Design of an Environmentally Benign Thread Compound for Oil Well Joints

ELIO SCAVO

Graduation Committee

Chairman and Program Director of PDEng
prof. dr. ir. D.J. Schipper   University of Twente

Thesis Supervisor
prof. dr. G.J. Vancso   University of Twente

Thesis Co-supervisor
dr. ir. J. Duvigneau   University of Twente

Members
dr. ir. R. Loendersloot   University of Twente
ir. D. Ernens   Shell Global Solutions International B.V.

Elio Scavo
Design of an Environmentally Benign Thread Compound for Oil Well Joints
PDEng Thesis, University of Twente, Enschede, The Netherlands
September 2018

DESIGN OF AN ENVIRONMENTALLY BENIGN THREAD COMPOUND FOR OIL WELL JOINTS

PDEng Thesis

to obtain the degree of
Professional Doctorate in Engineering (PDEng) at the University of Twente
on the authority of the rector magnificus,
prof. dr. T.T.M. Palstra,
on account of the decision of the graduation committee,
to be defended
on Friday the 14th of September 2018 at 13:30

by

Elio Scavo

born on 22nd January 1989
in Taormina, Italy

This PDEng thesis has been approved by:

Thesis supervisor: prof. dr. G.J. Vancso
Thesis co-supervisor: dr. ir. J. Duvigneau

Acknowledgment

This report is the result of two years of work in which many people have been directly or indirectly involved. I therefore feel the need to spend a few words to thank them.

First of all, I would like to thank the Professor G. J. Vancso for allowing me to start this wonderful experience in the Netherlands and for the immense support during the difficult times. Thank you very much also for the wisdom and the knowledge you shared during each of our meetings. After two years, I can firmly say that I would accept this position in your research group another thousand times. Particularly, Dr. J. Duvigneau was the person who considered me capable of carrying out this project and working as a PDEng trainee at the University of Twente. For this reason, for the trust given to me during these two years and for the time spent to provide me your useful feedbacks during both periods of research and writing of this report, thank you Joost. I also wish to acknowledge the Shell engineer Serge Roggeband for his wise feedbacks to this report and my Shell supervisor Dennis Ernens who has always directed me to the right direction for my research work providing meticulous information. Similarly, I would like to express my appreciation towards Rob Bosman for his smart suggestions during meetings and discussions. I am particularly grateful to Professor D. J. Schipper for the kind explanation of the PDEng program when I was just arrived in The Netherlands, as well as for the help provided to set up my defense and, above all, for the good mood and the positivity that he has always spread during our meetings.

Thank you Ezgi for the contribution on the synthesis of polymer particles and Jarvi as well as Maciek for the work on the hybrid core-shell particles.

I would like to extend my gratitude towards all the members of the MTP group. During these two years mostly spent on the 4th floor of Carré, I have always met pleasant people, at all times available to answer a scientific question rather than to share a relaxing moment. Thank you both Clemens and Marco for making the work atmosphere enjoyable and for the help always provided. Sida and Hubert, my office mates, thanks for help, enjoyment and the nice discussions.

Special thanks should be given to Prof. dr. G. La Rosa who, first, informed me about the existence of PDEng program and helped me to apply for this position.

Thank you very much to all the friends I met in Enschede for the good times spent together and to my girlfriend Zuzanna for making shorter the distance from home.

Finally, I would like to thank my beloved family, "mamma e papá", my brothers Salvatore, Filippo and Aurelio and my beloved niece Maria. Thank you for being by my side and supporting me in every moment of my life.

Elio Scavo
Enschede, August 2018

Table of contents

1. Introduction

1.1. Background

The constant growing demand for oil and gas, along with the reduction in available reserves, has led to the adoption of new drilling technologies, which allows drilling rigs to reach depths up to 13 km [1]. Under such extreme conditions, High Pressure/High Temperature (HPHT) wells need to assure the structural integrity over the full lifetime of the well. Casing and tubing strings are the main parts of a well construction [2]. Casing is the major structural component of a well due to the multiple functions it carries out. In addition, its cost covers the largest part of the total well-rig cost. It consists of multiple steel tubes joined at both ends. One or more casings are permanently installed into the wellbore to obtain the aforementioned structural integrity. Tubing is the conduit that actually transports oil and gas and its design relies on functional and economic considerations.

The so-called casing design loads are burst load (from internal pressure), collapse load (from external pressure) and axial load (tension or compression). In a more realistic context, a casing string has to be free from leaks while carrying mechanical, thermal, and chemical loads, for the whole lifetime of the well. For example, in HPHT wells, the cyclic thermal load experienced during the production phase, is a possible trigger for casing failure [3].

It is well known that, among all oilfield tubular failures, connection failures represent the majority of them [4]. Under HPHT well conditions standard API Connections [5] fail, meaning that safety and good performance are no longer guaranteed. In such a context, the so-called proprietary Premium Connections represent the currently preferred solution to meet the set performance requirements. They ensure superior structural and sealing performance [4]. A typical premium connection consists of a thread profile, commonly buttress threads for the structural function; a Metal-To-Metal (MTM) seal contact profile for sealability; and a torque shoulder next to the seal region, to control make-up of the connection and for additional sealability. Premium connections are described in more detail in Section 4.2.

The sealing performance of the MTM seal represents a critical aspect to be considered during both design and operation of the overall connection. It relies mainly on contact pressure, surface properties (roughness, coating, and hardness) and on the used thread compound[a]. The thread compound, also known as pipe dope, is applied to both threaded and seal surfaces prior to connection assembly, also known as make-up. During assembly and disassembly, it works as a lubricant to avoid galling while ensuring consistent frictional properties to obtain the recommended connection engagement. During service, the thread compound acts as a sealant that can withstand the high internal and external pressures.

In its more common composition, a thread compound is a mixture of base oil (mineral or synthetic) and additives such as thickeners (metal soaps, metal-complex soaps, or clays), anti-oxidants, and solid lubricants [6]. The most widely used and best performing thread

---

[a] Nowadays, the "dopeless technology", which allows avoiding the use of thread compounds, represents an effective, although expensive, alternative to the typical premium connections.

compound on the market is the API modified thread compound [6]. It consists of a mixture of heavy-metal particles (*i.e.* lead, copper, and zinc) and graphite powder dispersed in a base grease. However, the heavy-metal components must be replaced due to their proven high toxicity, as is discussed in more detail in Section 4.1.3. This project proposes polymer based alternatives to the toxic heavy metals used in API modified thread compound.

1.2. Motivation

In case of leaking connections, production is interrupted and the well is either abandoned or repaired. This results in significant economic losses due to decreased production and additional intervention costs. A well-designed thread compound helps to reduce the probability of both structural and functional failures. In particular properly designed polymer based particles are expected to improve a thread compounds' sealing properties and as such prevent oil leakages to the environment. In addition, for Shell it results in less production interruptions. Furthermore, a proper selection of the polymer particle composition is expected to yield more environmentally benign thread compounds that comply with current regulations. Today no satisfying alternatives are available on the market.

1.3. Company

The Shell Global Solutions International B.V. financed this project. Shell is a global group of energy and petrochemical companies with an average of 86,000 employees in more than 70 countries. Shell uses advanced technologies and takes an innovative approach to help build a sustainable energy future. Among others, the British–Dutch multinational oil and gas company is evaluating more environmentally friendly solutions that target set regulations while preserving or enhancing technical performances. Particularly, Shell is the first major-oil company that, during the last few years, has directed several efforts to the development of innovative thread compound compositions.

Next to this project, several PDEng and MSc students are still involved in the collaboration between Shell and the University of Twente in other projects that consider different design problems of oil and gas wells. In order to facilitate the exchange of knowledge among these projects, monthly group meetings both in Rijswijk and Twente were organized by Shell to allow the students to interactively exchange knowledge by presenting their progress and receive feedbacks.

1.4. Outline of this PDEng report

A more detailed project description is given in Chapter 2 before introducing the objectives of this project. In Chapter 3, the requirements are established and topics such as safety, reliability, maintenance, costs, legal requirements and sustainability are covered as well. Chapter 4 presents and discusses a literature study covering casing connections, microchannel fabrication methods, thread compounds and particle-packing theories. The design methodology behind the project is given in Chapter 5, while Chapter 6 describes the development phase, from the conceptual design to the results. Chapter 7 present the design deliverables and the conclusions. Finally, Chapter 8 gives the recommendations.

2. Objectives

2.1 Description of the design issue

A visual description of the design issue is given in Figure 2.1. Casing is a critical component of oil and gas wells. Connections are the parts of the casing most likely to fail. In order to face the severe performance requirements associated with HPHT wells, premium connections represent the currently adopted solution. Sealing performance of the metal-to-metal (MTM) seal is of crucial importance for the overall connection performance. Oil and gas leakages represent the (functional) failure mode as a result of sealing failure of premium connections. Leaking oil flows through nano and microchannels located between the two mating surfaces of the MTM seal [7]. The presence of these leak paths is strongly related to (axial) micro sliding of the connections and surface damage since they both compromise the "ideal configuration" for sealing that is initially determined by:

- Applied torque, which depends on the type of connection. It is specified by premium connection manufacturers.
- Connection material, which is selected depending on the severity of the environment (commonly L80, P110, Q125 grades [5]).
- Surface texture, as the result of turning and shotblasting, typically one part is rough (and softer) and the other part is smoother (and harder), respectively
- Surface treatment, which is generally manganese/zinc phosphate coating covering one or both surfaces.
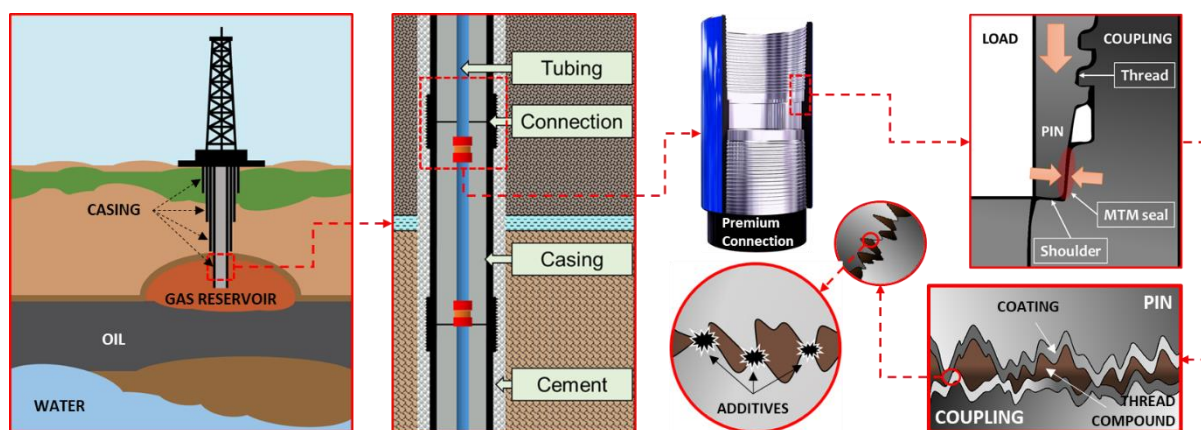

Figure 2.1. From the context to the design issue. Following the red arrows from left to right: Simplified diagram of an oil and gas rig; zoom-in a zone of the well; example of premium connection [8]; main elements of a premium connection; zoom-in of an MTM contact.

In terms of impact on sealing performance, both make-up and service phases are related to each other. During connection make-up improper engagement may lead to micro sliding of the connections in service. In addition, (axial) micro sliding can be caused (or increased) by the harsh and variable conditions inside the well, such as cyclic thermal and pressure loadings up to 250 °C and 1000 bar of differential pressure, respectively. Finally, micro sliding is a possible source of fretting fatigue failures [9] [10]. On the other hand, damage of the sealing surfaces can occur due to inappropriate lubrication during make-up/break-out. This mainly results in galling which is highly detrimental for the sealing performance of the connections.

It is important to realize that during service of the well, the impact of environment and all loading therein can not be fully controlled and therefore, not even meticulous compliance with make-up procedures can guarantee that leak paths are not created in the MTM seal.

As is shown in Figure 2.1, a substance called thread compound is applied to threads and MTM seal of premium connections to assist in lubrication and sealing against high internal and external pressure in service [6]. The most common composition API modified thread compound consists of a mixture of soft heavy metals (*i.e.* lead, copper and zinc) and graphite dispersed in a base grease (*i.e.* a base oil with thickening agents).

Besides the good lubrication performance given by the soft heavy metals in its formulation, the API modified thread compound seems to be the only pipe dope which has the necessary requirements to perform as a sealing compound for MTM seals at the extreme conditions in deep wells. Furthermore, the use of toxic heavy metals, such as lead, zinc and copper, is not anymore tolerated in many countries. Following the Norwegian environment agency (NEA), heavy metals are classified as "black" chemicals and, as such, they must be replaced with non- or less-hazardous components, such as "yellow" or "green" additives, as set out in more detail the next chapter. In addition, standard ISO 13679/API 5C5 full-scale tests are available to evaluate both lubrication and sealing performance of the connections. Nevertheless, these tests are not suitable to investigate the combined effect of thread compound, connections material and coating on both lubrication and sealing performance at the microscale. Therefore, new testing methodologies and set-ups must be developed as well.

2.2   Objectives of the design project

The main goal of the project is to propose, develop and evaluate the lubricating and sealing performance of environmentally benign alternatives to heavy-metal particles as thread compound additives.

3. Programme of requirements

This project stems from the need to replace heavy metals in thread compound compositions. In addition, the recent discoveries in the field of connection design and surface treatment require particular care for damage prevention of the premium connections main features, in particular the metal-to-metal seal. From a general point of view, thread compound requirements are classified in two macro categories, namely functional and non-functional requirements, as is shown in Figure 3.1.

The first category refers to performance requirements, most of which are listed in API 5A3 [6]. In addition to those, there also some requirements regarding the presence of coatings and their use with premium connections. In general, functional requirements include performance requirements during both make-up/break-out and sealing phases, *i.e.* (1) surface damage prevention and galling resistance (lubrication); (2) synergistic action with phosphates (and connection materials) not to affect the design surface treatment/texture; (3) adequate friction factor to allow connection engagement; (4) brushability and adherence to allow the application; (5) capability of filling and clogging leak paths and (6) extreme pressure (1,000 bar) and temperature resistance (250 °C).

Non-functional requirements concern compliance with local or global environmental legislation and market trends. Particularly, this category deals with the boundaries in terms of material selection, *i.e.* replace heavy metals by green/yellow alternatives (see Section 3.5) and with a particle size not below 100 nm. The latter was a communicated limit by Shell Hamburg based on environmental concerns.

Data regarding thread compound performance and impact on environment, health and safety must be included in the Technical Data Sheet (TDS) and in the Safety Data Sheet (SDS). These documents are provided with every new product entering the market.
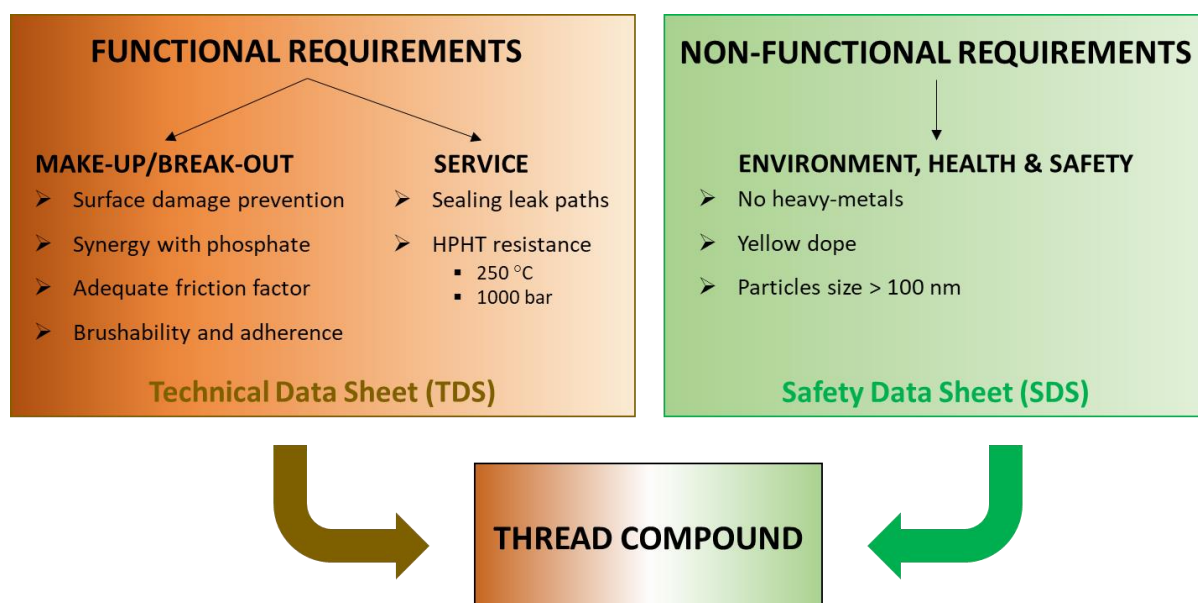

Figure 3.1. Thread compound requirements and related documentation for the use with premium connections.

3.1 Safety/Risks

The safety data sheet should inform about safety and health risks together with proper precautions for particular materials and conditions [6]. OSHA Hazard Communication Standard 2012 provides the format of such a document (29 CFR 1910.1200), which should contain general information about the chemicals.

3.2 Reliability

Following International Standard (*e.g.* API, ISO), an indicator of the reliability of thread compounds can be obtained by means of prescribed performance tests to evaluate dropping point, penetration, mass density, evaporation, oil separation, application/adherence, gas evolution, water leaching, frictional properties, extreme surface-contact pressure (galling), fluid sealing, corrosiveness, corrosion inhibition and compound high-temperature stability [6]. These tests provide reference values for minimum requirements of thread compounds for oil and gas wells. Nevertheless, the aforementioned properties do not really guarantee the reliability of the required sealing performance of premium connections. However, regulators suggest running supplementary tests for new specific applications, which are not evaluated, by the tests mentioned in the standards. In general, service applications and limitations should always be discussed by the user and manufacturer before selecting a thread compound. Finally, most of the provided tests refer to the performances of the thread compound itself without taking into account the combined effect between pipe dope and connection.

3.3 Maintenance

A thread compound is applied to the connections prior to make-up and it is intended to provide sealing while keeping its lubrication properties during the lifetime of the well. Well intervention strategies can follow different philosophies, *i.e.* continuous or periodic monitoring, load/usage bases, SH&CM (Structural Health & Condition Monitoring), etc. If the connections have to be broken out, the thread compound should support maintenance procedures by providing lubrication and friction properties to screw off the connections. In such cases, the washability of the thread compound is very important to allow for visual inspection and dimensional checks to be carried out [11]

3.4 Finances/Costs

The development of a thread compound requires a significant financial effort due to costs related to research, testing and material purchasing. From the standpoint of a regular thread compound manufacturer, the small profitability of the pipe dope market makes it impossible to direct large efforts to the development of new thread compounds while maintaining a positive economic balance. In the case of an oil company, this economic effort is justified by the large economic losses due to functional failures (such as leakages) and a subsequent decrease in production quantities. Increasing galling resistance, besides, can decrease the economic loss caused by the number of connections failed due to galling. In addition, the push from regulators makes these costs unavoidable for oil and gas companies. This project is expected to contribute to the purpose of reducing costs with the development of an effective design and a cheap while reliable testing set-up.

3.5   Legal requirements

The legal requirements of chemicals in thread compounds vary for different countries. Depending on the geographical area, the local legislation may allow the use of a chemical that is banned elsewhere. For example, the protection of the marine environment of the North-East Atlantic is regulated by the OSPAR (*i.e.* a legislative mechanism composed of 15 governments including The Netherlands) along with the European Union. The main legal guideline followed in this project has been developed by the Norwegian Environment Agency (NEA) and it is based on four categories that refer to four different chemical classes. Each category is named with a different color. Black and red chemicals are defined as components of special concern because they are hazardous and, therefore, they must be replaced. Yellow and green additives are considered non hazardous components, but concentration, time and place of discharge may cause environmental problems. Their substitution should be considered in case less harmful alternatives are available [12]. More information about the environmental properties of substances in chemicals is given in Appendix Table A1. Following this environmental framework, heavy metals are classified as black and as such, their use must be reduced and finally eliminated from thread compounds. Considering the value in Appendix Table A1, mineral oils are categorized as yellow with their biodegradability between 15% and 35% [13]. As a general trend, the use of filler particles having a size less than 100 nm is forbidden in thread compound compositions due to the high reactivity of nanoparticles.

3.6   Environmental/Sustainability

This project is strongly related to environmental concerns and sustainability. The environmental impact is given by the chemicals in the thread compound composition. For this particular project more environmentally benign alternative thread compound additives were targeted. Several European and international eco-labels exist to certificate eco- and sustainable performance and to guarantee the quality of the product, such as EU Ecolabel, Nordic Swan, Milieukeur, and many others.

4. Literature review

Considering the performance requirements of a thread compound as established in Chapter 3, it is clear that the role of additives is not only to aid in lubrication but they also play an important role in sealing. In Section 4.1, necessary background is provided about the role, typical composition and "green" alternatives of thread compounds to level knowledge with current standards and solutions. Premium connections are presented in Section 4.2 with special attention to the causes and the topography of leak paths in MTM seals. In order to be able to develop a single-channel testing methodology and set-up, microchannel fabrication methods along with fundamental concepts related to the flow in microchannels are introduced in Section 4.3. An overview on particles-packing theories is presented in Section 4.4 as an alternative method to design ideal particle size distributions for sealing.

4.1   Thread compounds

4.1.1   Role of thread compound in thread connections

Following regulations [6], a *thread compound is a substance applied to threaded pipe connections prior to make-up for lubrication during assembly and disassembly and for assistance in sealing internal and external pressures*.

Connection manufacturers [8] [11] recommend the use of thread compounds listed in tables provided with (online) available catalogs. Per each thread compound, these tables also give the proper torque factor to be used in the calculation of the final torque for a specific connection. Furthermore, several recommendations are provided for thread compounds to properly work, such as stirring at regular intervals prior to and during use and checking for contamination from water, mud or drilling fluid. Both stirring and contaminants, indeed, affect the friction factor and consequently, the lubricating efficiency of the thread compound. Prior to applying the pipe dope, connections are always checked from damage or corrosion. To actually apply the thread compound to the (dry) connections, a strictly dry brush (Figure 4.1, left) or motorized applicators are used. The correct amount of thread compound to be applied is cataloged as well and it varies depending on the type of connection.
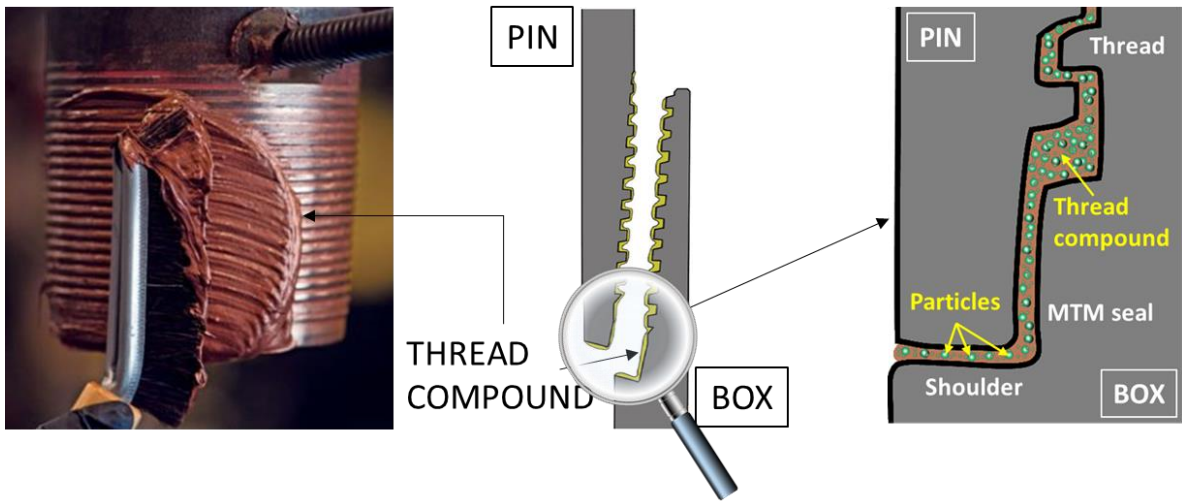
Figure 4.1. Applying thread compound to an OCTG connection (left) [14]; schematic example of properly applied thread compound (middle) [11]; detailed view with emphasis on the presence of solid particles (right).

In order to meet the definition of thread compound given above, control and performance tests are recommended by API, as designated in Table 4.1. However, the user and manufacturer are encouraged to perform supplementary tests for particularly severe applications [6]. The performance requirements listed in Table 4.1 are classified as properties ensuring friction, lubrication, sealing (leak tightness), physical and chemical stability (both in service and in storage[b] conditions), brushability and adherence.

These requirements are intended to allow proper and uniform connection engagement, to resist damage or galling (Figure 4.2) during make-up/break-out, and to seal thread type connections.

Figure 4.2. Example of a "galled" connection [15].

---

[b] Differently from running compounds, storage compounds are applied to the machined parts of connections to prevent the ingress of water and delay the corrosion process.

Table 4.1. Modified thread compound control and performance tests [6].

Test	Requirement
Penetration, mm x 10^{-1} worked at 25 °C (NLGI [a] Grade No. 1) after cooling at -18 °C (see procedure annex C)	310 to 340 200 min.
Dropping point, °C (ASTM D 566)	138 °C 88 min.
Evaporation, % mass fraction 24 hat 100 °C (see annex D)	2,0 max.
Oil separation, % mass fraction, nickel cone 24 hat 66 °C (see annex E)	5,0 max.
Gas evolution, cm^3 24 hat 66 °C (see annex G)	20 max.
Water leaching, % mass friction after two h at 66 °C (see annex H)	5,0 max
Brushing ability (see annex F)	Applicable at -18 °C
[a] National Lubricating Grease Institute, 4635 Wyandotte Street, Kansas City, MO 64112-1596, USA	
NOTE The Information presented in this table applies only to the API modified thread compound formula.	

The sealing requirement specific for MTM seals is indirectly addressed by ISO 13678/API 5A3 standard since it is herein only mentioned that thread compounds must "not inhibit the properties of the non-thread sealing connections" (*e.g.* MTM seals) [6]. However, thread compounds also play an active role to avoid leakages in MTM contact. Sealing tests conducted on ring-shaped specimens simulating actual premium connections (common material grade, turning machining and phosphating treatment) under field-like conditions (sliding, high temperature and contact stress) proved that grease is essential for the performance of metal-to-metal seals, especially when gas tightness is required [16]. Furthermore, the tribological layer formed by the phosphate coating performs most of the functions associated with lubrication [17]. Hence, more specific requirements should be given when thread compounds are intended to be used on premium connections. In particular, in addition to supporting phosphates without damaging them during lubrication, the thread compound should also fill

and clog micro-gaps (channels) between seal surfaces under operation conditions. These functions can not be guaranteed by means of the tests provided by API as listed in Table 4.1. Therefore, alternative tests should be developed.

4.1.2 Composition of thread compounds

Thread compounds are multi-phase non-Newtonian fluids composed of a base oil and several solid components, such as a thickener.

Lubricating oils are mineral (long chain hydrocarbons) or synthetic, such as silicones, polyglycol esters or polyesters, based oils. The use of vegetable oils is an eco-friendly solution, however, they are currently not able to fulfill the requirements for the deep wells. The operational temperature limit of mineral oils is around 150 °C while synthetic oils can withstand temperatures exceeding 450 °C [18] [19]. Besides good thermal stability, base oils for thread compounds should also have a high viscosity to face, along with the thickener, the pressure conditions typical for oil and gas wells. The viscosity-temperature dependence is well described by the viscosity index (VI), which has high values for small viscosity variations with temperature [20].

The thickener is the additive that most of all affects the physical character of the grease and its semi-solid structure. The most common thickeners used are metal soaps, metal-complex soaps, and clays. When a soap is used as a thickener, its interaction with the base oil forms a sponge-like matrix with even 75% of the oil locked in the coherent network of thickener particles. A combination of mechanical occlusion, capillary phenomena, and molecular forces balances the amount of trapped oil. The final skeleton of the microstructure depends upon shape, surface topography and size of soap particles [21] [22]. Examples of this type of thickener are lithium, lithium complex, calcium complex, and aluminium salts soaps. The thickening mechanisms of clay particles, such as bentonite, is governed by the formation of individual aggregates called platelets. In such a case, surface modification techniques allow tailoring the oil-clay interaction to reduce particles agglomeration in olephilic applications [23]. Thickener particles have a maximum size of 100 µm in case of soaps while clay particle sizes are typically below 1 µm [21]. Two important parameters for the characterization of greases (base oil and thickener) are consistency (NLGI grade) and dropping point (°C). They are used to describe grease flow-ability and high-temperature behavior [20].

Other additives include extreme pressure (EP) additives, corrosion inhibitors, anti-wear additives, friction modifiers, sealants and anti-oxidants [24]. Their roles are either preventing surface damage and thread compound oxidation or increasing the lubrication and sealing performance. For instance, anti-oxidants act as sacrificial compounds to prevent oxidation while EP additives such as sulfur, phosphorus or chlorine compounds become important when the lubrication regime passes from hydrodynamic to boundary/mixed [20].

API recommends proportions of solids and grease base in order for a thread compound to comply with the control and performance test requirements. Precisely, thread compounds that are realized following these recommendations are designed as "API modified thread compounds", an example is given in Table 4.1. This composition represents the current standard for connection manufacturers and users. Thus an API modified thread compound is

composed of a mixture of solids (*i.e.* amorphous graphite, lead powder, zinc dust and copper flake) uniformly dispersed in a base grease. Lithium 12-hydroxystearate is recommended as a thickener in such a composition, due to its superior thermal stability, although it has a lower water resistance compared to calcium and aluminum soaps [20]. Graphite is often used as a high-temperature lubricant due to its high-temperature resistance and lubricity. The latter derives from the typical lamella crystal structure of graphite having weak carbon bonds among layers located in different planes [25].

Table 4.2. Proportions of solids and base grease of API modified thread compounds [6].

Component	Mass fraction (%)
Total solids	64,0 ± 2,5
Amorphous graphite	18,0 (±) 1,0
Lead powder	30,5 (±) 0,6
Zinc dust	12,2 (±) 0,6
Copper flake	3,3 (±) 0,3
Base grease	36,0 ± 2,5
Base oil	Variable
Thickener	Variable
Total	100,0

4.1.3   Role of heavy metals in thread compounds

Mixtures of soft heavy metals have been widely used in thread compound compositions. Their combined effect results in excellent performance for both lubrication and sealing of threaded connection seals. Particularly, they form a tribological film composed of low melting point particles (*i.e.* lead and zinc particles) surrounded by graphite and copper particles. It is supposed that this configuration, known as a sandwich structure, helps to prevent lead particles from sticking to the metal surfaces and zinc particles from gluing together [26] [27]. Lead alone is extremely difficult to remove from the thread roots [28], but the sandwich structure is broken up after break-out and is easily removed [27]. Malleable and soft metals such as lead, copper and zinc have relatively low yield limits that help them to perform under load or pressure [29]. This characteristic is due to their close-packed structure, which has little corrugation among the various planes formed by sheets of metal atoms [30]. These so-called slip planes provide lubricating properties [31]. The tribological film is created while applying torque to the connections, as a result of shearing strain deforming the soft metal particles [27]. Copper, with its high thermal conductivity, disposes heat in the contact, thus producing a protective medium against pressure-welding and galling [28].

The synergistic action of lead, zinc and copper, together with amorphous graphite, fulfills the API requirements presented above. Indeed, the formed tribological film has several benefits, namely (1) increased load-bearing capacity of the connections (by increasing the contact surface); (2) higher impact resistance; (3) prevention of uncontrolled tightening (by additional deformation of particles); (4) prevention of wear and corrosion and (5) sealing resistance even at extreme differential pressures [27].

The main drawback of the use of heavy metals in thread compound compositions is their proven high toxicity, which gave rise to numerous environmental concerns. For this reason, heavy metals must be replaced, although they are still being used in several countries where no regulation exists about their use as thread compound additives [32]. In addition to that, soft heavy metals catalyze the oxidation process of the base oil, thus decreasing the overall performance of the grease [33].

4.1.4   Alternatives for heavy metals

A possible alternative for heavy metals in thread compounds is based on the use of different (non-toxic) metals. For example, bismuth has very similar properties to lead, but it is not considered as a toxic material [32] [34]. However, synthetic materials such as polymers offer a higher tunability of their properties to meet the desired specific requirements.

Polymers are already used as additives for lubricants [35] [36] [37] [38]. By varying size, distribution and shape of polymer particles along with their surface properties, it is possible to obtain a wide range of potential materials for replacing the heavy metals in thread compounds. In the oil and gas industry, polymers are used as components of fluids or additives during all well phases, *i.e.* drilling, completion and intervention [39]. For example, polyacrylamide is the most common polymer used in enhanced oil recovery applications [40]. It is thermally stable at the operational conditions and non-toxic by itself [41].

In the form of particles dispersed in a base grease, polymers may act as lubricating and sealing agents for casing connections. For this purpose, special attention must be directed to selecting polymers that have suitable physical and thermal properties. Considering the given background knowledge on premium connections, thermal stability and hardness are crucial parameters to decide whether a material is expected to be suitable or not for the use in metal-to-metal seals. Promising polymers are those that assist phosphate coatings in their excellent lubricating action, without damaging the surface of the metal-to-metal seals. If damage during make-up occurs it affects the MTM seals performance eventually resulting in functional failure of the overall connection. During service of the well, instead, the used polymers should resist the high operating temperatures (up to 250 °C) without excessive degradation and form a barrier against oil and gas leakages between the metal-to-metal surfaces. Finally, by selecting polymers having a relatively high biodegradation rate and non toxic discharges, it is possible to comply with the desired law limits.

Besides polymers, inorganic nanoparticles (NPs) can be used as alternatives to heavy metals due to their direct and indirect effects on lubrication and sealing [42]. The most known NPs alternatives are silica or diamond [43], graphite/graphene [44], calcium carbonate ($CaCO_3$) [45], molybdenum (MoS_2) [46] and tungsten disulfides (WS_2) [47]. Particularly, titanium

dioxide (TiO_2) is a well-known lubricant additive [48] [49] [50] [51] and it is classified as a "green" material. It represents a good candidate to replace heavy metals in thread compound compositions also due to its high availability and low price. Unfortunately, NPs suffer some drawbacks related to agglomeration and dispersability but their surface can be modified to reduce this tendency. For instance, surface-initiated atom transfer radical polymerization (SI-ATRP) can be used to create hybrid-core shell particles having tailored features [52] [53]. For example, a soft polymer (shell) can be attached to a hard material such as TiO_2 particles (core), thus preserving the sliding/mating surfaces from damage. Furthermore, the high-temperature resistance of TiO_2 is desired in high-temperature applications such as sealing in MTM seals for oil and gas wells.

4.2   Premium connections

The interested reader can find an overview on casing connections in Appendix Section B. The so-called *premium* connections are developed by private companies (*e.g.* Hydril, Vallourec, Mannesmann) to improve reliability, leak resistance and performance (*e.g.* fatigue resistance) of standard OCTG [54], whose design typically relies on static loading. These proprietary (non-API) connections are used in High Pressure/High Temperature (HPHT) wells, especially in applications where API standard connections fail. Applicability of standard and premium connections in terms of type of well, depth and pressure, is shown in Table 4.3.

Table 4.3. Applicability of API and premium connections [55]*.*

Gas Wells	Offshore	Premium Connections		
	Onshore	Standard Connections		
Oil Wells				
Well Depth [km]			3.0	6.0
Bottom Hole Pressure [bar]		275	550	

Likewise API connections, premium connections can be distinguished in (a) threaded and coupled and (b) integral connections, as is shown in Figure 4.3. The first group has a higher tensile strength and is less sensitive to stress concentrations, whereas integral connections are typically used when the radial clearances have to remain small, while the load/pressure capacity is still moderate/low [54].
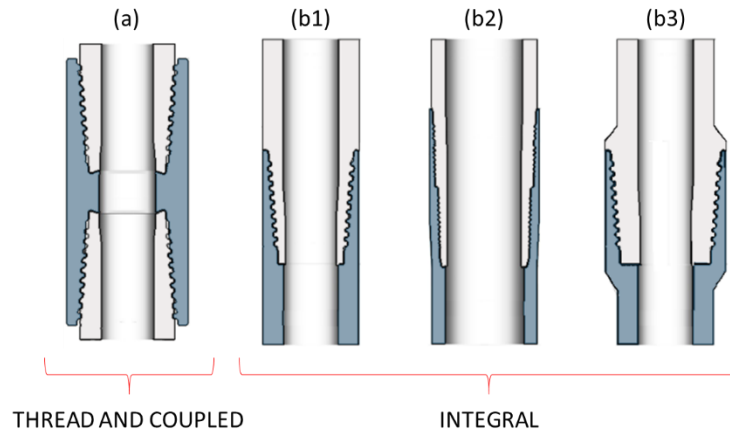
Figure 4.3. Different types of premium threaded connections: (a) thread and coupled; (b1) integral flush; (b2) integral semi-flush; (b3) integral upset [54]*.*

A more detailed description of a typical premium connection geometry is provided in Appendix Section B.3.

4.2.1   Sealing: Metal-to-metal seal

Sealing is required during service operations. Chemical exposure in a mud environment (water or oil based) inside the well with mainly hydrocarbons, carbon dioxide (CO_2), and hydrogen sulfide (H_2S) are a possible trigger for environmental cracking (especially sulfide stress cracking) to occur. Temperature conditions inside the well can vary from 30 °C up to 250 °C, while the differential pressure between internal and external pressure can reach 1000 bar. Furthermore, (axial) micro sliding due to cyclic loading in the well, may cause fretting fatigue failure [56]. In premium connections, sealing is primarily ensured by the metal-to-metal seal while the threaded part is designed to maximize structural integrity. More precisely, the metal-to-metal seal portion serves to ensure gas tightness under high pressure and extreme temperature [16]. The contact stresses in the metal-to-metal seal of premium connections can reach 1 GPa [17].

Oil and gas leakages are regarded to as functional failures that, due to economic losses and environmental concerns, make seals a critical component of the well. Understanding mechanisms and behavior of leakages is important to develop predictive capability to design optimal configurations for sealing. Metal-to-metal seals are based on the contact between two metal surfaces pressed against each other. Therefore, the sealing performance is strongly affected by the contact interface, which, in turn, depends on surface texture, shape distortion, interaction with the lubricant and any other factor causing degradation [17]. Only the (ideal) case of two perfectly flat surfaces under sufficient contact pressure would result in no leakages, but this is impossible to be actually achieved [57]. However, API standard [58] defines 0.9 cm^3 / 15 min as a leak and, therefore, values below the established threshold can be neglected. Finally, leakage is a function of surface topography at both microscopic and component length scales, as is shown in Figure 4.4. The presented geometry emulates a real MTM seal of a premium connection by an axial contact of a crown / circular geometry.
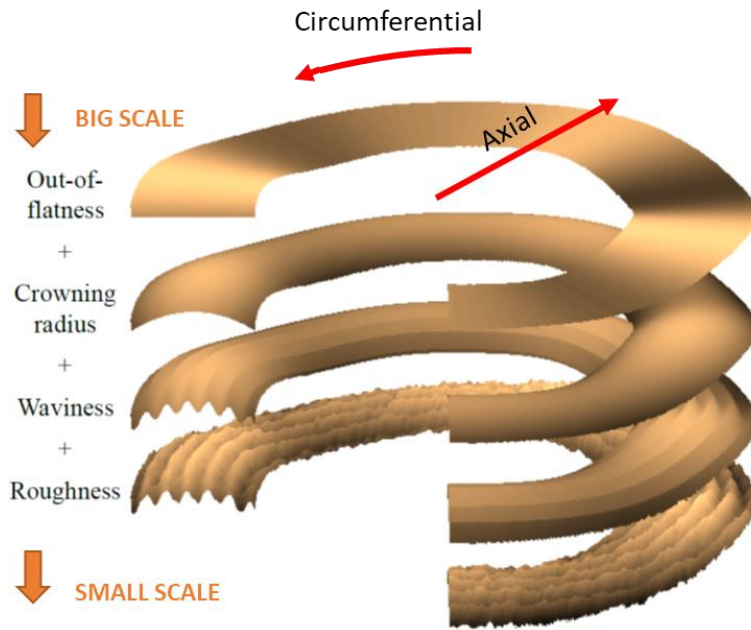
16

Figure 4.4. Surface topography of a metal-to-metal seal at different length scales [7].

Starting from the largest scale, errors of form (out-of-flatness) are always present and their impact can be reduced by (costly) manufacturing processes. Instead, the crowing radius is desired and its design relies on misalignment reduction and control of the contact width. These kind of feature are only applicable to the axial and circular seal geometry as indicated in Figure 4.4. MTM seals on premium connections do not have a flatness type feature, or a "crown". They have different features (roundness, seal round-off radius, etc.) at this length scale. Metal face seals are usually obtained by turning, which creates a spiral groove (waviness) that properly acts as an active sealing element when there are no flaws in the axial direction [59]. Roughness represents the smallest scale of the seal surface topography and, in turn, it exhibits different properties at different magnifications. Leak paths are always created due to the multi-scale nature of the roughness (neglecting plastic deformation and surface tension effects) and other small-scale features such as defects (*e.g.* scratches) [7]. The latter ones are mainly caused by to improper storing, make-up, axial micro sliding, pressure/temperature cyclic loading, lubricant failures or insufficient quantities applied

All studies on leak flow patterns through spiral grooves in metal-to-metal contact [60] [61] [59] agree upon the existence of two principal directions of flow, namely circumferential, along the spiral groove and axial, when the flow crosses the ridges of the waviness. Taking into account the high hydraulic resistance along the length of the spiral groove, circumferential leakage can be considered negligible compared to the axial one. However, a more realistic representation of leakages is based on the concept of a meandering flow pattern, which has been experimentally observed [62] and developed by means of models [7], as is shown in Figure 4.7 (upper right part). The (fluid) pressure drop mainly occurs in one of the ridges in contact, as confirmed by the color change at the third ridge from the left in Figure 4.7. The axial leak paths are visible in yellow (refer to the flow intensity scale) with the circumferential flow connecting the channels crossing the ridges.

17

The preferred configuration for sealing consists of a soft surface with waviness against a harder and smoother one [7]. To understand the reason for this choice, it should be realized that, as shown above, leakages depend on the evolution of the contact pattern and this last, in turn, is affected by the magnitude of the normal load. This concept is clarified in Figure 4.5. In order to obtain full sealing, the contact at the spiral summit crests should be continuous as it happens once a certain threshold load value is reached.
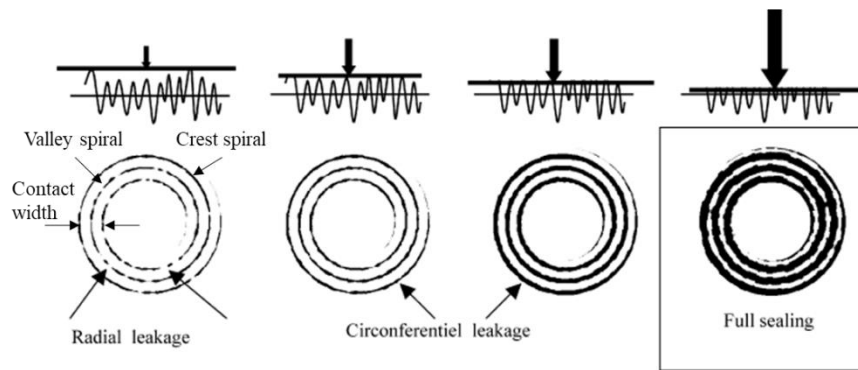

Figure 4.5. Contact area evolution and possible leak path for an increased contact load [61]*.*

A comparison between different micro geometries confirmed that the ideal configuration for sealing is characterized by surface textures with irregular valley altitudes and a regular crest altitude [61], as is shown in Figure 4.6. The red circle on the right part highlights how the contact within the channel is increased by the variations in valley depths. The turning process alone is not able to provide the described microgeometry and a partial polishing of the highest asperities could be a proper post-treatment of the surface. However, the choice of using a configuration in which a rough and soft surface indents another harder and smooth face seal represents an alternative method to reduce the variability of summit altitudes. Finally, taking advantage of the plastic deformation capability of phosphate coatings, it is possible to reproduce the ideal configuration of sealing (microgeometry) that has been described above. A typical example relies on one side coated by phosphates (*i.e.* a rough and soft surface) and bare steel on the other side (*i.e.* harder and smooth surface).
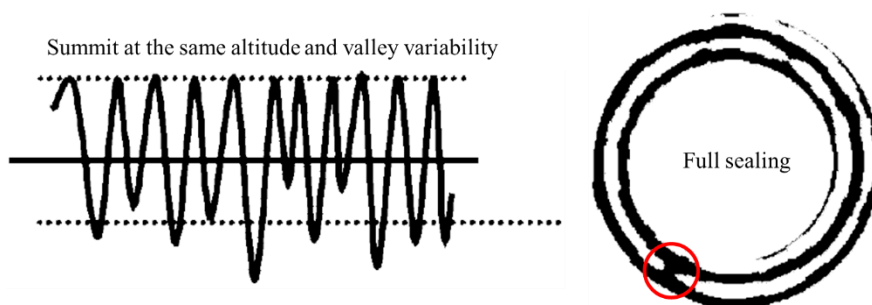

Figure 4.6. Contact pattern for a microgeometry ideal for sealing. The red circle indicates the point where the spiral-like channel is blocked [61].

It was previously mentioned that, as a more specific requirement for sealing, a thread compound should have the ability to flow inside the leak paths in metal-to-metal seals and efficiently clog them to prevent oil and gas leakages. Therefore, in collaboration with Shell it was decided to perform single-channel clogging tests at the microscale in order to study the clogging behavior of particles and eventually to be able to design an optimal particle size distribution for sealing those channels. Figure 4.7 provides an overview that justifies this choice. Leakages occur through a few channels that are formed in the axial direction. Hence, only a limited number of channels is responsible for leakages. In turn, it is assumed that each of these channels can be idealized with a rectangular or circular cross-section that simplifies the problem. Due to the complexity of the contact geometry, the actual dimensions of the leak paths is unknown. Considering models and numerical analysis of leakage through MTM seals [7], widths or diameters of channels cross-section are assumed to be in the range of 100 nm to several μm.
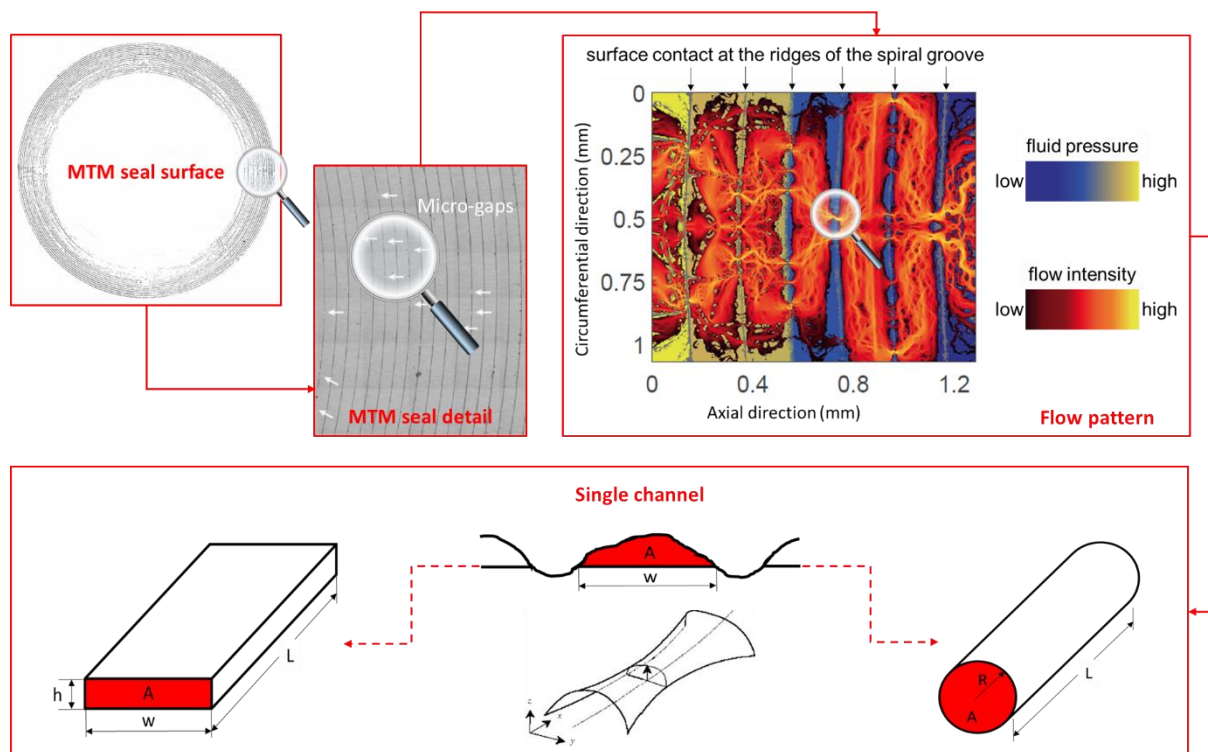

Figure 4.7. Magnification of the MTM seal surface up to the single-channel level [59] [7].

4.3   Microchannels

Therefore, different methods of fabricating microchannels were evaluated, as reported in Appendix Section C. The goal of this study was to identify the fastest realizable processes within the scope of this project among the currently available processes. Depending on the type of application and requirements (*e.g.* chemical, biological, or electronics and mechanical engineering-related), microchannels are fabricated on silicon, polymer, glass or metallic substrates. They typically have circular, half circular, rectangular, or square cross-sections [63]. Considering that glass capillary tubes having an internal diameter equal to 300 µm are incredibly cheap (1,10 € per meter), we decided to produce microchannels based on this type of capillary tubes. Exposing their central section to a blowtorch while pulling the two ends of the capillary tube allows to deform the glass and narrow the initial internal diameter. The final result is a balance of exposure time, intensity of the flame, tube-flame distance and intensity of the pulling force. This method has the advantage to create microchannels with diameters in the order of few microns in an extremely cheap and fast process. Furthermore, clean room facilities as for most of the other presented techniques are not required for the production of glass capillary tubes. The main drawback is the lack of a system that allows to accurately control the final channel dimensions. In addition, glass microfluidic chips with 5 µm nozzles can be purchased, as is discussed in more detail in Section 6.2.

4.3.1   Flow rate and pressure in a microchannel

Some concepts of flow in microchannels are herein covered as well. Understanding the physics related to this type of flow helps to evaluate the relevant parameters needed to assess the sealing behaviour of particles. For example, pressure and flow rate are the parameters that are commonly used to monitor the tightness of premium connections and it is investigated how are they related to each other inside microchannels.

The science and technology that deals with the control of fluids flowing through microchannels is called microfluidics. It developed in 1990s consequently to miniaturization and MEMs (*micro-electro systems*). Common size range for this discipline goes from 300 µm down to the nanoscale [64].

In such a small size range, viscosity forces exceed inertia forces leading to very low *Reynolds* (*Re*) numbers and, therefore, a laminar flow regime exists. The behavior of this orderly fluid regime is highly predictable, especially when Re < 1 and *Stokes* flow occurs [65].

Two governing equations regulate the fluid flow, *i.e.* (1) the continuity equation, which leads to the conservation of mass and (2) the *Navier-Stokes* equation, which determines the *Eulerian* velocity of a viscous fluid [65]. This last equation has a non-linear term (v·∇)v that results in several difficulties during calculations. However, the assumption of small velocities flow (commonly valid in microfluidics) makes the non-linear term negligible and the *Navier-Stokes* equation is thus reduced to the simplified Stokes equation, as is shown in Equation 4.1

$$0 = -\nabla p + \eta \nabla^2 v \qquad (4.1)$$

where ∇p = pressure gradient; η = dynamic viscosity and ∇v = velocity gradient.

The latter is assumed to describe the (Stokes) flow of particle dispersions. The most used solution to the *Navier-Stokes* equation is based on the assumptions that the fluid is viscous and incompressible, in laminar flow, while the channel has a constant channel cross-section and that the system is at steady state conditions (*i.e.* no acceleration of fluid flow). These assumptions lead to the so-called *Hagen-Poiseuille*'s law, which relates the pressure drop over the channel to the (volumetric) flow rate under the previous mentioned conditions. Such conditions are similar to those typical in microfluidic systems. Assuming no-slip boundary conditions, a second order partial differential equation for the velocity field is obtained and its analytical solution is possible only for certain cross-section shapes. However, approximations are used to calculate the velocity also for more complex cases. Knowing the velocity, the volumetric flow rate (Q) can be calculate as well [64] [65].
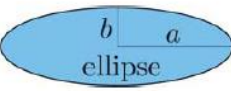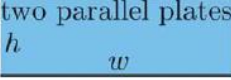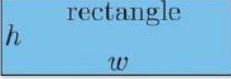
According to the *Hagen-Poiseuille*'s law, the flow rate ($[Q] = m^3/s$) and applied pressure drop ($[\Delta P] = Pa = kg/m \cdot s^2$) are proportionally related as is shown in Equation 4.2:

$$\Delta P = R_h \cdot Q \qquad\qquad (4.2)$$

where $[R_h] = Pa \cdot s/m^3 = kg/m^3 \cdot s$ and is referred to as the hydraulic resistance.

Some expressions of R_h for different cross-section shapes are shown in Table 4.4. An analogy between hydraulic and electric systems exists. Indeed, under the assumptions used before, the hydraulic resistance can be calculated as the same manner as the electric resistance in electrical systems, using the same concepts for serial and parallel circuits.

Table 4.4. The hydraulic resistance for water flowing through straight channels with different cross-sectional shapes. The numerical values are calculated using η = 1 mPa s, L = 1 m, a = 100 mm, b = 33 mm, h = 100 mm, and w = 300 mm. Note that the areas (A) are different [65].

Shape and parameters	R_{hyd} expression	$R_{\text{hyd}}\left[10^{12}\dfrac{\text{Pa s}}{\text{m}^3}\right]$
a — circle	$\dfrac{8}{\pi}\eta L\dfrac{1}{a^4}$	25
b, *a* — ellipse	$\dfrac{4}{\pi}\eta L\dfrac{1+(b/a)^2}{(b/a)^3}\dfrac{1}{a^4}$	393
a, *a*, *a* — triangle	$\dfrac{320}{\sqrt{3}}\eta L\dfrac{1}{a^4}$	1850
two parallel plates — *h*, *w*	$12\eta L\dfrac{1}{h^3 w}$	40
rectangle — *h*, *w*	$\dfrac{12\eta L}{1-0.63(h/w)}\dfrac{1}{h^3 w}$	51
square — *h*, *h*, *h*, *h*	$28.4\,\eta L\dfrac{1}{h^4}$	284
parabola — *h*, *w*	$\dfrac{105}{4}\eta L\dfrac{1}{h^3 w}$	88
perimeter $\mathcal{P}$, area $\mathcal{A}$	$\approx 2\eta L\dfrac{\mathcal{P}^2}{\mathcal{A}^3}$	—

4.4   Particle-packing theories

As was shown in the previous Section, the main design issue associated with this project is the presence of leak paths on metal-to-metal seal surfaces. In this context, particles-packing theories were closely examined in order to obtain insight in what are optimized particle size distributions to enhance the sealing performance of a thread compound. Considering that particles are widely used as additives for lubricants due to their lubricating effects [42], an increase in their packing density could lead to an improved sealing capability as well. Packing theories assume that adding fine particles to a packed particle structure helps to fill up the voids in between the particles (see Figure 4.8, right) [66]. In case of particles confined within a porous structure such as the network of leak paths in MTM seals (channels), the previous statement implies that the denser the particle packing, the less space is left for oil and gas leakages to occur.

In 1611, Johannes Kepler reported that, in a volume filled by identical spheres (*congruent balls in Euclidean three space*), the face-centered cubic packing (Figure 4.8, left) has the greatest packing density, equal to $\pi/\sqrt{18} \approx 0.74$. This value represents the so-called *virtual packing density*, being 0.74 the maximum packing density achievable under the previous conditions, considering that each particle keeps its original shape and it is placed one by one [67]. This conjecture, recently accepted as a theorem [68], is also valid for hexagonal close packing. Commonly, particles are randomly packed and their *physical packing density* will be lower than the virtual packing. For example, the physical packing density of a random close packing of mono-sized spheres is close to 0.60/0.64 [69] [70]. It is worth mentioning that in the literature, there is a distinction between Random Close Packing (RCP) and Random Loose Packing (RLP), depending on whether the container is shaken or not, respectively after particles are randomly packed.
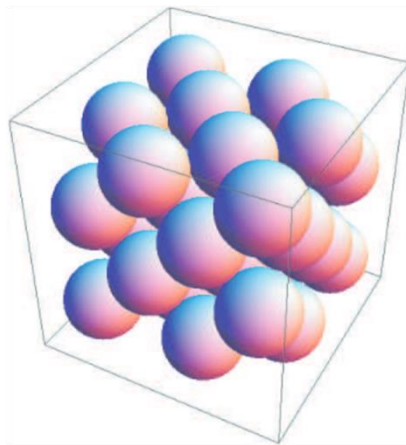
Mono-Sized Sphere Regular Packing

The highest packing density of mono-sized spheres in the 3-dim space is:

$$\frac{\pi}{\sqrt{18}} \approx 0.74048$$
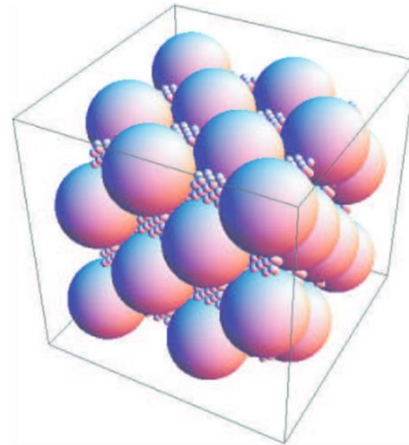
Multi-Sized Sphere Regular Packing

Increasing the ratio of the two sizes of spheres, the following density can be reached:

$$1 - \left(1 - \frac{\pi}{\sqrt{18}}\right)^2 \approx 0.93265$$

Figure 4.8. Kepler's Conjecture for Mono-Sized Sphere Regular Packing (left) and Multi-Sized Sphere Regular Packing (right). In the second case, the packing density is increased after adding smaller spheres to fill up the vacancies between the particles of the mono-sized sphere packing [71].

The concept of packing density is widely encountered in science and engineering for diverse applications. For instance, in concrete mix design, minimizing inter-particle voids (porosity) between the constituents, helps to reduce the slurry demand while ensuring certain minimum properties such as consistence, strength, and durability [66].

The aim of particles-packing theories is to maximize the packing density (ϕ), which is defined as the solid volume (V_s) in a unit total volume (V_t) [67], or equally, as the ratio of the volume of solids to the bulk volume of the solid particles [66]. The packing density can be expressed also in terms of void content (e), as shown in Equation 4.3.

$$\phi = \frac{V_{solids}}{V_{total}} = \frac{V_{solids}}{V_{solids} + V_{voids}} = 1 - e \qquad (4.3)$$

As anticipated above, a reduction in void content or an increase in packing density is achieved by means of smaller particles filling the voids between larger particles. In turn, smaller voids in the packing of small particles will be filled with even smaller particles, and so on. The most significant factor used to characterize multi-component compositions is the particle size distribution. From a viewpoint based on this factor, particle-packing models fall in two categories, namely discrete and continuous models, as is shown in Figure 4.9. Once a relation between the packing density and the particle size distribution is established, the purpose of these models is to predict the optimum particle composition leading to the maximum packing density.
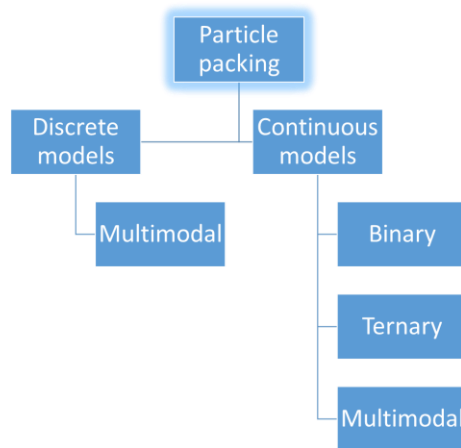
Figure 4.9. Classification of particle packing models [72].

The continuous approach assumes that the particle distribution in a system contains all possible sizes and the effect on the packing density is indirect. The fundamental step of this methodology provides for the development of an ideal particle size distribution (PSD) curve along which the maximum packing density is produced. This curve is known as Fuller's "ideal" curve and it was proposed in the first work reported on this topic by *Fuller* and *Thomson* in 1907 [73]. Their model deals with a continuous grading curve ranging from 250 µm to the maximum size [66]. A more general case is represented by the *Andreasen* model (1930) [74], which was later modified by *Dinger* and *Funk* (1994) [75] to account for the minimum particle size, as is shown in Equation 4.4:

$$\frac{CPFT}{100\%} = \frac{D^n - D_S^n}{D_L^n - D_S^n} \qquad (4.4)$$

where

CPFT	=	cumulative percent finer than
D	=	particle size
D_s	=	smallest particle size
D_L	=	largest particle size
n	=	distribution modulus, ranging from 0 to 1 (commonly selected based on experience)

A visual comparison among these models is given in Figure 4.10. Other continuous approaches refer to different distribution functions, such as the *Rosin-Rammler* distribution [76], which are used to represent particle size distribution. The relation between these functions and the porosity strongly affects the design of dense packing of particles.
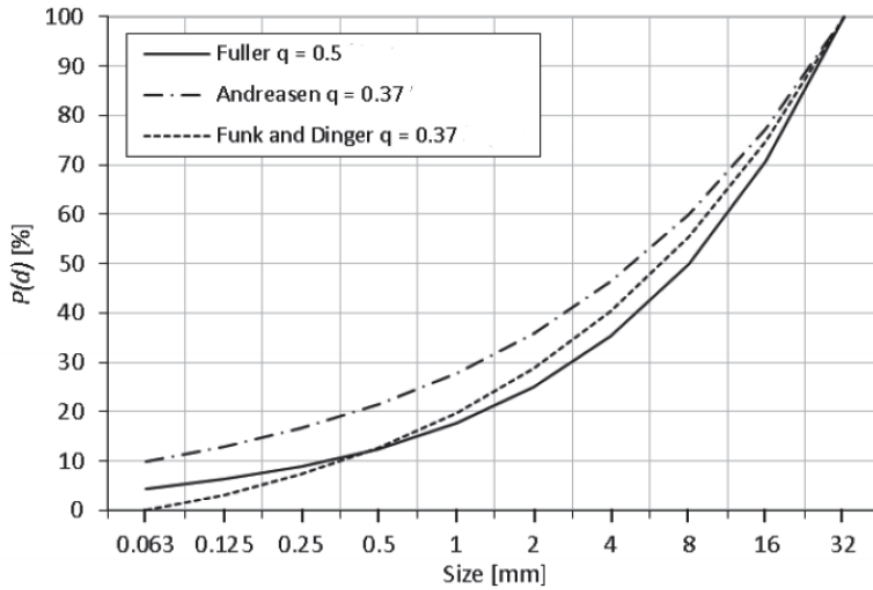
Figure 4.10. Ideal curves according to Fuller, Andreasen & Andersen, and modified A&A (Funk and Dinger). For a minimum and maximum particle size of 32 mm and 63 μm, respectively [77].

A typical application of the continuous approach is the design of reservoir drill-in fluids (RDF) to effectively seal the formation surface. In this regard, bridging agents are selected following the so-called Ideal Packing Theory (IPT), which provides the ideal size distribution required to seal all voids, including those created by bridging agents [78] [79]. An example of such an application is given in Figure 4.11, where the target line is based on the assumption that 90% of the particles of bridging agents (D_{90} rule) are smaller than the largest pore size for the given formation. Therefore, a straight line is drawn by connecting the origin of the Cartesian system to the $D_{90}^{1/2}$ point. In order to optimize the particle packing, bridging agents should be blended thereby producing particle size distribution approaching the target line.
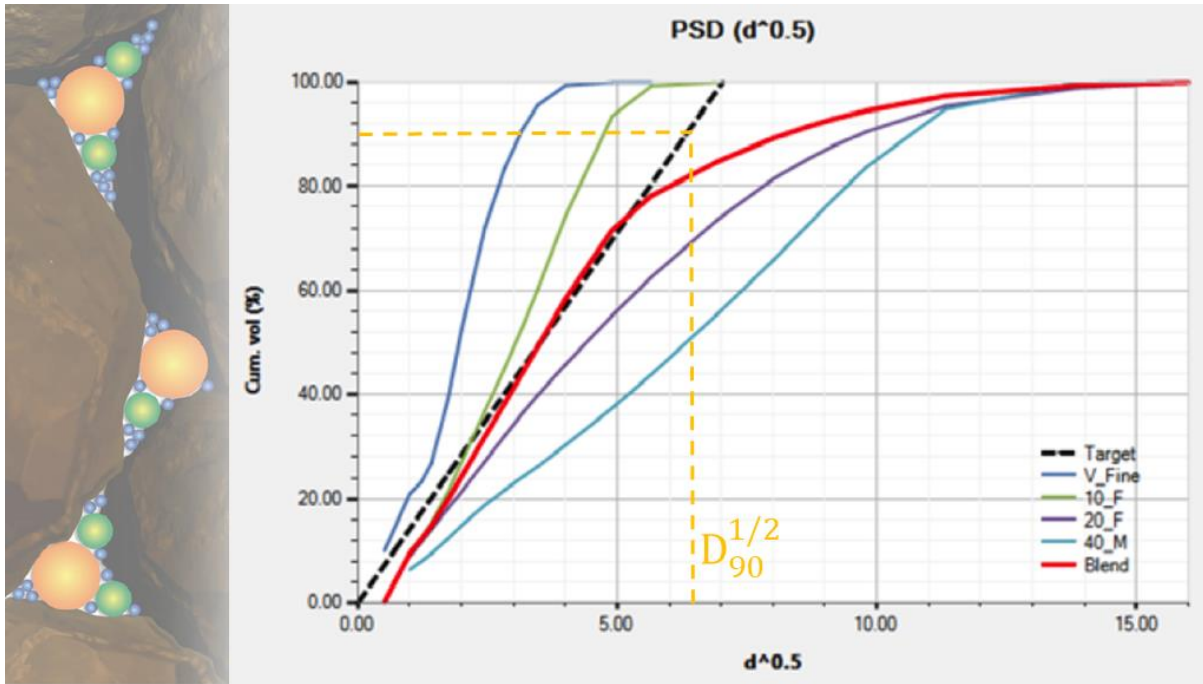
Figure 4.11. Ideal Packing Theory (IPT) in practice for designing reservoir drill-in fluids (RDF) [78].

Practicality and simplicity are the advantages of using a continuous approach. However, it does not consider some phenomena affecting particle packing such as wall, loosening, and compaction effects. The discrete approach compensates for this lack. Theories based on this approach refer to packing systems containing classes of discrete sized particles, assuming that each of those classes will pack following its maximum density in the volume available [72]. Based on the number of discrete size classes contained in the system, discrete models can be classified as binary, ternary, and multimodal mixture models (Figure 4.9). *Furnas* (1928) [80] developed the first analytical packing model to predict the void ratio of binary systems. Figure 4.12 shows the packing porosity of a binary mixture as a function of the percentage of large particles in the overall volume and of the size ratio between large and small particles. In the figure, it is shown that, in order to minimize porosity, an optimum proportion between large and small particles is needed. Furthermore, particle size ratio affects porosity since, for a given solid fraction, an increase in the ratio between small over large particles leads to an increase in void content. This model is valid in case of binary mixtures without interaction (diameter$_{grains\_1}$ >> diameter$_{grains\_2}$), which means that local arrangements of the two assemblies of grains do not affect each other [67]. As is shown in Figure 4.13 (a) and (b), two situations are distinguished in this case: (1) *coarse grains dominant*, when the volume fraction of coarse particles is larger than the volume fraction of fine particles (y_1 >> y_2) and (2) *fine grains dominant*, in the opposite circumstance (y_1 << y_2) [72] [67].
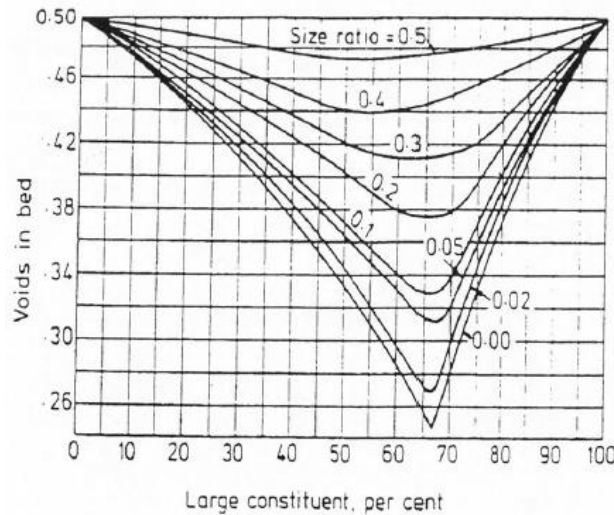
Figure 4.12. Typical binary packing results in terms of packing porosity [81].

Another (ideal) case depicted in Figure 4.13(c) regards binary mixtures of grains having similar diameters but different residual packing densities (*e.g.* grains have different shapes). In such a situation, the mixture is said to have total interaction and the overall packing density is given by the maximum between the residual packing densities of class 1 and 2. Binary mix with partial interaction refers to the case in which diameter$_{grains\_1}$ ≥ diameter$_{grains\_2}$. It is assumed that two interactions effects occur between the particles, namely *loosening effects* and *wall effects*, represented in Figure 4.13 (d) and (e), respectively. However, more complex models exist and these include other parameters, *e.g.* a so-called *wedging effect* (small particles entrapped in the gaps between the big particles instead of filling into the voids) [82]. The loosening effect happens when coarse grains (class 1) are dominant with the small grains filling the matrix of coarse particles. Hence, the porosity is locally increased due to not-filled voids created in the packing of class 1. In this case, in order to take into account the effect of the particle interactions, a so-called loosening effect coefficient is used, *e.g.* it is set equal to zero or one for the ideal cases of "no interaction" (Figure 4.13 (a) and (b)) and "total interaction" (Figure 4.13 (c)), respectively. When fine grains (class 2) are dominant, the wall effect takes place. The presence of some isolated coarse grains, indeed, increases the porosity in the vicinity of the contact zone with the sea of fine grains. In this second case, another coefficient called wall effect coefficient is used to introduce the particle interaction effect.
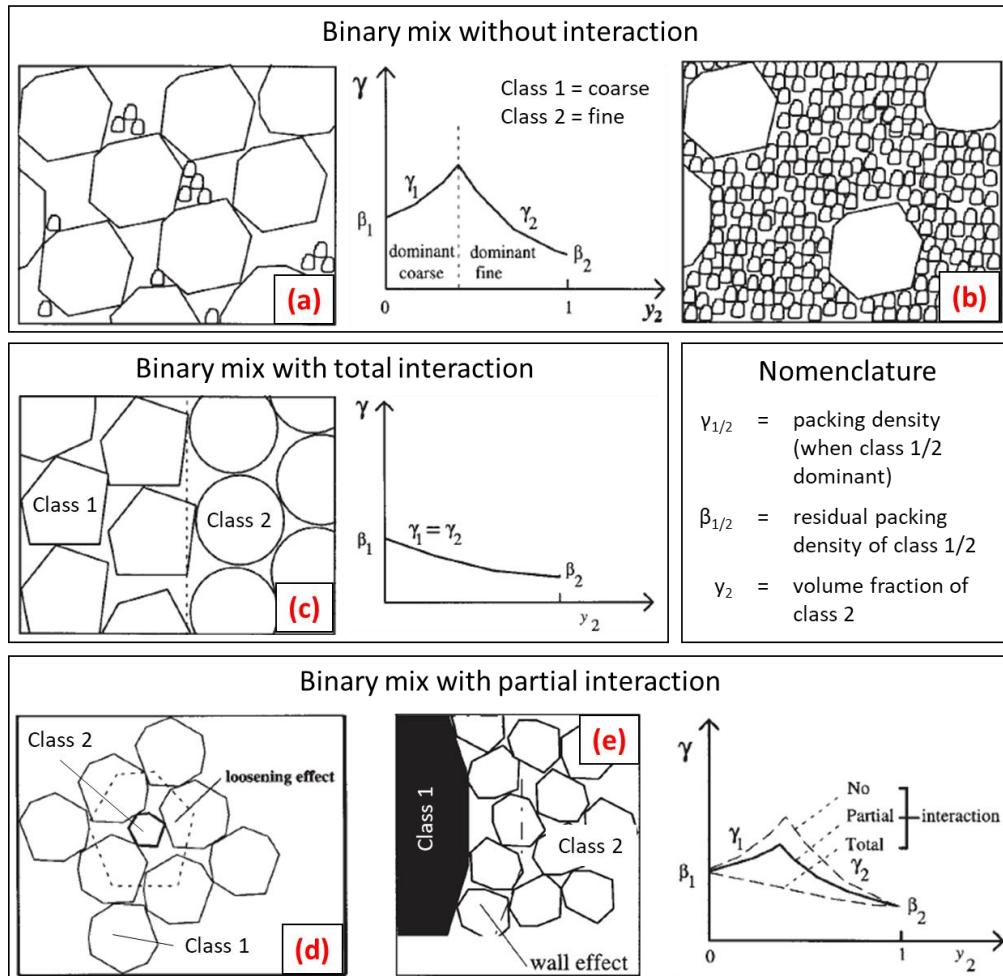
Figure 4.13. Binary mix without interaction: coarse grains dominant (a) and fine grains dominant (b). Binary mix with total interaction (c). Binary mix with partial interaction due to loosening effect (d) and wall effect (e) [67].

Toufar et al. (1976) [83] reported a model to calculate the packing density of binary mixtures of grains having a diameter ratio in the range of $0.22 < d_1/d_2 < 1.0$. The model included only the wall effect, but it has later been modified by *Goltermann et al.*, 1997 [84] to take into account the loosening effect as well. Multicomponent systems were also included in this model by assuming that any two components form a binary mixture [72], but the accuracy decreases with the number of size classes.

Referring to multicomponent systems, the *Linear Packing Density Model (LPDM)*, proposed by *Stovall et al.* (1986) [85], is able to predict the packing density for several particle classes. In order to create a more user-friendly application, LPDM was implemented in the so-called *4C-Packing* software by the Danish Technological Institute [86] to calculate the packing density by means of the "Eigen packing" concept. The latter refers to coefficients (μ-values) that, once properly calibrated, estimate the degree of packing in a unit volume for each individual aggregate fraction. The LPDM was later transformed into the solid suspension model (*de Larrard et al.*, 1994 [87]) and then, refined in the *compressible packing model (CPM)* [67]. This last offers the opportunity to consider the effect of the packing method by including a *compaction index (K)* in the calculation of the actual packing density from the virtual one.

The previous coefficient, indeed, depends on the compaction energy related to the packing method. For instance, K has an infinite value in case of the virtual packing density while, K = 4.1 for loose packing [67]. From Figure 4.14 (a) it is easy to understand that the LPDM is a particular case of CPM for which K → ∞.
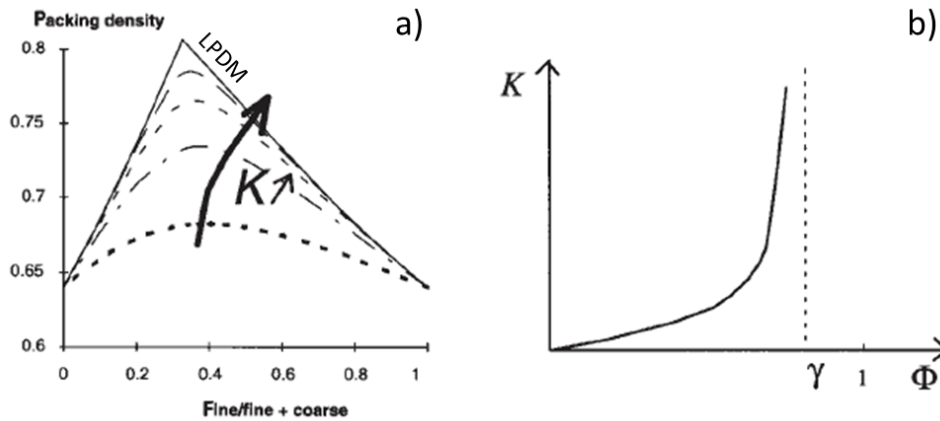

Figure 4.14. a) Packing density of binary mix of grains with a size ratio of 1/8 using the compressible packing model. Actual residual packing densities of the two classes are assumed to be equal to 0.64, and the different curves stand for low to high K values. b) Variation of compaction index (K) vs. Φ (actual solid volume) [67].

A comparison among the most common packing models, *i.e.* 4C, modified Toufar and CPM, is shown in Figure 4.15 together with experimental results for binary mixtures with the purpose of designing the proportions of concrete ingredients [66]. All theories confirm that there is a certain particle size distribution, given by an optimum proportion between fine and coarse particles, which maximizes the packing density.
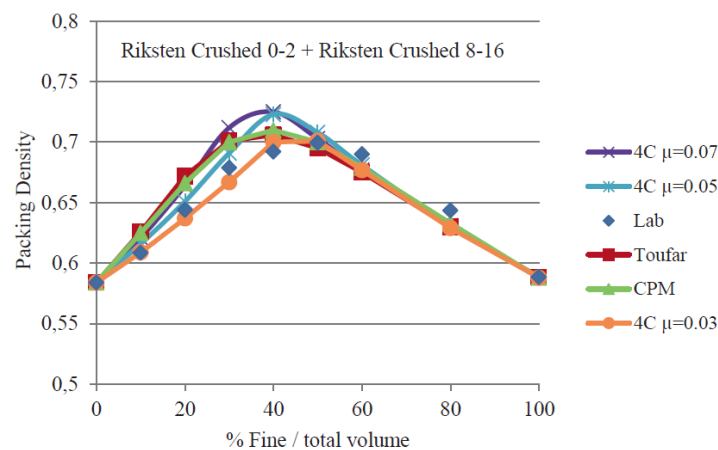
Figure 4.15. Loose packing density of a binary mix from Riksten quarry in Sweden, CPM (with K = 4.1), modified Toufar and 4C models (with three different µ values) vs. lab data [66].

Taking into account the inter-particle forces involved, coarse particles are dominated by the gravitation force and assumed to be non-cohesive while fine particles (d < 100 µm) are dominated by the van der Waal's force and assumed to be cohesive [81] [88]. Data in the literature confirmed that porosity increases for a decreasing particles size, as is shown in Figure 4.16 for the experimental results reported by *Yu et al*. (1970) on white fused alumina

powders [89]. Evidently, due to the generated agglomerations, bridging and arching, fine cohesive particles have different packing behavior from that of coarse particles. This behavior was described by *Feng* (1998) [90] by means of an equation that allows calculating the porosity by using the inter-particles force ratio between the van der Waal's force and the gravitation force.
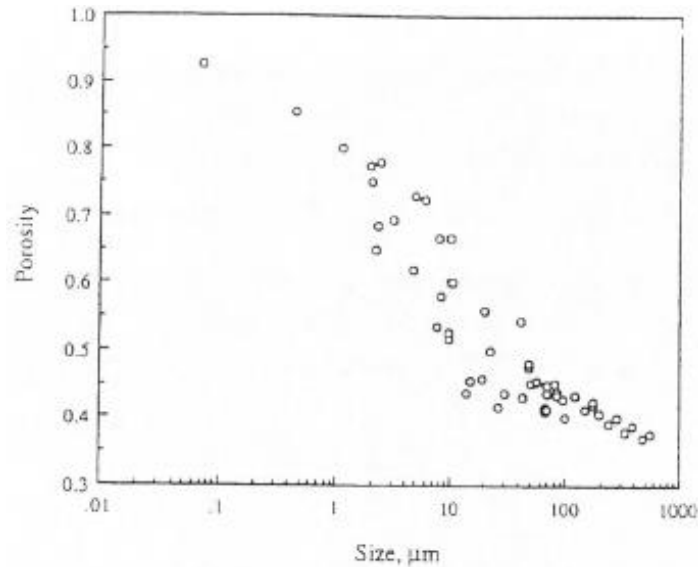
Figure 4.16. Experimental results of the porosity of packed white fused alumina powders as a function of mean particle size [89].

In one of its design phases, this project aims to apply the concepts described above to nano- and micrometer-sized particles (ranging in this case from 0.15 µm up to 5 µm) while evaluating a relation between particle size distribution and particle sealing properties of several dispersions. For this purpose, particles dispersed in water with different size distributions were tested in their ability of clogging single channels, using channel pressure and leak rate as performance parameters to compare different size dispersions (see Chapter 6).

5. Design Methodology/Design steps

The goal of this project is to design a thread compound that satisfies the functional and non-functional requirements, as discussed in Chapter 3. The engineering cycle is shown in Figure 5.1. It is important to clarify that both mechanical- and chemical-related knowledge is required for the development of a thread compound, *i.e.* from the synthesis of solid additives to the design of testing methodologies. Therefore, a research group was formed that, in addition to the supervisors and this PDEng position, included two master students with the aim of separately addressing the mechanical and chemical requirements. Since particle synthesis is covered by the resulting Master of science Thesis's [91] [92], it is not presented and discussed in detail in this report.
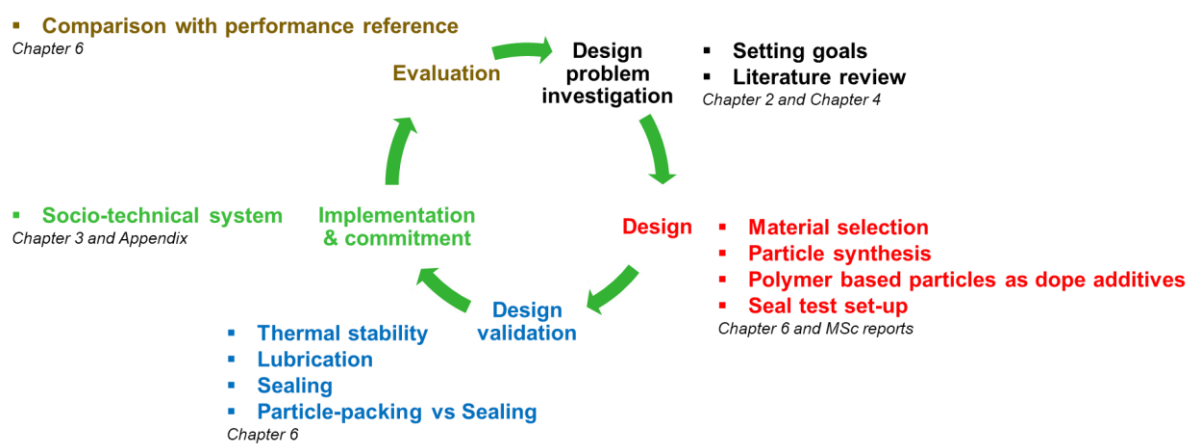
Figure 5.1. Engineering cycle followed during this design project.

The first phase of the engineering cycle relies on a detailed <u>problem investigation</u>, which mainly consisted of the identification of stakeholders, understating of the needs as well as exploring possible improvements of current designs. Meetings with both university and Shell supervisors played a key role at this stage. The stakeholders of this project were classified in three main categories, namely (1) customer (Shell), (2) external stakeholders (environment, connection thread suppliers, operators and competitors), and (3) supplier (University, Engineer and Chemist), as is shown in Appendix Figure D1. The literature review (Chapter 4) together with the supervisors supported the establishment of project requirements (Chapter 3) and goals (Chapter 2).

Based on the acquired knowledge, the <u>design</u> phase took into account the main aspects of the design issue, *i.e.* lubrication and sealing. Different materials were selected and polymer based particles were synthesized accordingly by various techniques [91] [92]. The synthesized particles were then dispersed in a base grease made of a mineral base oil and bentonite as thickener. Furthermore, particle size distributions were designed to evaluate and optimize their sealing capability. Lubrication performance was treated as a tribological system composed of two sliding and lubricated surfaces subjected to a specific contact stress, under certain environmental conditions. The sealing issue was addressed at the microscale assuming that the opening of leak paths in the metal-to-metal seal is the most relevant factor

to consider. Finally, lubrication and sealing test methodologies were established and designed, as is described in more detail in Chapter 6.

During the <u>design validation</u> phase, both testing methodologies and particle designs were validated as is described in Chapter 6. Several design parameters were considered for the validation of particle design, such as degradation temperature, coefficient of friction (COF), pressure and leakage flow rate. In order to evaluate the performance of the proposed replacements, tailored tests were developed at the University of Twente in the laboratories of the Materials Science and Technology of Polymers (MTP) and the Surface Technology and Tribology (OPMTR) groups.

The <u>implementation & commitment</u> phase for a thread compound is represented as is shown in Appendix Figure D1. However, the artefact was not implemented in the real (petroleum) world and, consequently, the <u>evaluation</u> phase was based on the results obtained by laboratory tests and the comparison with a performance reference.

6. Development phase

This chapter first proposes concept designs for alternative thread compound additives based on polymer particles, their preparation methods, characterization and performance in terms of lubrication. Next, a concept for the seal test and particle size distributions for effective clogging are presented, evaluated and discussed.

6.1 Polymer based particles as additives for yellow thread compounds

6.1.1 Concept of design

Considering the requirements of a thread compound provided in Chapter 3 and Chapter 4, two different particle systems seemed to be promising for the use as additives in thread compounds, namely solid polymer and hybrid core-shell particles. Their hardness can be tuned by changing parameters such as size, material composition, crosslink density, grafting density, etc. [93] [94]. Besides, depending on the particle composition, they can resist required high temperature ranges and due to their solid character and tunable diameters, they may also be suitable for sealing. Finally, the wide range of possibilities enables the selection of non-hazardous materials that can comply with the environmental requirements. Due to all these tunable properties, polymer and core-shell particles were considered possible alternatives to the toxic heavy metals.

Regarding polymer particles, the idea was to select three different materials having sufficient thermal stability and biodegradability as well as different hardnesses. Polyacrylamide (PAM), polystyrene (PS), and polydimethylsiloxane (PDMS) were the selected polymers. PS and PDMS have great differences in hardness values being PDMS much softer (30-80 shore A[c] [95]) than PS (90 Rockwell[c] R [96]), as is shown in Figure 6.1. PAM was taken into account as a reference considering that it is widely used in the oil and gas industry. All of them are thermally stable up to 250 °C but, while PAM and PDMS are considered biodegradable or environmentally inert [97], PS is not biodegradable.
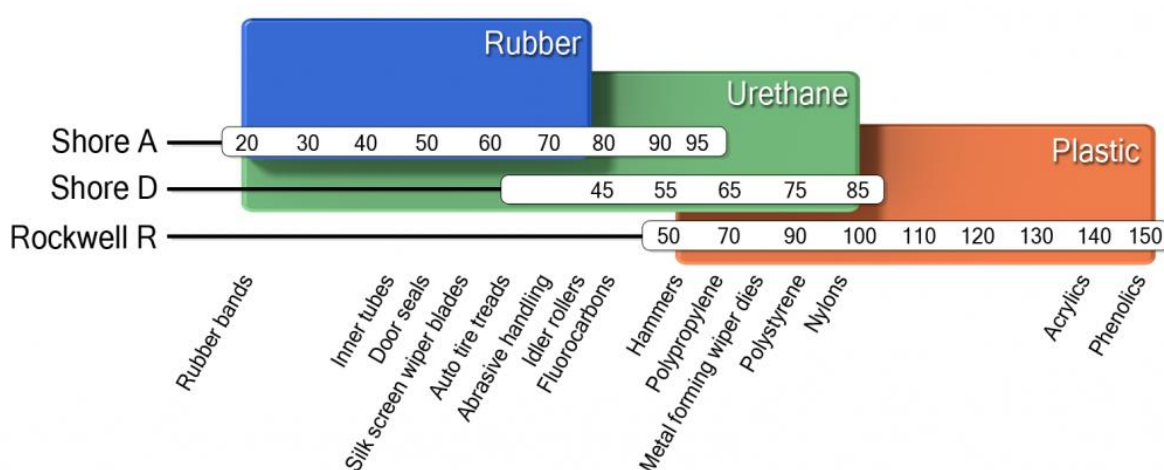

Figure 6.1. Hardness of polymers [96]

---

[c] Shore A hardness scale is chosen for rubber/elastomer such as PDMS while Rockwell hardness is generally used for 'harder' plastics such as polystyrene.

Instead, core-shell particles were selected due to the opportunity to combine the properties of a hard core resistant to high temperatures and extreme (contact) pressures, with the properties of a softer polymer shell, which surrounds the core and prevents its direct contact with the system substrate/coating. The shell was believed to be effective for lubrication while the core, with its high density, compressibility strength and melting point values, could fulfill the HPHT requirements needed for sealing. Furthermore, grafting polymer brushes reduces agglomeration of nanoparticles, which is believed to be favorable for their lubricating performance as well [42]. In this case, TiO_2 hybrid core-shell particles were synthetized by grafting poly(butyl acrylate) (PBA) or Poly(methyl methacrylate) (PMMA) brushes from the initial TiO_2 particles. As mentioned in the literature review (see Section 4.1.4), TiO_2 was selected due to its high availability and because it is a well-known lubricant additive as well as for its promising mechanical properties. Indeed, TiO_2 has a density that is about 4 times higher than polymers such as PS ($1.04 - 1.065$ g/cm^3) or PMMA (1.190 g/cm^3) [98] and a compressibility strength of 680 MPa [99] against 83 MPa for PS or 83-124 Mpa for PMMA [98]. Furthermore, TiO_2 nanoparticles have a melting point equal to 1.843 °C [99], which is definitely larger than the set operation limit of 250 °C (see Chapter 3). On the other hand, the high hardness value (880 HV 0.5 [99]) of TiO_2 may lead to surface damage of the connections during both make-up phase and micro sliding. This justifies the choice of grafting a soft polymer (PMMA) shell surrounding the hard core (TiO_2). Finally, its use does not create particular environmental concerns and, therefore, it is considered as a "green" alternative for heavy metals.

6.1.2   Material and methods for (hybrid) polymer particle preparation

The particles were synthesized by E. Ispirogullari [91] and J. Spanjers [92] who conducted their Master of Science projects as a part of the Shell consortium in support of this particular PDENG project. Below some brief details are presented. For the details, reference is made to the corresponding master thesis reports [91] [92].

Materials used for solid polymer particle preparation. Divinyl benzene (DVB) 80% technical grade, p-xylene 99% anhydrous, polyvinylpyrrolidone (PVP) with an average molecular weight of 40.000 g/mol, styrene 99%, acrylamide 98% GC grade, poly(vinyl methyl ether) (PVME) 50% solution in water, ammonium persulfate (APS), ethylene glycol dimethacrylate (EGDMA) 98%, potassium persulfate (KPS) 99%, butyl methacrylate (BMA) 99% and 5.0 M sodium chloride (NaCl) solution were purchased from Sigma Aldrich (St. Louis, MO, USA). α,α'-azoisobutyronitrile (AIBN) 98% and calcium chloride (CaCl2) were purchased from Merck (Darmstadt, Germany). 2-propanol (IPA) 98% GC grade, methanol (MeOH) 98% GC grade, chloroform 98% GC grade and acetone 99% GC grade were purchased from Biosolve (Valkenswaard, the Netherlands). Sodium dodecyl sulfate (SDS) 98% was purchased from Fluka (Seelze, Germany). Monomethacryloxypropyl terminated polydimethylsiloxane (MCR-M11) with an average molecular weight of 1000 g/mol and methacryloxypropyl terminated polydimethylsiloxane (DMS-R11) with a molecular weight of 1200 g/mol were purchased from Gelest (Morrisville, PA, USA). Milli-Q water was produced by a Millipore Synergy system (Billireca, MA, USA). All the chemicals were used as received.

Materials used for hybrid core-shell particle preparation. Dopamine hydrochloride, tris buffered saline, n-butyl acrylate (BA), methyl methacrylate (MMA), triethylamine (99%) (TEA), tris(2-pyridiylmethyl)amine (TPMA), α-bromoisobutyryl bromide (BiBB), ethyl α-bromoisobutyrate (EBiB) and copper wire (99.999%) were purchased from Sigma-Aldrich. TiO_2 particles (mixed phase anatase/rutile, d~300 nm, S_{BET} = 16.66 m^2/g) were donated by Artecs B.V. (Hengelo, The Netherlands). Monomers were passed through a column of basic alumina to remove inhibitors. Cu wire was cleaned in a mixture of hydrochloric acid (HCl))/methanol (MeOH) (1:4 v/v) for 20 min, rinsed with ethanol and dried under stream of air directly before use. Other materials were used as received. Solvents were of analytical grade and supplied by Sigma-Aldrich or Biosolve (Valkenswaard, The Netherlands).

Methods. Polyacrylamide (PAM), crosslinked PAM and highly crosslinked polystyrene (PS) particles were synthesized by dispersion polymerization reactions. Instead, PS, crosslinked PS and polydimethylsiloxane (PDMS) spheres were synthesized with emulsion polymerization. PDMS particles were also obtained by grinding bulk PDMS gel produced using AIBN. More details about the preparation methods of the polymer particles are presented in [91]. The synthesis of the hybrid core-shell particles was based on three main steps, *i.e. i)* coating of TiO_2- NPs (diameter 300 nm) with polydopamine (TiO_2-PDA), *ii)* subsequently derivation with an ATRP initiator (TiO_2-PDA-BiB) and *iii)* followed by the surface-initiated SARA ATRP. In the last step, poly(methyl methacrylate) (PMMA) or poly(butyl acrylate) (PBA) were grafted from the PDA-modified TiO_2 in DMF at room temperature via supplemental activator reducing agent atom transfer radical polymerization (SARA-ATRP). Hybrid core-shell particles with high organic contents (40–88 wt%) and grafting densities (0.16–0.25 chains nm^{-2}) were obtained, as is discussed in more detail in [92] and [100].

Thread compound preparation. Shell provided three different base greases whose lubrication performances and thermal stability were evaluated. These greases are shown in Table 6.1. From Table 6.1 it is clear that the main differences in composition are the different values of base oil viscosity (especially for base grease_1) and that different types of thickener were used. For reasons of confidentiality no additional information was provided by Shell.

Table 6.1. Base greases provided by Shell.

Base grease	Base oil	Base oil kinematic viscosity (cSt @40 °C)	Thickener
Base grease_1	Mineral oil	900 – 1000	Bentonite
Base grease_2	Mineral oil	120 - 140	Li complex
Base grease_3	Mineral oil	90 – 100	Al complex

Among the three base greases shown in Table 6.1, base grease_1 was the best in terms of both thermal stability and pin-on-disc results, as is shown in the Appendix E. Therefore, base grease_1 was used during the course of this project. The compositions of the thread compounds prepared are shown in Table 6.2. The required range of weight percentage of additives to obtain the overall thread compound composition was suggested by Shell. Polymer particles were directly added to the base grease_1 and mixed by hand. Instead, in

order to disperse the particles grafted with the polymers (core-shell particles), base grease_1 was sonicated for 30 minutes along with a mixture of grafted particles in THF. The tribological tests were executed the following day to allow the THF to evaporate overnight under ambient conditions.

Table 6.2. Composition of the thread compound composed of base grease_1 and the synthesized additives used for lubrication tests.

Component	wt% with polymer particles	wt% with TiO₂ based particles	Description
Base oil	64.78	64.78 – 74.78	Mineral oil (900 – 1000 cSt @40 °C)
Thickener	4.95	4.95	Bentonite
Anti-oxidant	0.27	0.27	Undisclosed
Additives	30	20 - 30	Polymer / Core-shell particles

6.1.3 Evaluation methods/experimental methods

Thermal analysis. Considering that it was not possible to test lubrication and sealing at high temperatures, the thermal stability in terms of weight loss was used as a parameter to evaluate the temperature-related performance of the additives. A Shimadzu GC-14 (Kyoto, Japan) oven in a nitrogen environment was used to measure the isothermal weight loss (T = 250 °C for 66 hour) of the three provided base greases (see Appendix Table E1) and thread compounds with polymer particles. American Petroleum Institute (API) modified (ISO 13678:2010, Jet-Lube, USA) thread compound was tested as well since it represents a standard for pipe dope and could be used as a reference. Instead, the weight loss of hybrid core-shell particles was measured using a Pyris 1 thermogravimeter (PerkinElmer, USA) in the range from 40 °C till 600 °C in steps of 15 °C/min, under a nitrogen-flow. Compared to the polymer particles, core-shell particles were not dispersed in the thread compound during the thermal test. The change in procedure was required due to the difference between the two particle systems.

Lubrication. Lubrication performance was evaluated by means of pin-on-disc tests following the same testing methodology used by *Ernens et al.* [17]. The tests were performed on a UMT Tribolab tribometer (Bruker, USA) in the laboratories of the University of Twente. The characteristics of ball and disc together with the parameters used for the tribo-tests are given in Figure 6.2 while the chemical composition of the two steel materials is shown in Table 6.3. The assumptions for the choice of these parameters were set to obtain a contact stress, which is assumed to be similar to the MTM-seal contact stress, *i.e.* 1 GPa. By controlling the vertical load and measuring the friction force, the machine automatically calculates the COF. The tests were repeated three times for each specimen and the results were averaged to obtain a single curve of the COF. Before each tests, disk and ball were cleaned with isopropanol and sonicated for 15 minutes. In total, three discs (7x7x2 cm each) were used, two for the polymer particles and one for the core-shell particles. The ball was changed after every measurement. The grease was applied by means of a cotton stick on both disc and ball surfaces to cover the contact area. The test was performed at ambient temperature.
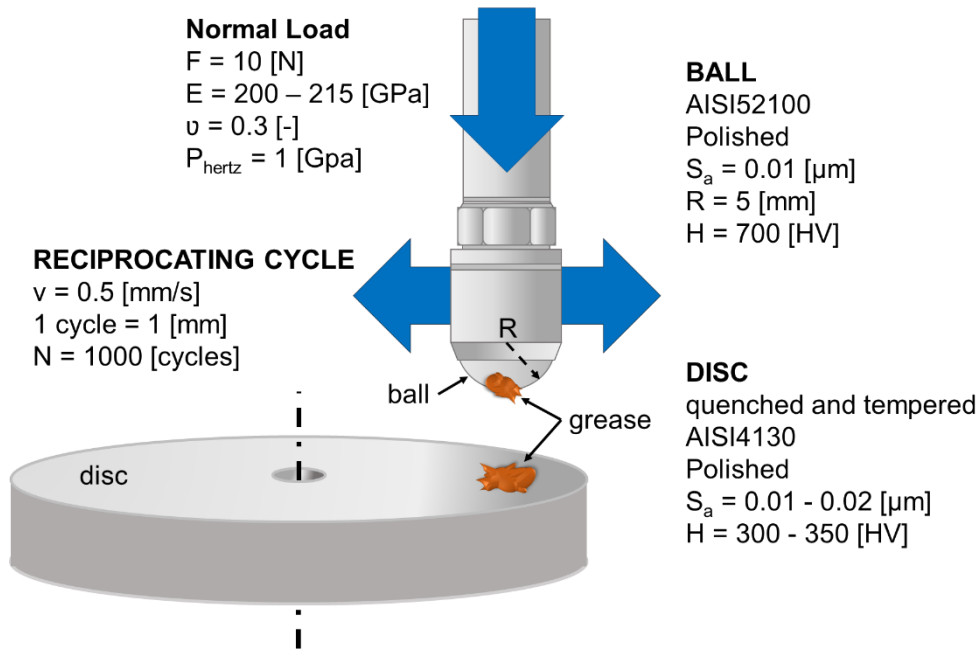
Figure 6.2. Schematic view and parameters of the reciprocating pin-on-disc.

Table 6.3. Chemical composition of ball and disc used in pin-on-disc experiments.

	Chemical composition (%)						
	C	Si	Mn	P	S	Cr	Mo
AISI4130	0.28 − 0.33	0.15 − 0.35	0.40 − 0.60	≤ 0.035	≤ 0.04	0.80 − 1.10	0.15 − 0.25
AISI52100	0.95 − 1.10	0.15 − 0.30	≤ 0.25	≤ 0.03	≤ 0.025	1.30 − 1.60	-

Microscopy. A VK-9700 confocal microscope and the accompanying software VK analyzer (Keyence, Japan) were used to determine depth and width of the wear scars after pin-on-disc tests. Images of the scars on the discs were obtained with 20x magnification and characterized using the software. We assumed that most of the damage was on the disc due to its lower hardness in comparison with the ball (see Figure 6.2). The analysis procedure to follow was suggested by Shell and it relied on the removal of the tilt from the image (3 point plate method) as a first step. Subsequently, the scars depth was measured by considering three sections of the scratches perpendicular to the sliding direction (equal to the main length of the scar) and analyzing the average profile over the three measurements. Particular attention was given not to consider the polishing lines in the calculation. The wear scar depth was selected as the height difference of the disc surface and the deepest point of the scar. The scar width, instead, was evaluated measuring the distance between two points lying on the same plane, along the direction perpendicular to the sliding direction.

Others. FTIR spectroscopy was performed on an Alpha FTIR spectrometer (Bruker, USA). Scanning electron microscopy (SEM) images were recorded on a JSM6330F microscope (JEOL, Japan). The hydrodynamic particle size was measured on a Zetasizer Nano ZS (Perkin Elmer Inc., USA). This device uses a 4mW 633nm laser and measures the backscattering at an angle of 173°. A delay time of 60 seconds after sample insertion was used for each measurement. The particles were loaded in disposable containers in water. Gel permeation chromatography (GPC) was performed on a Waters system (pump: Waters 515, USA, injector: Hewlett-Packard 1050 USA, detector: Waters 2414 and Waters Styragel HR3-6 columns) at 50 °C with DMF 50mM LiCl as eluent (1 mL/min). Polymer molar masses were calculated using linear polystyrene standards for PBA or PMMA standards for PMMA.

6.1.4 Results and discussion for the thread compound performance

The synthetized solid polymer particles and their size are listed in Table 6.4 while the prepared hybrid core-shell particles are listed in Table 6.5. The particles sizes shown in Table 6.4 were obtained from DLS measurements. The sample compositions are all based on base grease_1 and are explained as follows:

- PAM and PAM_CR samples refer to thread compounds containing PAM and crosslinked PAM particles, respectively.
- PS_MM indicates that the thread compound contains highly crosslinked PS microbeads while thread compounds PS and PS_CR contain submicron PS particles and submicron crosslinked particles, respectively.
- PDMS_GEL thread compounds contain gelled PDMS particles while thread compounds PDMS and PDMS_CR contain PDMS and crosslinked PDMS particles, respectively.
- TiO2 indicates thread compounds containing bare titanium dioxide particles (d~300 nm).
- PMMA-40 and PMMA-88 samples contain hybrid core-shell TiO_2 particles obtained by grafting PMMA with 40 and 88 wt % organic content, respectively.
- PBA-40 stands for thread compounds prepared by grafting PBA from PDA-modified TiO_2 particles with a 40 wt % organic content.

Note that all the samples in Table 6.5 were grafted from the same TiO_2 particles (d~300 nm).

Table 6.4. Type and size of polymer particles selected for lubrication tests [91]. The particles sizes shown in the table were obtained from DLS measurements of diluted particle dispersions in water since particle fusion during drying made it impossible to get a particle size count from SEM images for some of the samples.

Sample name	Polymer	Crosslinked	Particle size (nm)	Standard deviation (nm)
PAM	PAM		106	14
PAM_CR	PAM	✓	180	61
PS_MM	PS	✓	1950	227
PS	PS		112	8
PS_CR	PS	✓	131	23
PDMS_GEL	PDMS	✓	46000	45980
PDMS	PDMS		133	58
PDMS_CR	PDMS	✓	198	89

Table 6.5. Core-shell particles used for lubrication tests [92] [100]. Bare TiO_2 particles (300 nm) without polymer shell (sample name TiO2) were tested as a comparison.

Sample name	Polymer	Organic content (TGA)	M_n(g/mol)[d]	M_w/M_n
TiO2	-	-	-	-
PMMA-40	PMMA	0.42	100,700	1.23
PMMA-88	PMMA	0.88	1,108,000	1.23
PBA-40	PBA	0.4	116,000	1.13

The results from the thermal analysis of the polymer particles in the thread compound, the API dope and base grease_1 are shown in Table 6.6. In order to evaluate only the weight loss ascribed to the grease, the weight loss percentages of the thread compounds were normalized to the base grease_1 weight percentage, assuming that the particles added to base grease_1 did not decompose during the thermal stability test. The high weight loss value of the API dope was not expected since the presence of metals in its composition (see Table 4.2) should not catalyze the oxidation reactions in the absence of oxygen (the thermal tests were performed in nitrogen environment). However, the reproducible high weight loss percentage obtained for the API dope could not be explained. Particularly, considering that the percentage of solids of the API dope is around 60 wt % (Table 4.2), a maximum value around 40 wt % loss was expected from the thermal analysis result of this pipe dope. The good thermal performance of base grease_1 in comparison with the other two base greases (see Appendix Table E1) is attributed to the different dropping points of the grease containing bentonite from those having Li or Al complex soaps. Indeed, the base oil bleeds from the thickener matrix once a certain temperature (dropping point) is reached, causing higher

---

[d] Analytically calculated assuming the same value of grafting density of the reactions with sacrificial initiator [92] [100].

weight loss in greases having lower dropping point [101]. Further information on the composition of the grease was not shared and, therefore, a detailed comparison was not possible. Evidently, crosslinking had a positive effect on the thermal stability of polystyrene considering the notable weight loss difference of PS_CR and PS_MM thread compound compare to PS samples. Furthermore, the particle size did not seem to affect the thermal stability of PS particles. Finally, while PDMS and PDMS_CR thread compounds showed a good performance, PAM, PAM_CR and PDMS_GEL samples had the highest weight-loss percentage. In addition, FTIR analysis performed before and after the thermal tests (the data is reported in [91]) confirmed that the addition of polymer particles to the thread compound does not present any particular problem and, therefore, the analyzed compounds are promising for further evaluation.

Table 6.6. Weight loss percentages of thread compounds with synthesized polymer additives in comparison with their base grease (base grease_1) and the performance reference (API dope, highlighted in yellow). Experimental conditions: oven, 250 °C, 55 hours, nitrogen environment.

Sample name	Weight loss (%)	Weight loss (%) normalized to base grease_1
API dope	83.9	
Base grease_1		38.5
PAM	53.8	69.1
PAM_CR	51.0	75.2
PS_MM	27.7	38.4
PS	40.0	49.8
PS_CR	29.7	39.5
PDMS_GEL	45.6	60.0
PDMS	24.1	39.5
PDMS_CR	30.2	47.2

The TGA results for the hybrid core-shell particles are shown in Figure 6.3. From Figure 6.3 it is obvious that at the temperature requirement for the MTM seal *i.e.* 250 °C (vertical dashed line), PBA-40 (blue line in the graph on the left) had less than 5 % weight-loss percentage. Instead, PMMA-40 (blue line in the graph on the right) and PMMA-88 (green line in the graph on the right) had values of around 95 % and 88 %, respectively. Since the weight loss percentage for this system is ascribed to the presence of the polymer shell, enough organic material around the TiO_2 particles would be still present at the selected temperature. However, the testing conditions used to evaluate the thermal stability of hybrid core-shell particles were not isothermal as is the case for the polymer particles. Therefore, a higher thermal degradation of the polymer brush is to be expected from thermal tests performed for a longer time. Nevertheless, the titanium oxide core would in principle still be suitable to ensure the required sealing performance while any remaining organic material at high temperatures would reduce the surface damage of the connections under (axial) micro sliding.
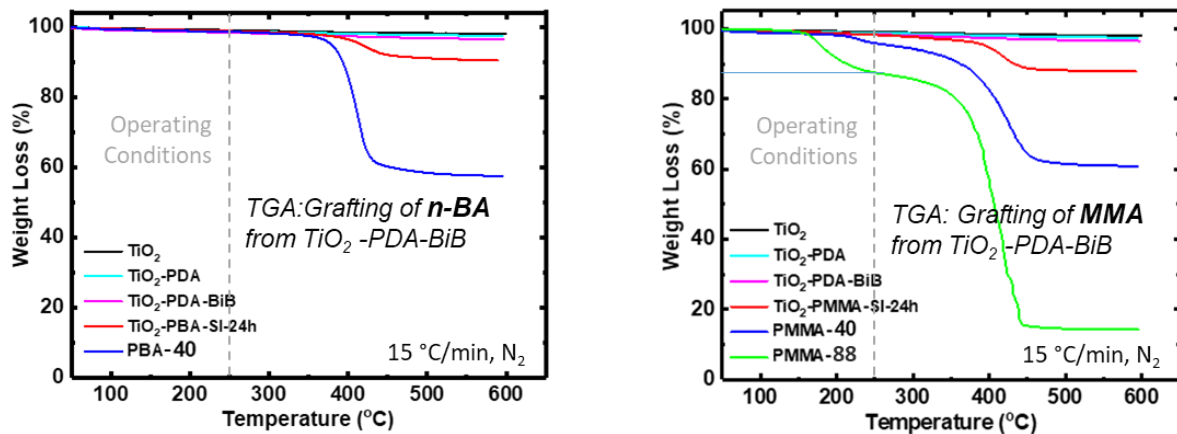
Figure 6.3. Thermograms (TGA) from 40 °C till 600 °C in steps of 15 °C/min (under a nitrogen-flow) of PBA-40 (left), PMMA-40 and PMMA-88 (right). Note that the other curves refer to the bare TiO$_2$ particles other steps of the synthesis, such as deposition of a thin PDA layer, immobilization of the ATRP initiator (BiB) and reaction with the sacrificial initiator. The grey vertical dashed line indicates 250 °C [92] [100].

The results from the pin-on-disc tests of polymer particles are given in Figure 6.4 (initial phase of the test) and in Figure 6.5 (last 10 minutes). In Figure 6.5 it is shown that the COF curves of base grease_1 and the reference API dope containing heavy-metal particles have similar steady states. Hence, the positive effect of the boundary film formed by the bentonite thickener (base grease_1) had comparable lubrication performance to the tribolayer composed of a matrix of heavy metals and graphite (API dope). Figure 6.4 shows that most of the lubricants reach a stable value of the COF after 50 seconds with PS thread compounds as an exception, for these it took around 140 seconds to stabilize. Overall PS_CR thread compounds had the worst performance. The difference in running-in times depends on the mechanisms involved in the formation of the tribolayer, whose presence between the sliding surfaces is necessary to prevent surface damage and decrease friction. The bad performance of PS_CR was explained with the typical increase in hardness due to crosslinking agents [102]. The last 10 minutes of the tests (Figure 6.5) were assumed as steady-state conditions for all the lubricants. In general, all the tested thread compounds showed comparable performance with base grease_1 and slightly better than API dope. The exception was PS_CR probably due to the increased hardness of the crosslinked particles compared to non-crosslinked particles (PS).
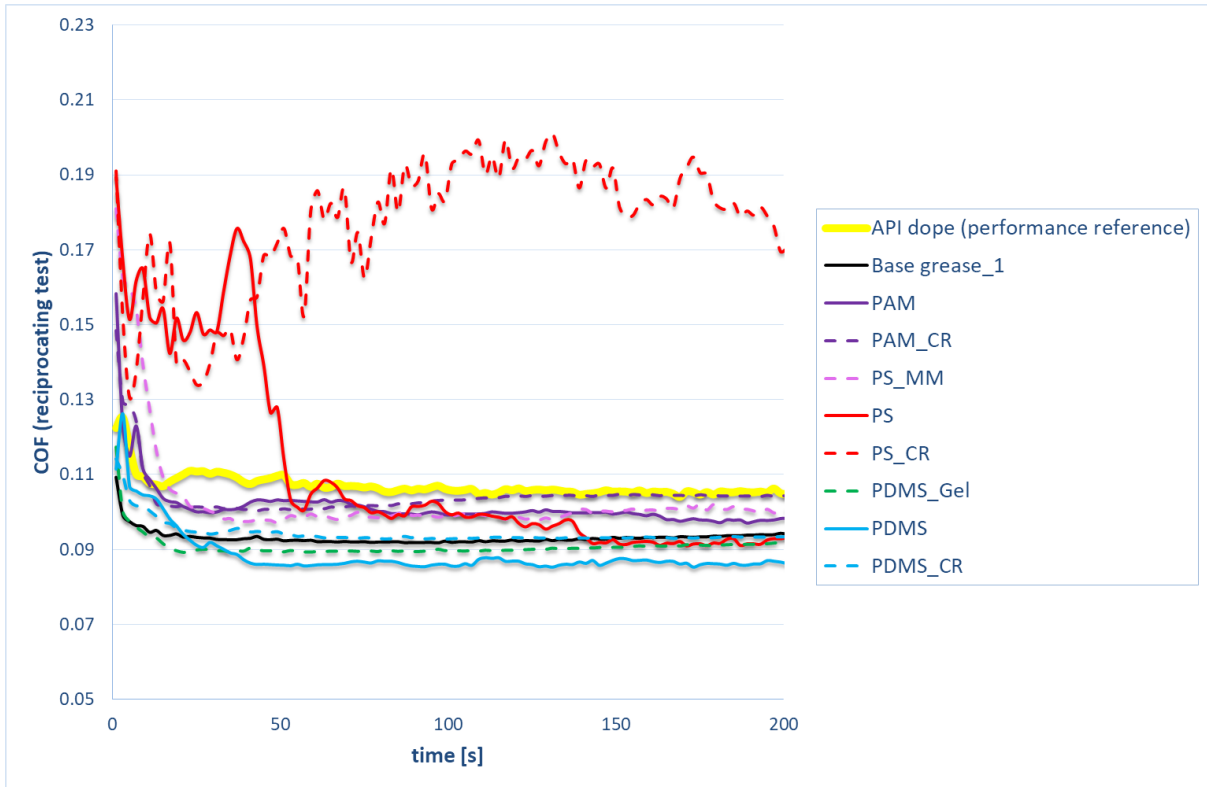
Figure 6.4. COF vs time (first 200 seconds of tests) for polymer particles in comparison with their base grease (base grease_1) and the performance reference (API dope, in yellow).
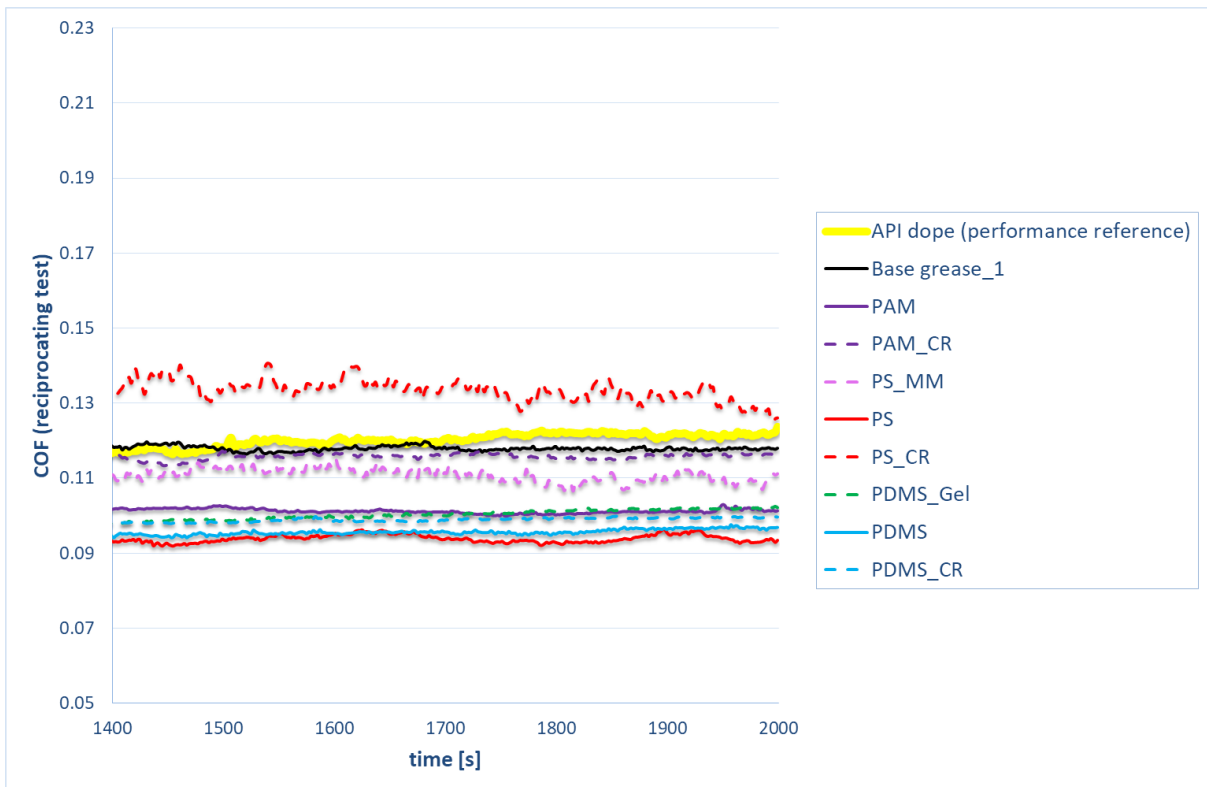

Figure 6.5. COF vs time (last 10 minutes of tests) for polymer particles in comparison with their base grease (base grease_1) and the performance reference (API dope, in yellow).

44

For TiO$_2$ particles and corresponding core-shell particles both initial (Figure 6.6) and final phase (Figure 6.7) of the tests clearly shows the positive effect of grafting polymer to TiO$_2$ on reducing the friction. Indeed, compared to the thread compound prepared with base grease_1 and bare TiO$_2$ particles, the samples containing the hybrid core-shell systems showed a lower coefficient of friction. Referring to the type of polymer, the PMMA shell resulted in positive impact on the lubrication performance. Particularly, a higher amount of organic content in the particles led to further benefits (PMMA-88 vs PMMA-40), probably due to the viscoelastic properties [103] of thicker brushes. However, further analysis of the wear scars was needed to prove that both polymer and core-shell particles could be suitable candidate for lubrication during micro sliding.

Scar depth and width were taken as the two main parameter to evaluate the surface damage after the pin-on-disk tests. Clearly, the worst case occurred when the two sliding surfaces were in direct contact, leading to cold welding and subsequently galling [104]. Assuming that the performance of the base grease_1 was good because it is comparable with API dope (Figure E1 and Figure E2 in Appendix), the goal of this further analysis was to evaluate whether the particles increased or not the surface damage during micro sliding in comparison with their own base grease. As explained in Chapter 4, the micro sliding of the connections is related to the opening of leak paths. Therefore, an evaluation of the wear scars in terms of width and depth values may help to evaluate the most promising particles, *i.e.* those that do not excessively damage the metal surfaces. The scar width and depth values of all the thread compounds prepared in this project are shown in Figure 6.8. Here API dope and base grease_1 serve as reference values. The corresponding confocal microscope images are shown in Appendix Figure E4.
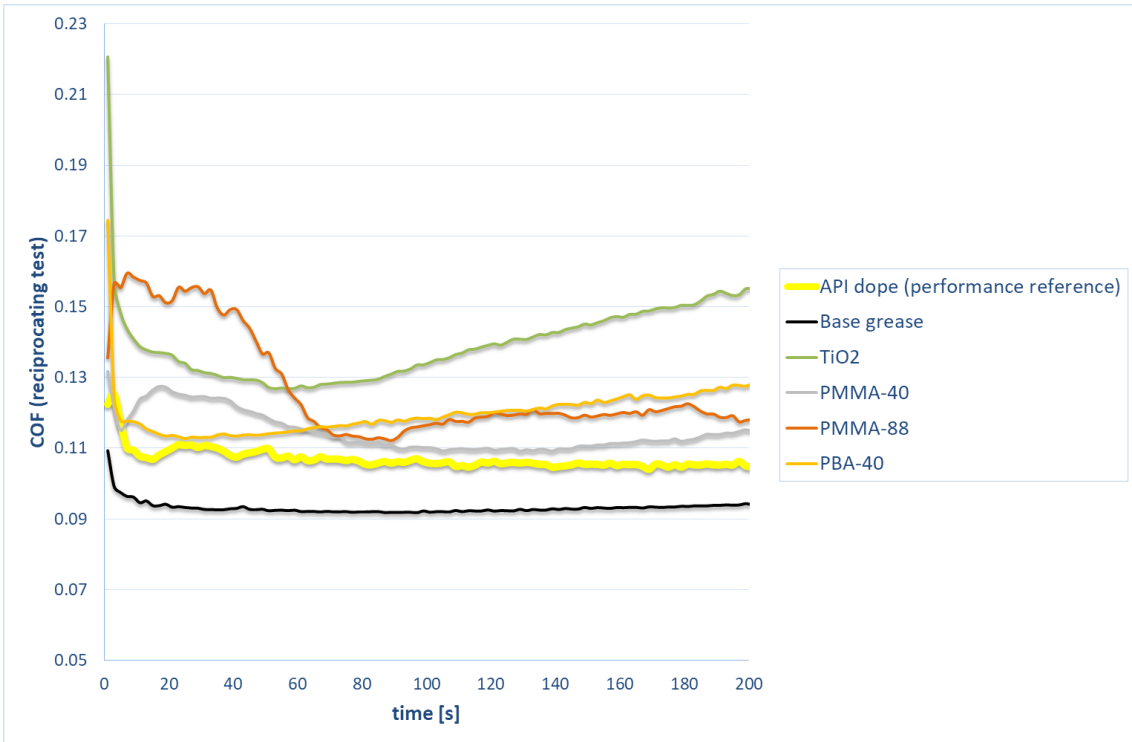
Figure 6.6. COF vs time (first 200 seconds of tests) for bare TiO2 particles and hybrid core-shell particles in comparison with their base grease (base grease_1) and the performance reference (API dope, in yellow).
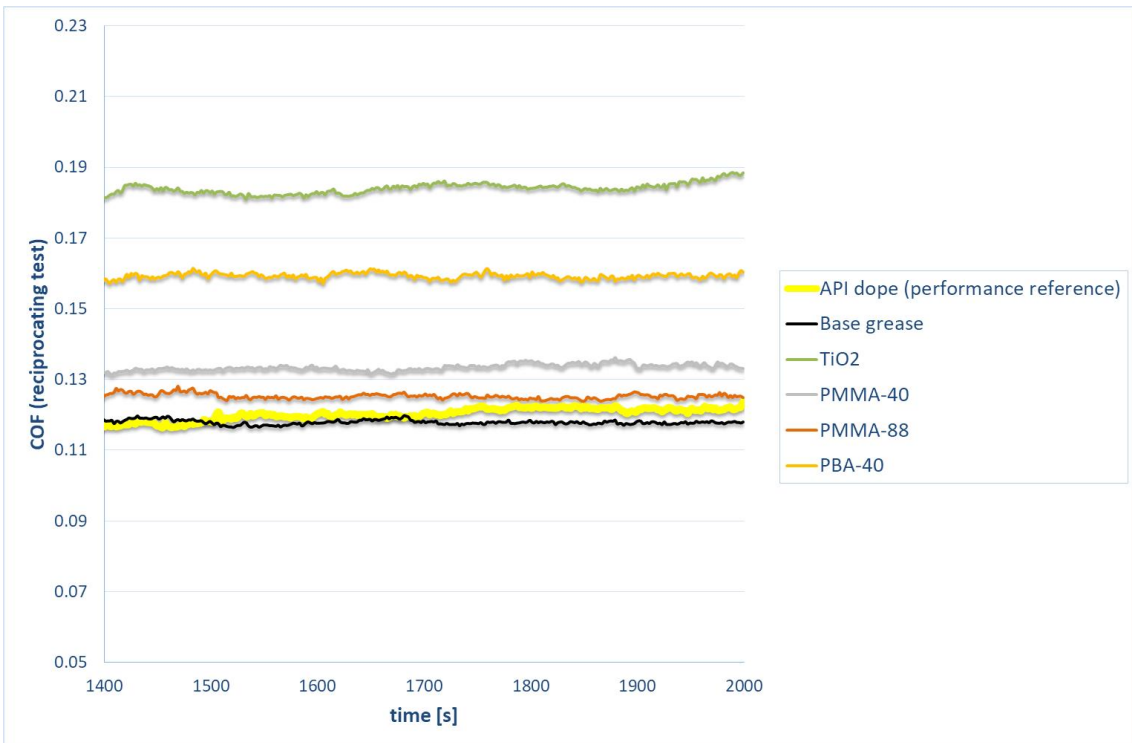

Figure 6.7. COF vs time (last 10 minutes of tests) for bare TiO2 particles and hybrid core-shell particles in comparison with their base grease (base grease_1) and the performance reference (API dope, in yellow).
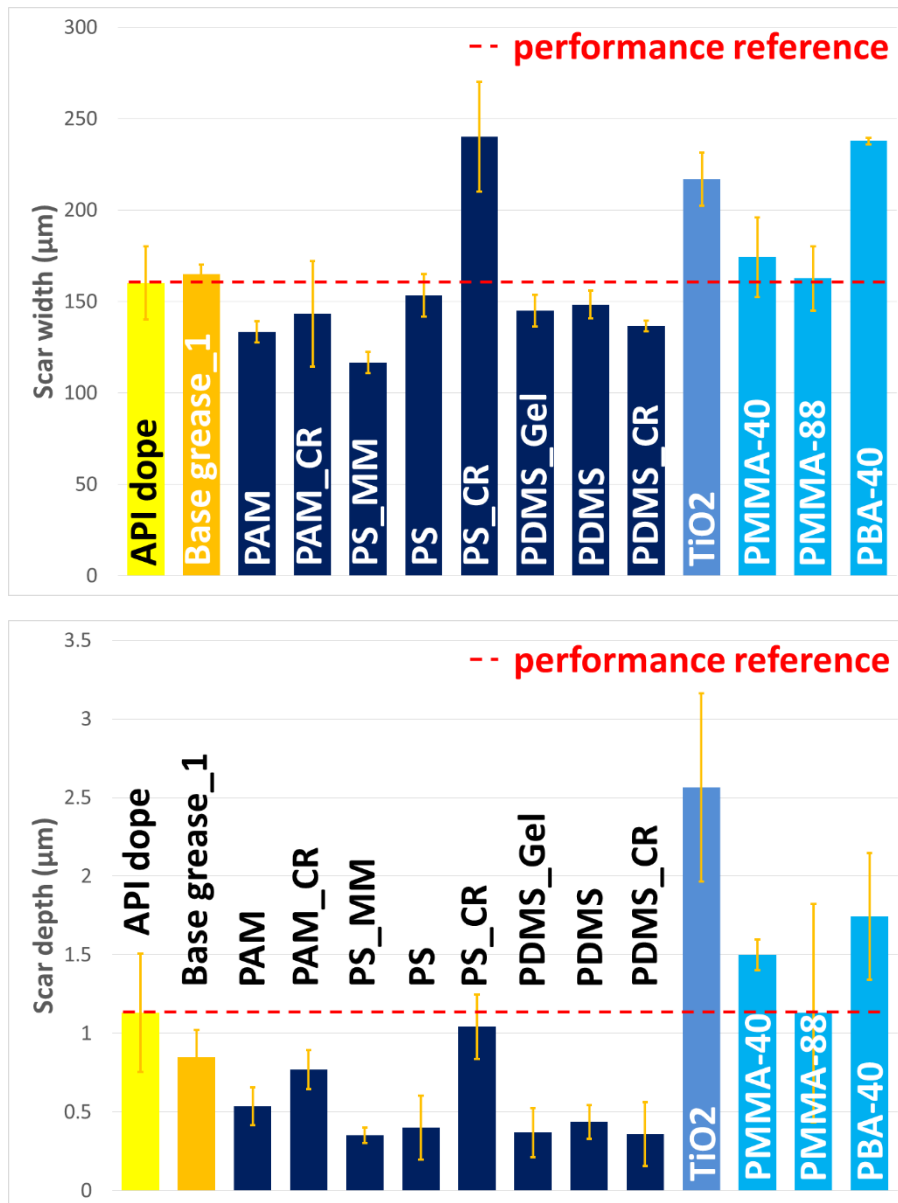
Figure 6.8. Scar width (previous page) and depth (above) as calculated from confocal microscope images for Base grease_1, API dope (performance reference in yellow and red dashed line), polymer particles (dark blue) and core-shell particles (light blue). The error bars indicate the standard deviation (n=3).

Figure 6.8 shows that, among polymers (dark blue in the figure), only PS_CR has much higher amount of damage than the base grease alone. The increase of hardness due to crosslinking creates an abrasive effect on the surface, as shown in Appendix Figure E4. On the other hand, it is worth noting that grafting PMMA from TiO$_2$ particles modified with PDA helps in reducing both scar width and depth compared to bare TiO$_2$ particles. As confirmed by the COF values, it can be said that the higher the amount of organic content, the better the lubrication performance. The agglomeration of PBA-40 particles due to stronger cohesive forces among particles may be the reason behind their worse lubricating behavior. Referring to wear scar images (Appendix E) and taking the scar image of the base grease_1 as a reference, it can be

seen that the boundary film created by the bentonite thickener was strongly compromised only in the case of PS_CR and TiO$_2$. However, we can not say that the particles improved the already good performance of the base grease. Nevertheless, the observed damage may be acceptable during a single make-up phase. Finally, the possibility to improve the chemistry of particles makes PDMS and PMMA-88 two promising solutions to consider for further investigations. Particularly, ATRP is a versatile tool, which allows the grafting of different polymers from (or to) different core materials. Using particles that do not damage the surfaces during make-up enables the design of particles for sealing. However, further analysis should investigate the impact of the lower thermal stability of PMMA-88 on sealing.

6.2 Seal test set-up

6.2.1 Concept of design

In this section, the design of both additives for sealing and a seal test set-up at the microscale (with the corresponding methodology) are discussed. The design of additives to increase the sealing performance of the thread compound relies on the concepts described in Chapter 4 about particle-packing theories. Figure 6.9 clarifies the concept in the case of binary mixtures.
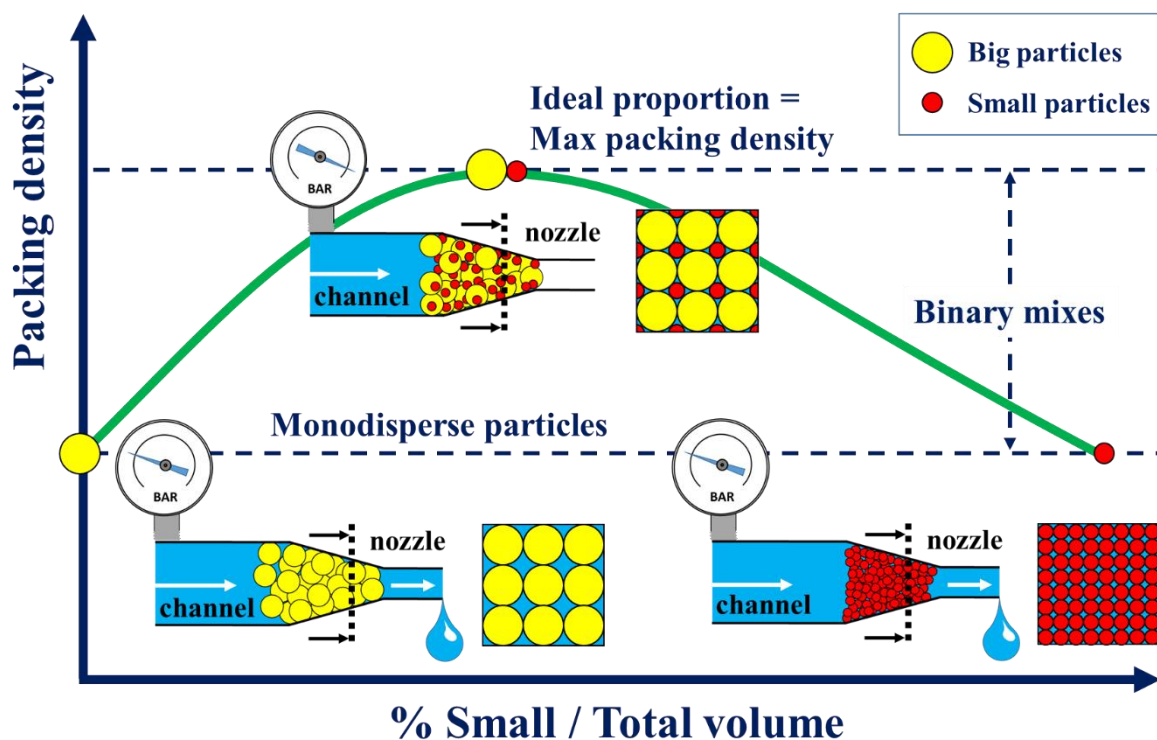

Figure 6.9. Concept of particles design for sealing in the case of binary mixtures: prediction of the relation between particle-packing density and leakage. Note that, ideally, the packing density does not change by changing particle size (horizontal line associated with monodisperse particles). However, several authors reported that nanoparticles have a lower packing density due to agglomeration, as discussed in the literature review. Nevertheless, the mixing of both nano and microparticles should lead to an increase in packing density.

At both x = 0 % (only big particles) and x = 100 % (only small particles), the packing density is lower compared to the case of 0 < x < 100 % (small and big particles mixed in a certain proportion). Particles proportions were established based on the data from the literature to develop an optimum particle size distribution that maximizes the packing density of the particles. In turn, the increased packing density should have led to a reduction of leakage flow due to the decreased volume between the bed of particles inside the microchannel. For instance, monodisperse particle distributions were expected to give a lower sealability (and resist lower pressure) than polydisperse particle distribution. It is important to mention that particles having different sizes and narrow distributions were needed to test the sealing performance of monodisperse particles in comparison with model particle size distributions. For this reason, standard polystyrene (sPS) particles were purchased with four different particle sizes with a small standard deviation. The particle sizes were selected according to the fact that for a given three sizes of particles, with $d_1 < d_2 < d_3$, the value of d_2 that maximizes the virtual packing density is given by the geometrical mean of the extreme diameters, *i.e.* $d_2 = \sqrt{d_1 d_3}$ [67]. For this reason, particles were selected in such dimensions that this proportion was nearly respected. Several monodisperse and polydisperse (binary and ternary) mixtures were prepared to test the effect of particle size and particle size distribution on sealing and to relate this effect to the packing density of the particles. Hybrid core-shell particles were also tested in their sealing performance. In this case, mixtures of either Tetrahydrofuran (THF) and bare TiO_2 particles or THF and TiO_2-PMMA-88 (see Table 6.5) were used to evaluate the impact of the polymer shell on the sealing performance. The use of this solvent was required to overcome the agglomeration of the TiO_2 particles grafted with polymers. Although the two systems (polymer *vs.* core-shell particles) have different sizes, it was of interest to investigate if these particles would be able to effectively clog a microchannel.

Creating a perfect reproduction of the same conditions as in the MTM seal contact was a difficult undertaking, it was therefore decided to idealize the problem and focus on the demonstration of the particle-packing concept in minimizing leak flow through model channels. Factors such as high temperature, channel materials, effect of oil and surface interactions were not considered in this design. Two types of microchannels were selected. The first geometry consisted of microchips with 5 μm nozzles purchased from Micronit Microtechnologies B.V. (Enschede, The Netherlands). Additional information about the overall geometry is shown in Figure 6.10 (top) and more in detail in Appendix Figure E5. Since we were not interested in the original use of the device as a droplet generator, we cut the chip in the section far enough from the nozzle to remove the part containing the two filters. The microchip is used in conjunction with a cartridge and a chip-holder that allowed the use of standard laboratory equipment such as syringe pumps and inverted microscopes for operation and visual observations during the experiments. This auxiliary equipment is available within MTP. In addition, buying the microchannel chips allowed saving a significant amount of time compared to developing and producing our own chips. However, the cost of these chips was around 450 € per 3 chips and once they were clogged there was no way to clean and reuse them. For this reason, another channel geometry was selected. This consisted of a DURAN (Wertheim, Germany) capillary tube (price only 1,10 € per meter), that was

heated followed by stretching to reduce the inner tube diameter. A blowtorch, safety glasses and a bit of skill in working the glass with the flame allowed to manufacture a geometry as shown in Figure 6.10 (bottom). Around 30 microchannels were prepared with this technique. The original tube had internal and external diameters of 0.3 mm and 4 mm, respectively. Microcapillary tubes with an inner diameter between 10 µm and 30 µm were selected and used to simulate (scaling-up) the voids/channels in the roughness pattern of a MTM seal. Both model channel systems were made of naturally hydrophilic borosilicate glass. The schematic of the microfluidic set-up used for the clogging tests is shown in Figure 6.11 and is described in the following section.
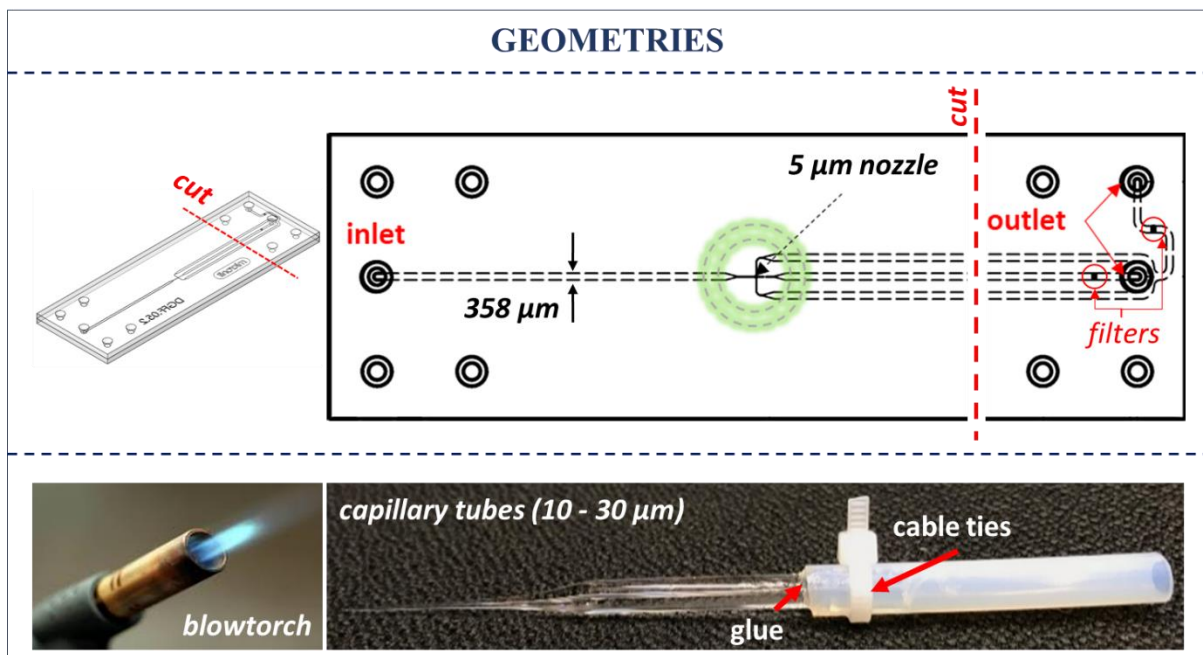

Figure 6.10. Geometries of the microchips used as model channels for the clogging tests.
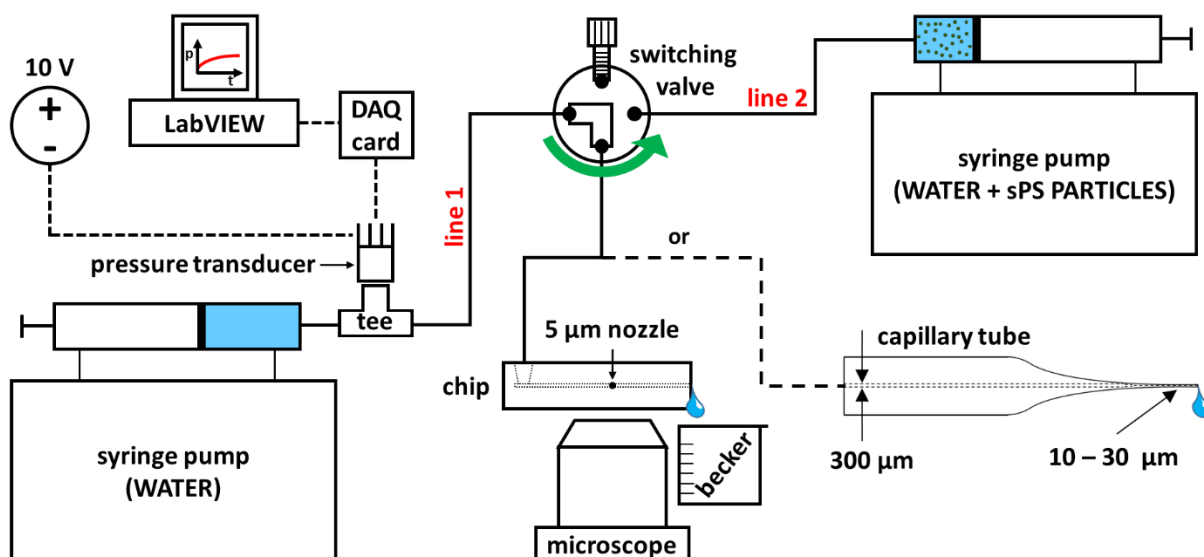
Figure 6.11. Schematic of the microfluidic set-up used for the clogging tests with model particle suspensions.

6.2.2 Materials and methods for the seal tests

Particles and suspensions. Stabilized aqueous suspensions of monodisperse polystyrene particles (sPS) with four different particle sizes were purchased microParticles GmbH (Berlin, Germany), *i.e.* 0.147 µm (SD = 0.007 µm, 5 % w/v), 0.919 µm (0.026 µm, 5 % w/v), 2.23 µm (0.04 µm, 10 % w/v) and 5.31 µm (0.10 µm, 10 % w/v). Bare TiO_2 particles were donated by Artecs B.V. (Hengelo, The Netherlands) and TiO_2-PMMA-88 (see Table 6.5) particles were synthesized from them by SI-ATRP as mentioned above [92] [100]. PS particles were tested in Milli-Q water by diluting the original solutions (for monodisperse suspensions) and mixing for the preparation of polydisperse suspensions. Titanium dioxide particles were dispersed and tested in THF to avoid agglomeration. All the suspensions used during the tests had a final concentration of solids in the range of 0.5 - 1 % w/v (percent of weight of solution in the total volume of solution). During the first tests, it turned out that sonication played a key role for the ability of particles to flow in the channels, therefore, a standard practice was to sonicate the samples for 3 hours and, immediately after, use them in the tests.

Connections of the devices to tubing and pumps. For glass chip devices obtained from Micronit, standard Perlast ferrules compatible with 1/16 inch OD Teflon tubes were used in combination with the chip-holder. For the capillary tubes, instead, a self-made solution was to apply suitable glue to the glass surface and embed the capillary tube with some intrusion inside a bigger tube made of Teflon. To further strengthen the contact, cable ties were applied in the overlap area between glass and Teflon tube, as is shown in Figure 6.12. The Teflon tube was connected to the set-up with PEEK fittings, suitable for hosting standard 1/16 inch OD Teflon tubes commonly used in microfluidic applications. In order to completely seal this part, Teflon tape was applied to the thread of the PEEK fitting before screwing it inside the big tube. However, most of the sealability was given by a Perlast ferrule applied as is shown in Figure

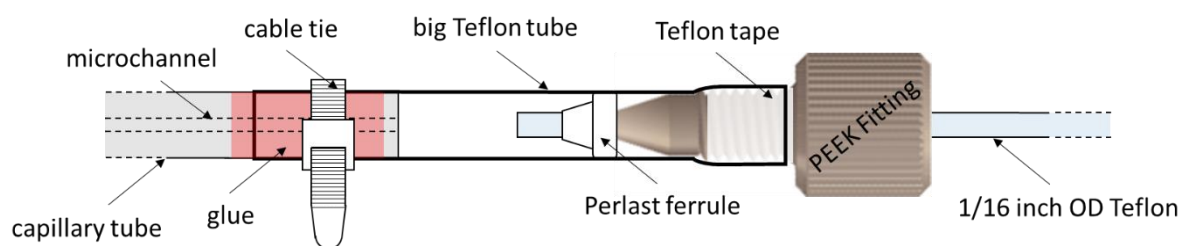6.12. No leakages were noticed up to 10-12 bar (max pressure detected by the pressure sensor, see further on).

Figure 6.12. Schematic of the connection between the capillary tubes and the standard Teflon tubing.

Seal test set-up. Two commercial plastic syringes (10 ml) equipped with rubber seals are operated by two separated syringe pumps (see Figure 6.11). Two different lines are used to separately send either only water (line 1) or particles dispersed in water (line 2) to the model channels. In the case of hybrid core-shell particles, only THF was sent from line 1 and THF + particles from line 2. The switching valve allows to isolate the two lines and switch from one to the other. Standard 1/16 inch OD Teflon tubes (ID = 250 µm), FFKM (Perlast) perfluoroelastomer ferrules, PEEK tee (P-727 PEEK Tee .020 thru hole Hi Pressure, F-300), manual switching valve (V-101L), PEEK fittings for syringe and corresponding valves were purchased either from Micronit (Enschede, The Netherlands) or IDEX Health & Science (Oak Harbor, Washington, USA). A Honeywell (Morris Plains, New Jersey, USA) pressure transducer (24PCGFB6G, 0 – 250 psi) is powered by a power supplier set at 10 Volt and connected to a USB-6008 DAQ card (National Instruments, Austin, Texas, USA) to convert the signal for read out with LabVIEW. The pressure sensor is placed in the only-water line so that its contamination (and possible disturbance of measurements) by particles is avoided. The pressure sensor was calibrated and the coefficients of the calibration curve were used in a LabVIEW script to acquire the internal pressure (with a sampling frequency 1 Hz), convert, visualize and store the signal. The tee valve hosts the pressure sensor, which is glued and kept under compression to ensure that it stayed in position. The overall microfluidic set-up was built up around an IX71 inverted microscope (Olympus, Tokyo, Japan) to allow channel inspection and video recording during the experiments. Specifications, drawings and further information of the set-up are available in the Appendix (from Figure E6 to Figure E14). In the case of devices with a nozzle, the microchip was directly placed in the sample holder of the microscope whereas a self-made solution was adopted to place the microcapillary tubes near the lens of the microscope. A BX60 optical microscope (Olympus, Tokyo, Japan) equipped with magnification lenses from 5x to 50x was also used to take images of the different microchannels geometry.

6.2.3 Experimental methods

The flow rate was Q = 0.3 ml/h for all the tests. It represents a good compromise between time and pressure. At high flow rate, *i.e.* exceeding 0.5 ml/h the maximum pressure of the set-up was reached. On the other hand, lower flow rates would result in really long times for a single test. The reader is directed to the Appendix (Figure E13 and Figure E14) for more details on the selection of the flow rate.

Ideally, the testing methodology consists of three steps, as is described in Figure 6.13.
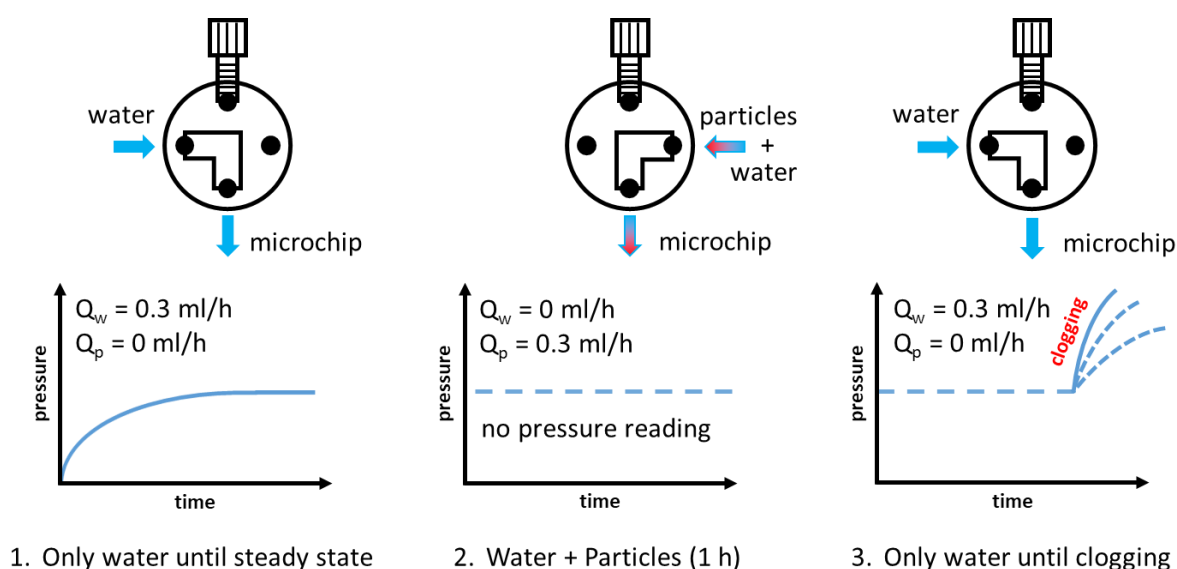

Figure 6.13. Clogging test methodology. Note that the same concept was applied in case of THF instead of water.

In the beginning, only water (or THF) is sent to the microchannel from the line containing the pressure sensor. This phase proceeds until a steady state is reached inside the channel. Having a smaller cross-section, the device with the nozzle requires a higher pressure (around 4 bar) and time (more than 3 hours and a half if no contamination occurred) to reach the steady state. Once the pressure and flow rate are (nearly) constant, the valve is switched to send a (just sonicated) particle dispersion from the other syringe pump with a slight overpressure. The flow from the first line is stopped immediately after switching the valve. The particle injection phase is usually 1 hour. However, in some tests, it was necessary to send particles again to obtain the desired result. It is important to understand that during this phase, the pressure sensor measures a (nearly) constant value of pressure (theoretically equal to the last value that was measured before switching the valve). This happened because the line containing the pressure transducer is isolated while the actual pressure inside the channel can increase due to clogging phenomena. However, this test aims to allow a certain amount of particles to reach the smallest section of the microchannels (*i.e.* the nozzle) and to evaluate their clogging effectiveness in terms of measured leakage flow rate at a certain pressure. For this reason, the third step consists in switching the valve back to the line with only water (or THF) thereby stopping the flow from the line with particles.

If particles do not completely clog a microchannel, the flow rate at the outlet of the microchannels is regarded as leak flow rate. This last is the most relevant parameter to compare the sealing performance of different particles size distributions. Measuring the leak flow rate was done as is shown in Figure 6.14. The droplets were collected over precise time intervals and the overall volume was evaluated by means of either a high precision syringe (for relatively high leakage flow rates) or measuring the size of single droplets (for low leak flow rates). Evaporation was not taken into account during measurement of the leak flow rates.
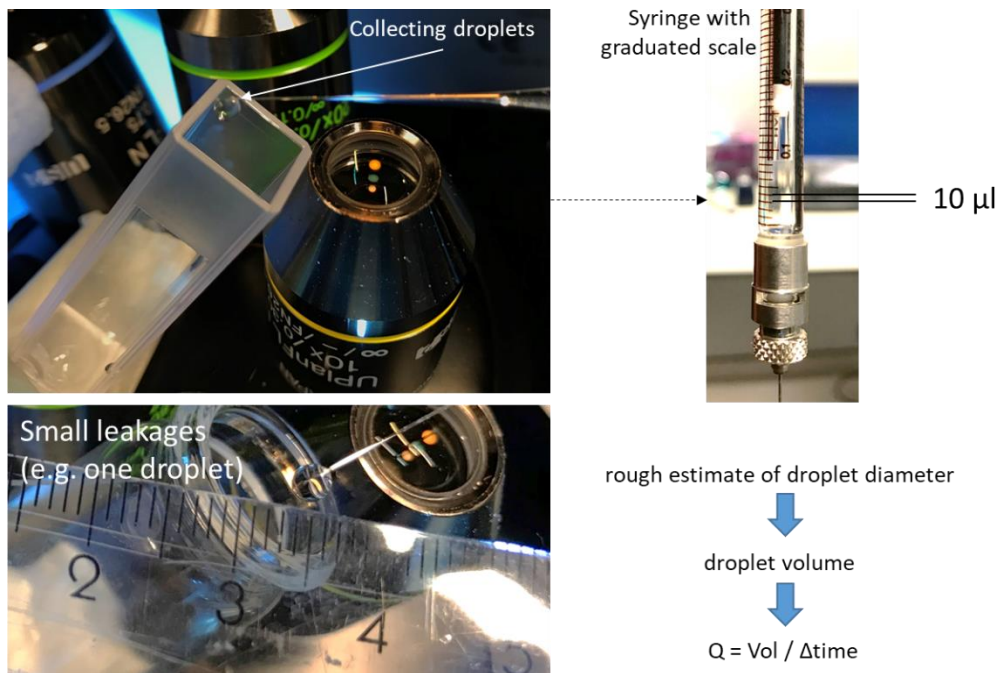

Figure 6.14. Measuring the leak flow rate for "high" leak flow rate (top) and "low" leak flow rate (bottom).

After each test, connectors and valves were immediately cleaned with ethanol or acetone and sonicated for long times (~24 h). Teflon tubes were changed and replaced with new ones having the same length. Before each new test, the set-up was built up again and subjected to a flow of ethanol (first) and water (later) to further remove possible contamination inside tubes, valves and connectors. In this case, the (cleaning) flow rate set from the pumps (one line at a time) was 1 ml/h. In total, the cleaning procedure before each test took around 1 hour, *i.e.* 15 minutes per line per solvent.

6.2.4 Results and discussion for the seal tests

Seal test set-up. The real version of the set-up is shown in Figure 6.15. The pressure in the set-up is governed by the syringe, which does not allow tests at pressure higher than 10 bar. Due to problems related with the video recording from the PC connected to the microscope, a laptop and a HD camera were used to record the screen of the PC while the microscope was in live mode. In a third screen, Labview was set to allow the simultaneous start of the measurements from all the devices. The power supply set at 10 V to power the pressure transducer is not visible in the figure. Note: it may be replaced with a battery for a more compact version of the single-channel clogging set-up.
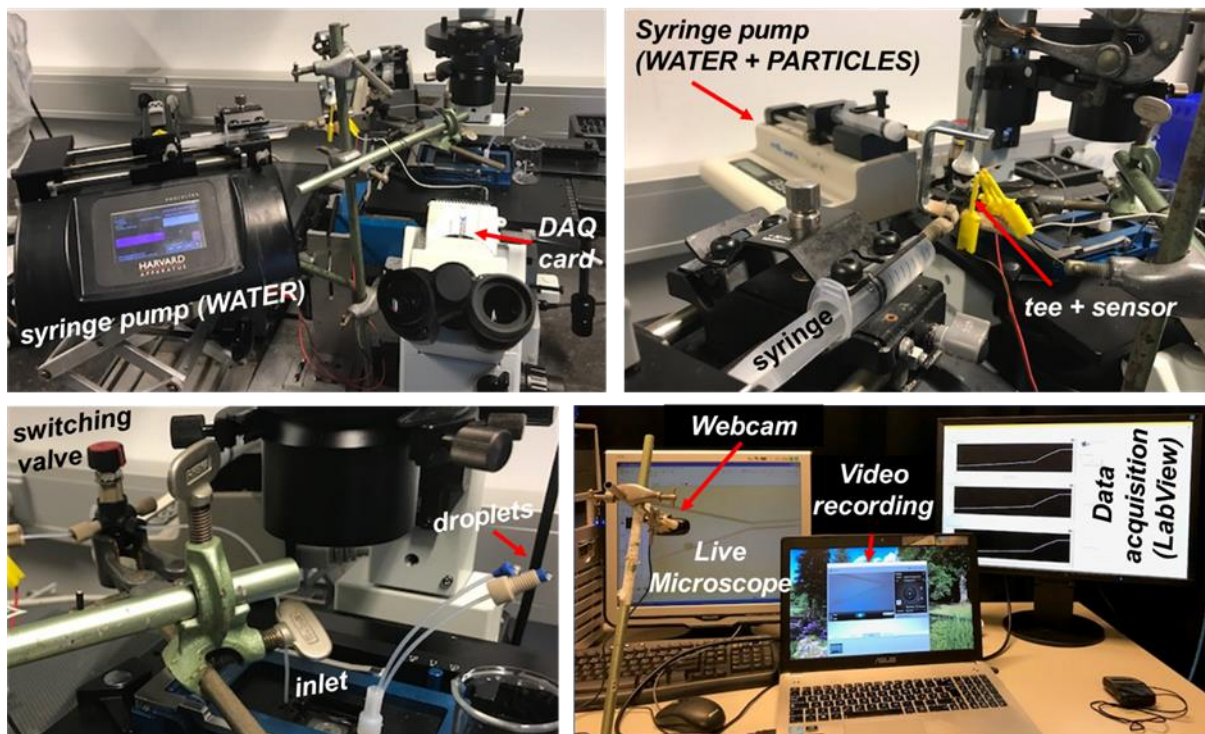

Figure 6.15. Microfluidic set-up for clogging tests with particle suspensions.

Seal tests with sPS particles. Figure 6.16 shows microscopy images after successful clogging tests for a purchased microfluidic chip (left) as well as for a capillary tube (right). Once clogging had occurred, particle loss downstream of the nozzle was negligible in both cases. This means that nearly all particles were involved in clogging and were able to resist the increase in pressure. However, in some tests performed using monodisperse particles in water (particularly with nanoparticles), it happened that the packing of particles (which was previously formed at or in the vicinity of the nozzle) was destroyed due to the increasing pressure inside the microchannels. Clogging was usually obtained within a few minutes from the moment the particles reached the nozzle.
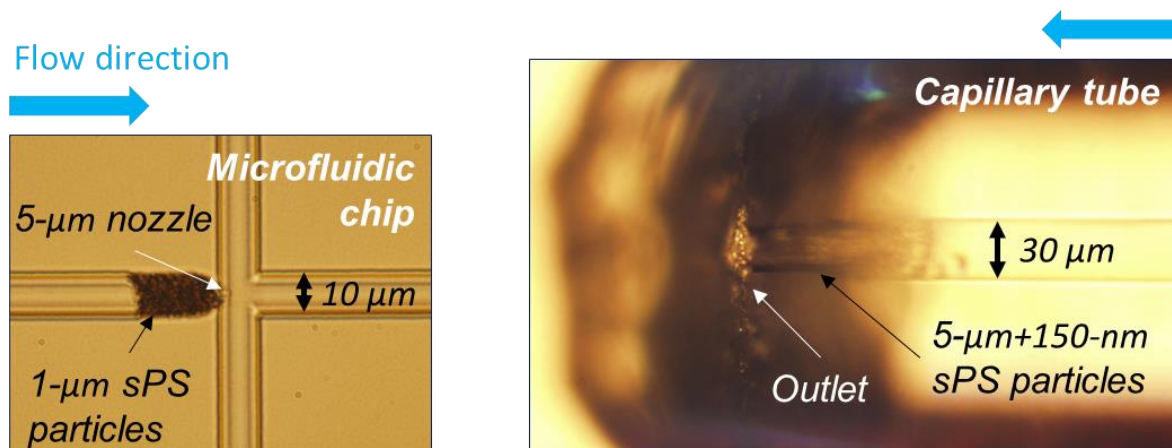
Figure 6.16. Optical microscopy images of the Micronit device and the capillary tube with their nozzles successfully blocked with PS particles. The size of particles used for the clogging test is shown in the corresponding image. Note that the block of particles on the left, although dense, did not clog the device and a low leak rate was observed.

Typical pressures and leak flow rates as a function of time for single-channel clogging tests for both sample geometries are shown in Figure 6.17. As mentioned above, the flow rate set by the syringe pump was 0.3 ml/h for all the tests presented and discussed in this report. The light blue refers to the "small" scale test, *i.e.* the test performed on a purchased microfluidic chip having a nozzle of 5 μm. The dark blue refers to a capillary tube stretched till a cross-section having a diameter of ~30 μm was reached. The red dashed line represents the syringe limit given by the deformation of the (plastic) syringe and obtained after calibration of the system (see Appendix Figure E14 for more details). The horizontal dotted and dashed light blue line refers to the steady-state pressure for microfluidic chip channels. From Figure 6.17 it is obvious that it takes about 3 hours to reach steady flow rate conditions. The stretched capillary tubes had significant larger diameters and as a consequence, they reach steady state almost directly at the start of the experiment. For both model microchannels, particles were injected once steady state was reached. In such a way, it could be assumed that changes in pressure or leak flow rate values only occurred due to the presence of particles. In Figure 6.17, the particle diameter used were 5.31 μm and 0.919 μm for the stretch capillary and purchased microchip, respectively. These diameters were selected to keep the ratio of the particle diameter to channel cross-section constant, *i.e.* ~0.2. *H. M. Wyss et al.* [105] reported that this value is within a range for partial particle-clogging phenomena to be expected and, therefore, it was chosen as a suitable value to study the effect of the particle-packing density on sealing, as confirmed also during preliminary tests (not shown in this report). The observed gradual pressure built up for both systems suggest that particles are clogging the channels as was optically observed as well. Despite that the maximum syringe pressure is nearly reached and the packed bed of particles appears dense (Figure 6.16), a significant leak flow rate is observed at the channel outlets of both model systems. This is in agreement with what can be expected for a monodisperse particle size distribution. When partial unclogging occurred, it was observed with the microscope and a corresponding pressure drop was measured (see the dark blue line).
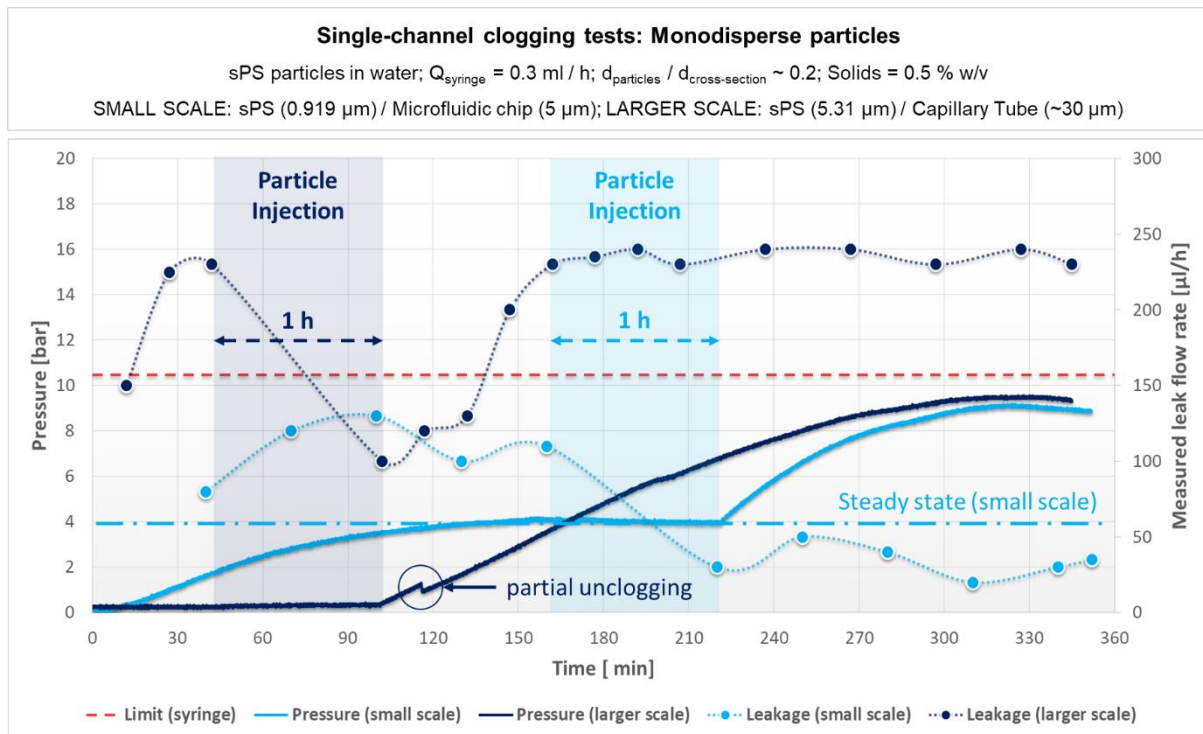
Figure 6.17. Typical pressure and leak flow rate curves of single-channel clogging tests for monodisperse sPS particles with a particle diameter to channel dimension ratio of ~0.2. Note that during particle injection the pressure is constant because the pressure transducer is situated in the other fluid line (see set-up description), which is isolated from the channel system during this phase. The dotted lines (both 'small scale' and 'larger scale' leakages) belong to the second y-axis.

Following the successful monodisperse sPS particle tests, binary mixtures of 50/50 vol%/vol% of micro and nanoparticle dispersions were prepared and used in clogging tests. For the microchip particles with average diameters of 0.919 μm and 0.147 μm were used while for the stretched capillary the particles with diameters of 5.31 μm and 0.147 μm were used. The overall particle concentration was 0.5 % w/v. The typical results of the clogging tests using binary mixtures are shown in Figure 6.18. Remarkably, the resulting leak flow rate right after particle injection is nearly zero for both model systems. Thus, it is concluded that binary mixtures of particles have better sealing performance than monodisperse particles, which is expected. The increase in sealing performance for binary mixtures may be caused by the presence of nanoparticles filling the gaps between microparticles [66]. Following the particle-packing theories, binary mixtures would have a lower porosity (*i.e.* higher packing density) compared to monodisperse particles. In turn, a lower porosity of the packed bed of particles may be related to the decrease in leak flow rate. Since pressure and flow rate in microchannels are related by means of the hydraulic resistance (see Chapter 4), in this case, particles act as an "infinite" resistance causing the measured pressure increase. The obtained entire sealing was not expected for binary mixtures since their overall packing density could be further improved with the addition of other particles within certain size and concentration ranges. It is not known whether the measured entire sealing was due to the effective clogging action of the binary mixtures or due to lack of a highly sensitive system to measure the leak flow rate.
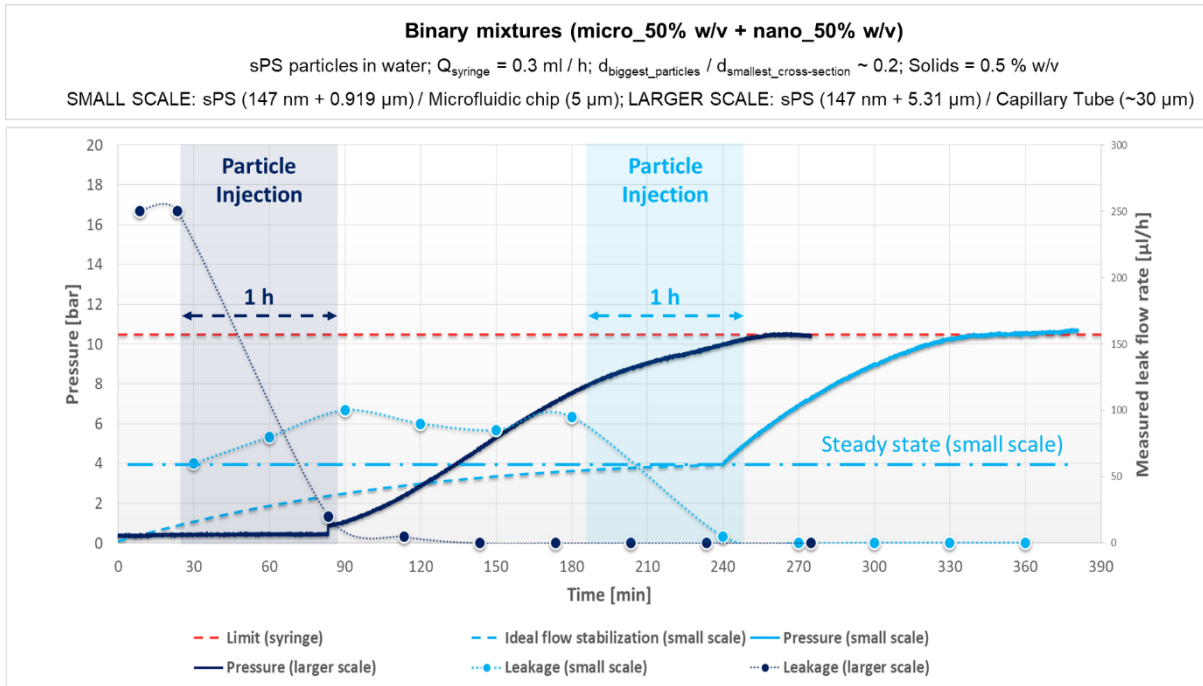
Figure 6.18. Typical pressure and leak flow rate curves of single-channel clogging tests for binary mixtures of sPS particles with a particle diameter to channel dimension ratio of ~0.2. Note that during particle injection the pressure is constant because the pressure transducer is situated in the other fluid line (see set-up description), which is isolated from the channel system during this phase. The particle mixture is given in the figure. The dotted lines (both 'small scale' and 'larger scale' leakages) belong to the second y-axis.

The clogging observed during the test with binary mixtures was basically perfect. Nevertheless, some tests were also run with ternary mixtures to see possible differences an example is shown in Figure 6.19. The results were comparable in terms of both pressure and leakage rate to the tests with binary mixtures. Although improvements were expected with the current system it was impossible to observe differences in pressure built up and decreases in leak flow rates during the particle injection phase.

Ternary mixture

sPS particles in water; $Q_{syringe}$ = 0.3 ml / h; $d_{biggest\_particles}$ / $d_{smallest\_cross-section}$ ~ 0.2; Solids = 0.5 % w/v

LARGER SCALE: sPS (147 nm [40 % w/v] + 0.919 μm [20 % w/v] + 5.31 μm [40 % w/v]) / Capillary Tube (~30 μm)
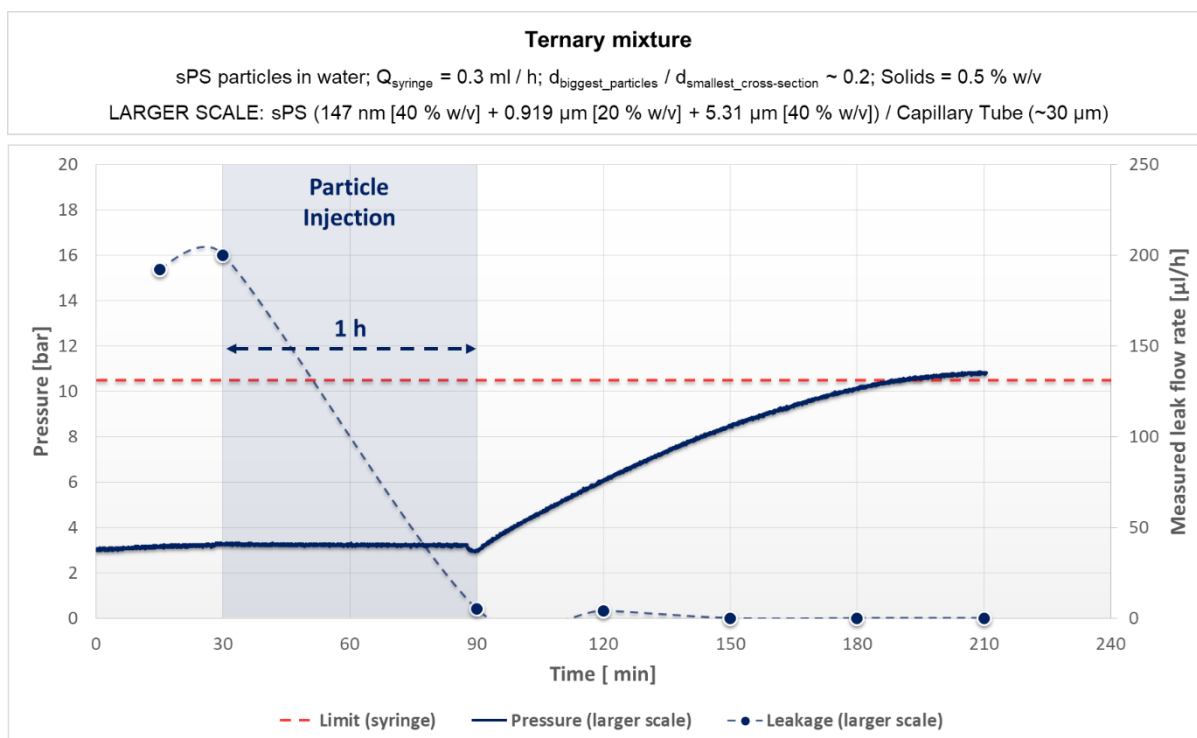
Figure 6.19. Single-channel clogging test for the stretched capillary channel clogged with a ternary particle mixture. Typical pressure and leak flow rate curves of single-channel clogging tests for ternary mixtures of sPS particles with a particle diameter to channel dimension ratio of ~0.2. Note that during particle injection the pressure is constant because the pressure transducer is situated in the other fluid line. (see set-up description), which is isolated from the channel system during this phase. The particle mixture is given in the figure.

Following the successful clogging tests, attempts to correlate the leak flow rate to a model packing density for various particle size distributions were not successful. The lack of a system which allows controlling the pressure instead of the flow rate (here controlled by the syringe pump) makes it impossible to normalize the obtained results for the two model channels. For each test, the leak flow rate values measured at a certain pressure should be related to the leak flow measured at the same pressure without particles. This in combination with flow model like used in packed columns would eventually allow to correlate the results to a packing density [106].

Seal tests with PMMA-88 in comparison with bare TiO₂ particles. Bare TiO$_2$ particles and PMMA-88 (see Table 6.5) were also evaluated for their sealing behavior by means of the developed microfluidic set-up, as is shown in Figure 6.20.
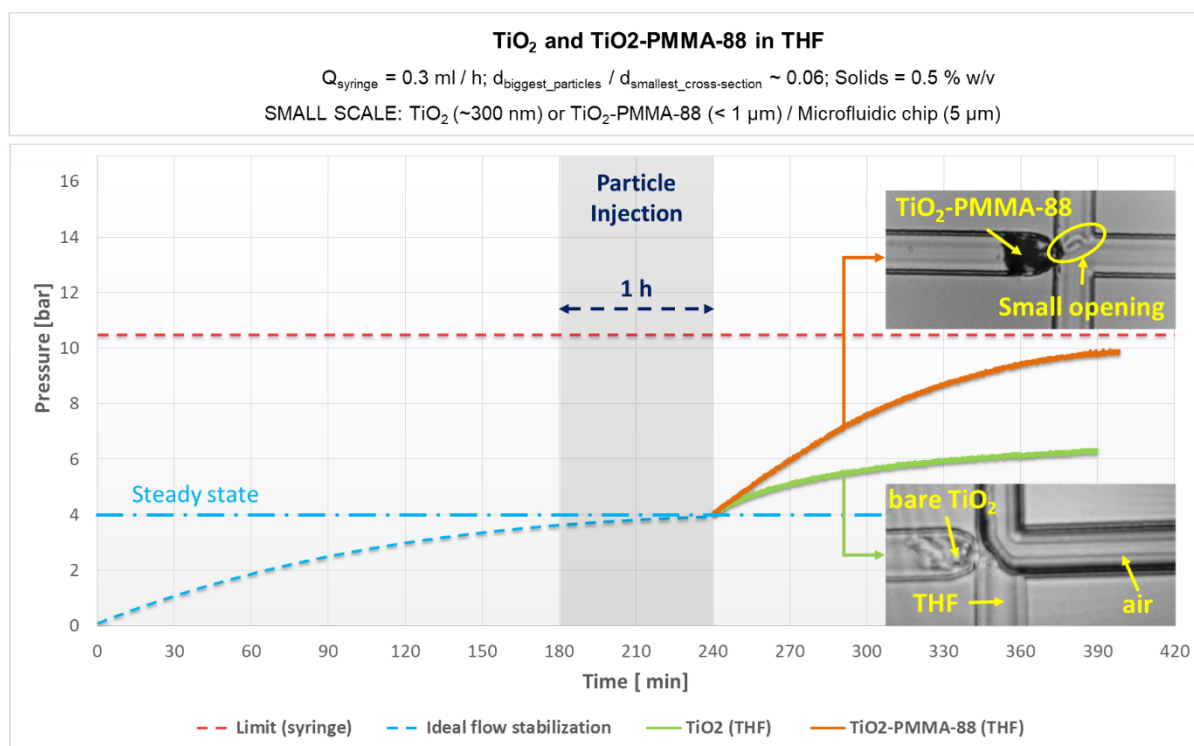

Figure 6.20. Single-channel clogging test with bare TiO$_2$ particles and PMMA-88 (see Table 6.5) in the case of microfluidic chip equipped with a 5-μm nozzle. Note that THF quickly evaporate and, therefore, it was not possible to evaluate the leakage rate in this case. The two inverted microscopy images shows the corresponding clogging with the solutions of THF-TiO$_2$ (bottom) and THF-PMMA-88 (top). Clogging with bare TiO$_2$ particles showed a certain amount of liquid (THF) passing through the particles while clogging with PMMA-88 had a small opening at the nozzle.

Due to the small size of the particles, this second particle based system (having average particle size around 300 nm and a division between 190-420 nm [92]) was tested using the microfluidic chip not to further increase the ratio of particle size to channel dimensions. Unlike what was done before with water, the core-shell particles were dispersed and tested in THF to reduce agglomeration. TiO$_2$ particles were also dispersed in THF to enable the comparison with the grafted system. Unfortunately, the use of THF made it impossible to evaluate the leak flow rate due to the high evaporation rate of this solvent compared to water. However, a rough evaluation of their performance was conducted by analyzing the pressure variations and the movies as well as the images taken with the inverted microscope. The green curve in Figure 6.20 refers to a test with bare TiO$_2$ particles dispersed in THF whereas the orange line represents a test performed using only PMMA-88. The percentage of solids in the overall THF/particles system was always 0.5 % w/v. It appears evident from the graph that the pressure bearable by core-shell particles was higher but it could not be said that they perfectly clogged the nozzle. Indeed, comparing the two microscope images shown in Figure 6.20, leakage of THF is visible in both cases. However, the magnitude of the

leak flow rate looks definitely lower in the upper microscope image corresponding to the test with hybrid core-shell particles (PMMA-88). Hence, although not perfect, the packing of particles grafted with PMMA was better than the packing of bare TiO_2 particles without a shell. In general, the obtained results using TiO_2 and PMMA-88 do not contradict the approach based on the particle-packing theories since a perfect clogging (no measured leakages) was not expected for a monodisperse solution of particles. Instead, the improvement in sealing performance could be caused by the use of a (soft) grafted polymer shell surrounding a (hard) core particle was a desired result.

It is hard to make a comparison between the results obtained with sPS and hybrid TiO_2-PMMA-88 particles. Effects of pressure media viscosity differences were to be expected however due to the high evaporation rate of THF no reliable differences in leak flow rates were observed to consider this in detail. In addition, the particle size distributions were not comparable.

Finally, an overview that summarizes the results of all the seal tests showed in this report is presented in Table 6.7. From the table it is obvious that, regardless of the device and the used particle system, monodisperse particle size distributions were never able to effectively clog the microchannels. Therefore, it is concluded that polydisperse particle size distributions increase the sealing performance as is confirmed by the results obtained with binary and ternary mixtures.

Table 6.7. Overview of the tests showed in this report. The corresponding particle concentrations are shown in the graphs from Figure 6.17 to Figure 6.20.

Test	Device	Particle	Clogging
Monodisperse	Microfluidic chip (5 μm)	sPS (0.919 μm)	No
Monodisperse	Capillary tube (~30 μm)	sPS (5.31 μm)	No
Monodisperse	Microfluidic chip (5 μm)	TiO2 (~300 nm)	No
Monodisperse	Microfluidic chip (5 μm)	PMMA-88 (~300 nm)	No
Binary	Microfluidic chip (5 μm)	sPS (147 nm + 0.919 μm)	Yes
Binary	Capillary tube (~30 μm)	sPS (147 nm + 5.31 μm)	Yes
Ternary	Capillary tube (~30 μm)	sPS (147 nm + 0.919 μm + 5.31 μm)	Yes

The main results of this section are a device and a corresponding testing methodology that allow to measure pressure and leak flow rate of particle dispersions while monitoring their flow inside the microchannels. Further work is required to relate the obtained values of pressure and leak flow rate to the particle packing densities such that the data from various sets can be compared.

7. Deliverables and conclusions

7.1 Deliverables of the project

The objective of the project was to design and develop a yellow thread compound as well as a new test method for evaluating the sealing performance of particles at the microscale. This design project delivers the following results:

- A literature study was carried out to clarify the current background related to the development of a thread compound (Chapter 4 and Appendix).
- Two systems of particles were developed, *i.e.* different polymer and core-shell particles and their lubrication performance was evaluated.
- A paper [100] was published on the developed hybrid core-shell particles grafted from modified TiO_2 particles.
- A methodology to develop a seal test set-up at the microscale (Figure 6.11 and Figure 6.15) and measure the most relevant performance parameters, *i.e.* pressure and leak flow rate (Figure 6.13 and Figure 6.14) was delivered.
- A proof of concept (based on particle-packing theories) which confirmed that polydisperse particle size distributions increase the sealing performance compared to monodisperse particle size distributions was delivered.

Thus, polymer particles and their inorganic hybrids appear to be promising candidates for the development of yellow thread compound. In addition, single micro channels are viable tools to study the clogging effectiveness of particle size distributions as a function of their composition. Eventually, the obtained results will aid in selecting and producing thread compound additives with the right composition as well as with the right particles size distribution.

7.2 Conclusions

The objective of this project was to design, develop and test suitable additives to replace heavy metals in thread compounds for OCTG connections. In particular, attention was paid to designed additives' performance in the MTM seal of premium connections. Besides the chemical and physical stability at high temperature (250 °C), the designed additives needed certain lubrication and sealing performances to *i)* prevent surface damage, *ii)* help make-up/break-out operations and *iii)* avoid leakages through micro leak paths in MTM seals during service. Development of testing methodologies and set-ups were required as well.

A literature study was carried out to understand the sealing mechanism of MTM seals and it turned out that connection material and the typically applied phosphate coating form a tribosystem together with the thread compound. The roughness of the two metal surfaces is designed in such a way that the sealing performance of the connection is enhanced. For this reason, it is crucial that surface damage is limited within an acceptable range in order not to compromise the originally designed configuration. Thread compounds containing heavy-metals particles are commonly used to protect the surface under severe sliding conditions due to their excellent deformation and lubrication capabilities. The most common example is the API modified thread compound, which was used in this report as performance reference.

For this reason and to be able to propose promising alternatives, the role of heavy-metal particles used in this thread compound, such as lead, copper and zinc, was investigated.

Based on the literature study and the established requirements, two systems of particles were developed, *i.e.* solid polymer and hybrid core-shell particles. In order to have a wide range of polymer system alternatives, PAM, PS and PDMS polymer particles were synthesized with and without crosslinking by means of emulsion and dispersion polymerization reaction. Core-shell system particles were selected consisting of PMMA or PBA grafted by SI-ATRP from TiO_2 particles, whose surface was previously modified by PDA treatment.

Weight loss measurements under nitrogen environment were used as a methodology to evaluate the short-term thermal stability of the thread compound and the particles. All the additives performed well at the temperature of 250 °C (Table 6.6 and Figure 6.3), which was established as an operation limit for this project.

Pin-on-disc tests were performed to evaluate the lubrication performance under micro sliding and 1 GPa of contact stress. For this test, the additives were dispersed in a provided base grease and applied on the surfaces of both pin and disc prior to the test. The majority of the polymer-based particles was able to ensure the required lubrication performance in terms of COF values and surface damage (wear scar analysis) as compared to the API modified thread compound as a reference, as is shown from Figure 6.4 to Figure 6.8 and in the Appendix (Figure E4). Among the core-shell particles, PMMA grafted from TiO_2 particles with 88 % of organic content was the best performing.

Sealing performance of the designed particle dispersions was evaluated at the microscale by means of a constructed microfluidic set-up. The dimensions of suitable particle diameters were obtained from particle-packing theories such that effective channel clogging was achieved. The results show that leakage is reduced or even stopped when using polydisperse particle solutions. (*e.g.* compare Figure 6.17 and Figure 6.18).

Overall it is concluded that the (hybrid) polymer based particle designs, prepared and evaluated are promising candidates to replace heavy metals in thread compounds and that single channel flow test are of interest to obtained optimum particle size distributions. In future work the best performing particles have to be prepared in larger quantities such that their performance in premium connections under model circumstances can be evaluated for a longer period of time.

8. Recommendations

PDMS seems an interesting material to be further investigated due to its thermal stability and lubrication performance, but also for its compliance with the environmental requirements. PS is not biodegradable and, therefore, further investigation is needed to evaluate the possibility to use it as a thread compound additive.

The repulsion/attraction interaction between particles is expected to have an important role in the formation of hydrodynamic arches and clogging as well. Particularly, repulsion between particles should create a pushing effect that enhances the robustness of the arches at the pore entrance [107]. Hence it is of interest to obtain particles with various surface compositions. The use of ATRP initiator modified inorganic core particles, not limited to TiO_2, seems a viable route to obtain various classes of hybrid core-shell particles that allows studying the effect of particle interactions on clogging and lubrication performance.

Regarding lubrication performance, in order to evaluate the interaction between connection material, coating and thread compound, the pin-on-disc test should be repeated with a phosphate coating on the flat substrate. Furthermore, these tests should be performed at a high temperature to have a more realistic reproduction of the real condition inside the well. The four-ball test can be another possibility to evaluate lubrication since many thread compound manufacturers refer to this test in the TDS and a lot of data would be available for comparison. Eventually, field-scale tests are necessary to give the final evaluation.

The sealing test confirmed that model microchannels are suitable for testing the sealing performance of particle dispersion. However to compare to a more realistic environment the test itself should be further downscaled to channels with submicron dimensions. This requires the development of new chips and a set-up that can operate at much higher pressures. The use of multiple channels in parallel may be advantageous here. In addition, the set-up could be improved by the implementation of flow rate sensors, which is substantially more expensive but readily available.

Moreover, the modification of the glass surface towards more hydrophilic/hydrophobic properties is recommended in order to study the influence of the metal surfaces instead of glass.

Eventually, it is highly recommended to select the best performing particles reported in this study and make enough quantities of those available for a pilot-scale test to study the make-up phase and sealing performance. Data within Shell is available for comparison with existing commercial API modified thread compounds.

Appendix

A.   Norwegian Environment Agency's color-category

Table A1. Evaluation criteria and categories for evaluation of the environmental properties of substances [108].

Emissions		Category[1]	Norwegian Environment Agency's color-category
WATER		200	Green
Substances on the PLONOR list		201	Green
Substance covered by REACH Annex IV[2]		204	Green
Substance covered by REACH Annex V[3]		205	Green
Substances missing test data		0	Black
Additive packages that are exempted from test requirement and not tested		0.1	Black
Substances that are believed to be or are harmful in a mutagenic or reproductive manner[4]		1.1	Black
Substance on the list of priority chemicals or on OSPARS priority list[7]		2	Black
Substance on REACH candidate list[8]		2.1	Black
Biodegradability <20% and log Pow ≥ 5[5]		3	Black
Biodegradability <20% and toxicity EC50 or LC50 ≤ 10 mg/l		4	Black
Two of three categories: Biodegradability <60%, log Pow ≥ 3, EC50 or LC50 ≤ 10 mg/l[5]		6	Red
Inorganic and EC50 or LC50 ≤ 1 mg/l		7	Red
Biodegradability <20% [4]		8	Red
Polymers that are exempted from test requirement and not tested[9]		9	Red
Potassium hydroxide, sodium hydroxide, hydrochloric acid, sulfuric acid, nitric acid and phosphoric acid		104	Yellow
Substance with biodegradation> 60%		100	Yellow
Substance with biodegradability 20% - 60%	Subcategory 1 - expected to complete biodegrade.	101	Yellow
	Subcategory 2 - expected to biodegrade to substances that are not hazardous	102	Yellow
	Subcategory 3 - expected to biodegrade to substances that may be hazardous	103	Yellow
Sum [10]			

B.   Casing connections

B.1   Casing in drilling operations for oil and gas wells

Tubes used for oil and gas production both onshore and offshore are referred to as *Oil Country Tubular Goods (OCTG)* and represent the main parts of the well construction. Particularly, the selection of size, material and type of connectors of casing, is a crucial design phase due to the tubes high cost in relation with the overall well cost as well as the severe performance requirements [2]. Indeed, at a set depth, a combination of mechanical, thermal and chemical loads act on the system that can lead to failure as the result of different failure mechanisms (overload, deformation, stress corrosion cracking, fatigue, etc.). In general, if the relative magnitude of these loads is higher than the load-carrying capacity of the system, it will fail [109].

A drilling process involves creating an open borehole to reach a targeted reservoir. Consequently, an external support is necessary to provide stabilization and keep the sides of the well from collapsing. In this regard, the casing has the function to line the walls of the drilled well [5]. In order to establish a cased wellbore, multiple strings of pipe are cemented in place and screwed together to form casing strings. Referring to the outside diameter, casing sizes vary from 4.5'' (114.3 mm) to 36'' (914.4 mm) [110]. The production tubing has smaller sizes and it is used within the cased wellbore to produce well fluids or to inject fluids. In its most common configuration, two male joint ends are connected together by means of external couplings equipped with female threads. Thread compound is applied to the connections to provide lubrication during make-up and ensure sealing during service [5] [111].

The drilling operations are commonly carried out following precise stages. As shown in Figure B1, at each stage, a borehole is drilled, cased and cemented with a decreasing diameter for increasing depths of the subsequent stages, *i.e.* the conductor, surface, intermediate and production stage.
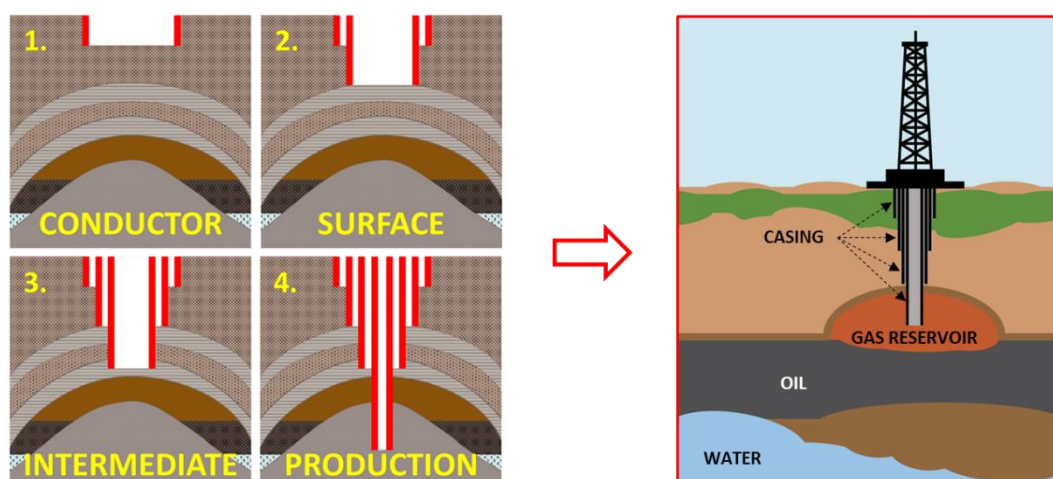

Figure B1. Drilling stages (left) and simplified diagram of an oil and gas rig (right).

Initially, the conductor casing is installed to isolate unconsolidated formations and water sands, but also to protect against shallow gas. The wellhead system is usually assembled onto this string [2]. Typical conductor pipes have diameter from 30'' (762 mm) to 42'' (1066.8 mm) for offshore wells, and 16'' (406.4 mm) for onshore wells [111]. Subsequently, the surface casing is set to provide blowout protection, isolate water sands, and prevent lost circulation. At a certain depth into the well, a transition zone from relatively low to high pressure exists. The intermediate casing functions in this area to isolate unstable well regions [2]. The last casing string is run directly into the producing reservoir and it is, therefore, called the production casing.

In some cases when drilling deeper is necessary while reducing cost, liners are used instead of casing strings. Unlike these last, liners do not extend back to the wellhead but, instead, hang from the bottom of the previously installed casing string, down to the lowest part of the borehole. In an alternative method, the liner string can be tied back to the wellhead before well completion. Figure B2 shows a comparison between typical shallow water (onshore) and deep water wells. Being longer, the latter ones need a greater number of casing strings, which leads to greater system complexity and, therefore, to higher cost as compared to onshore wells.
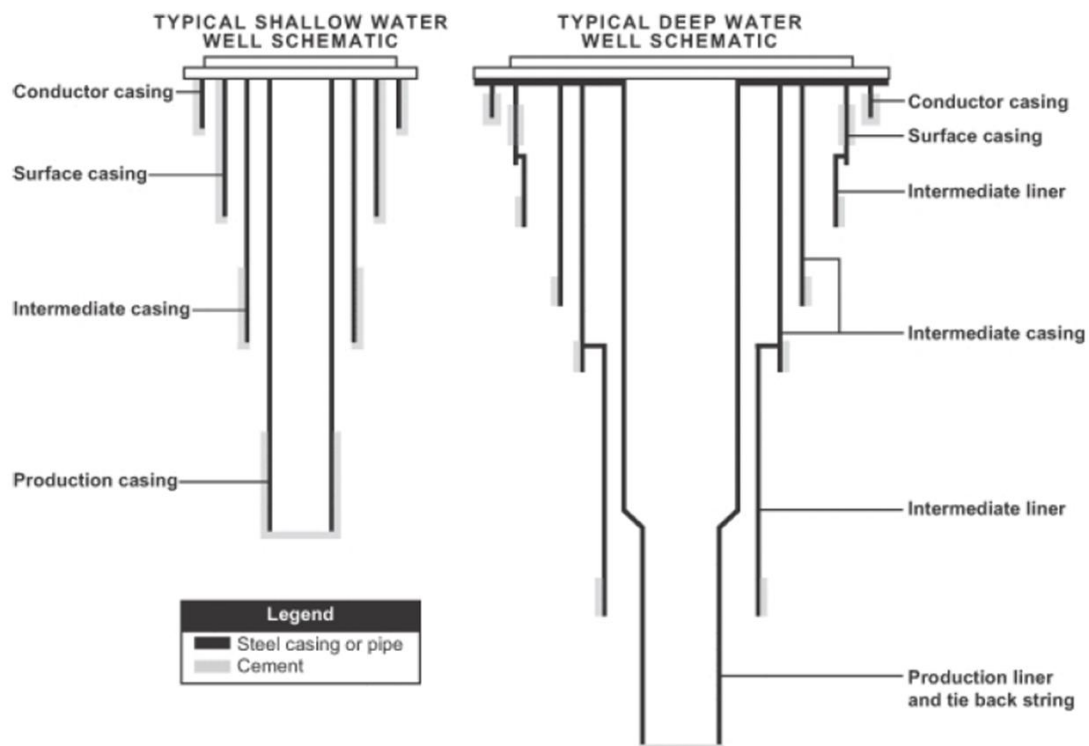

Figure B2. Typical casing strings schematic of shallow water wells (left) and deep water wells (right) [111].

B.2   API connections

The American Petroleum Institute (API) provides the reference in terms of testing and performance requirements for steel tubing used in the oil and gas industry. These imply Specifications [5] [112], Recommended Practices [113] [114] [115] [58], and Bulletins [116] [117] [118] [119]. Following API specifications [5], three main categories of connectors (Figure B3) exist: (1) non-upset tubing and couplings (NU), (2) external-upset tubing and coupling (EU), and (3) integral-joint tubing (IJ). By means of threaded connections, couplings are used to join two ends of the casing joints. In this case, the separate coupling has female threads while pipe ends are machined with male threads. In integral connections, instead, the pin end (male part) of one joint screws into the box end (female part) of another joint. External-upset connections refer to those showing an increase in wall thickness in certain sections to improve the mechanical resistance. Despite the considerable decrease in joint strength, API non-upset tubing has a cost that is only slightly lower compared to external-upset tubing. This explains why EU tubing is the most used group of connectors [120]. Three types of coupled connections are standardized by the API, namely (1) Short round-thread casing and coupling (STC); (2) Long round-thread casing and coupling (LC); and (3) Buttress-thread casing and coupling (BC), as is shown in Figure B4.
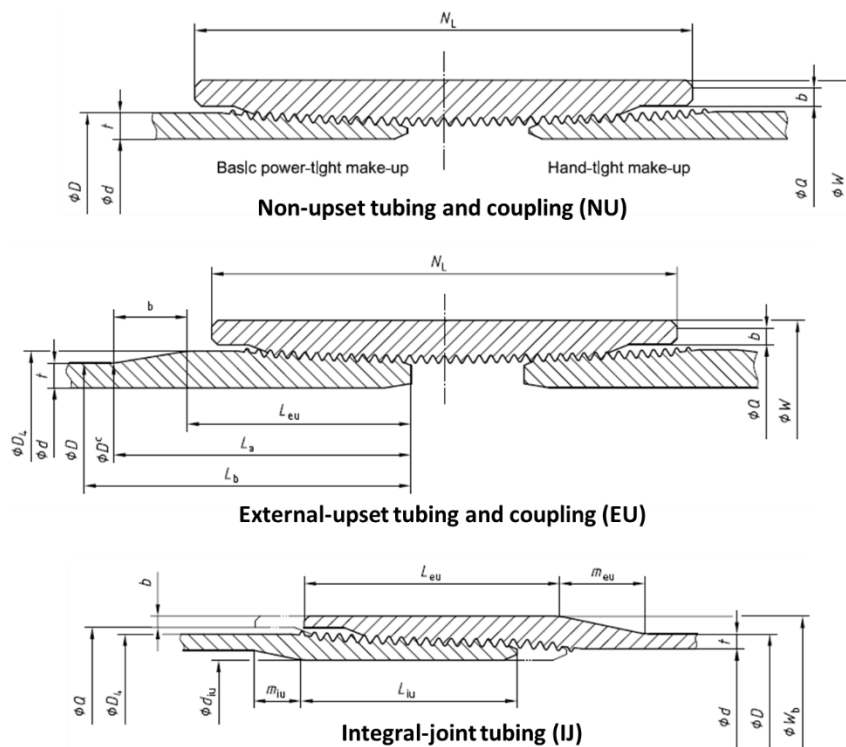

Figure B3. Drawings for the known main categories of API connections. Non-upset tubing and coupling (top), External-upset tubing and coupling (middle), and Integral-joint tubing (bottom) [5].
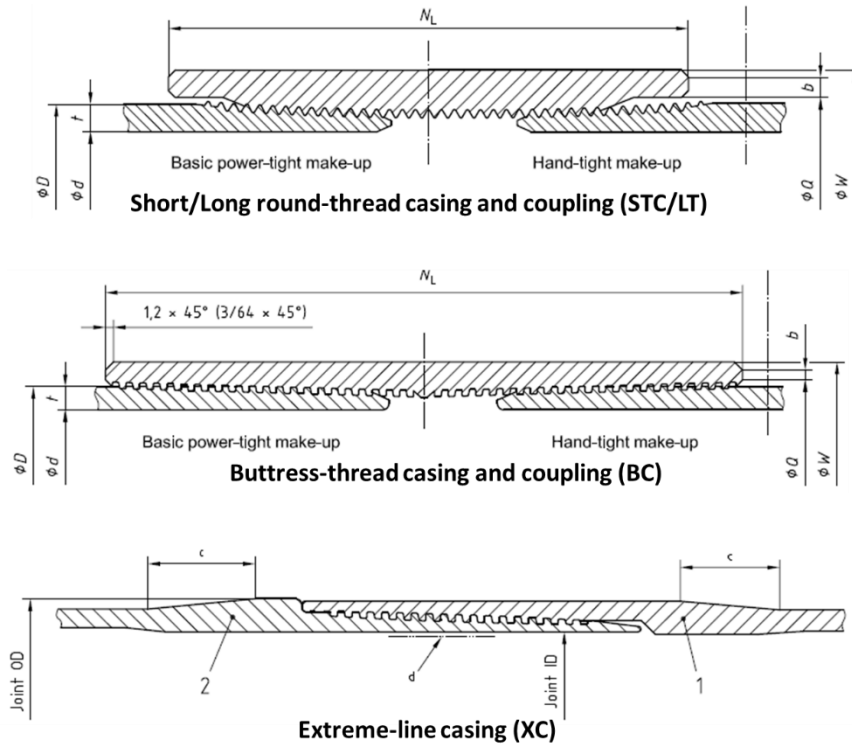
Figure B4. Drawings for Short/Long round-thread casing and coupling (top), Buttress-thread casing and coupling (BC), and Extreme-line casing (XC) [5] .

STC and LC (Figure B4, top) are similar, but the latter provides better strength and sealing properties as a result of its longer coupling region compared to the STC. Due to the reduced cross-section of the unengaged thread section of the pin, the STC connection shows a lower axial load carrying capacity than the material yield strength (Figure B5). This is often the reason for connection jump-out to occur. To solve this problem, API adopted the buttress thread form (Figure B4, middle) that, by means of two different flank angles, significantly increases the axial load strength of the connection. Extreme-line casing (Figure B4, bottom) also has a flat-crests thread type and is the only API connection equipped with MTM seal.
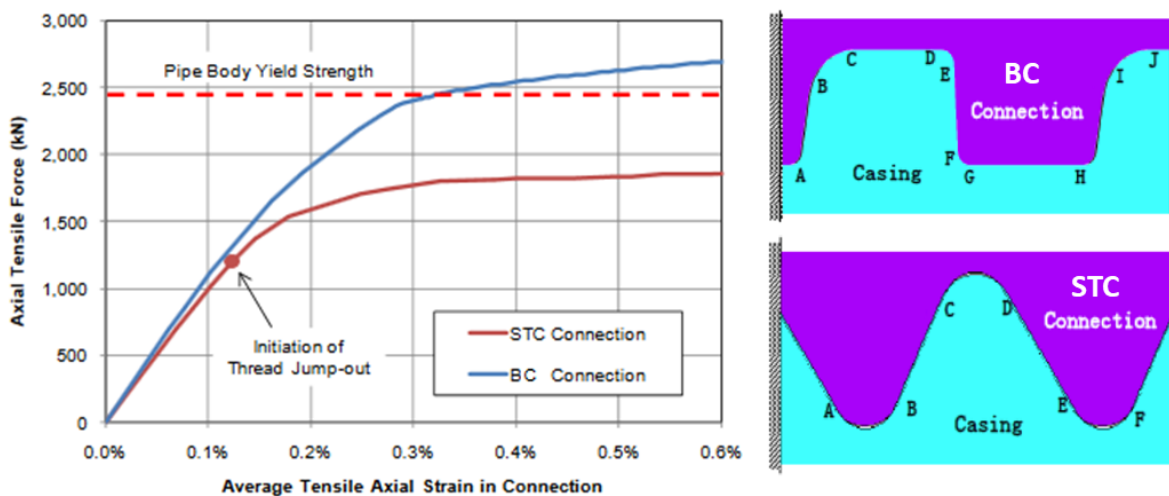

Figure B5. Axial force vs average axial strain of 177.8 mm, 34.2 kg/m Grade 80 API STC and BC connections under tensile loading [121].

71

B.3 Major geometrical characteristics of premium connections

Premium connections obtain their improved properties as the result of three major geometrical characteristics (Figure B6):

- Thread profile, which often relies on special buttress-like thread profiles with a combination of a negatively oriented load flank and a positive stab flank to maximize structural integrity and to avoid jump-out failures. Several failures analysis [122] [123] of such a type of connections agree on the root of the *last engaged thread* (LET) of the pin as the most susceptible location for fatigue damage. Anti-galling properties are improved by adopting the pitch change concept [124] to optimize the contact stress distribution over the threaded surface [54].

- Metal-to-metal seal, which ensures pressure integrity of the connections and eliminates the need of threads acting as a pressure seal. This design feature is particularly essential when gas tightness is required under high pressure and extreme temperatures. Since MTM seal represents the area of major interest for this project, it will be described in more detail later.

- Torque shoulder, which increases the contact surface to control make-up and for additional sealability. In order to further improve the structural strength while providing self-alignment to the connections, the angle of the torque shoulder and the load flank of the threads are designed to create the so-called wedge effect [11].

In addition to the elements listed above, a lubricant relief groove or dope pocket may be incorporated to accommodate excess of thread compound to avoid locally high stress levels in the threads during make-up, thus reducing the risk of connection failure.
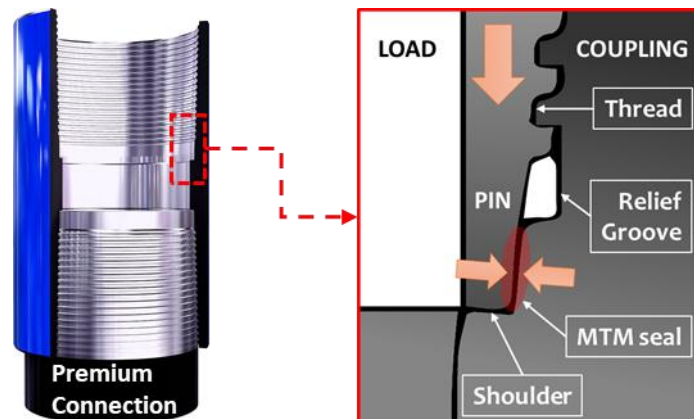

Figure B6. Premium connection (left) [8] and detail of major geometrical characteristics (right).

B.4 Lubrication: Connection make-up and break-out

Lubrication is required during connection make-up and break-out operations. These are performed within a wide range of ambient temperatures due to the variability of environmental conditions for different oil and gas wells around the world. This is particularly important for selecting a proper thread compound, which should be brushable and capable of adherence over a temperature range of -7 °C to 66 °C [6].

During make-up, one or more joints are connected by power tongs and lowered into the well. For this purpose, pipes are first aligned and then, the pin connection is placed with particular care not to create damage into the box or coupling connection (stabbing process). Based on factors such as diameter, material (steel grade), weight and connection type, the make-up torque is recommended by API (in case of API connections) [115] or connection manufacturers (in case of proprietary connections) [8] [11]. The actual make-up process consists in applying rotation (circumferential sliding) until the desired torque is reached. As mentioned above, make-up is carried out using power tongs while monitoring the joint make-up by means of computerized systems and assessing its goodness in accordance with recommendations. Back up tongs are used to break-out the connection. In order to provide the tong enough time for stalling before damage has occurred, manufacturers recommend low gear with low speed [11], *i.e.* below 5 RPM [8] for final make-up. A schematic of the torque application is given in Figure B7.
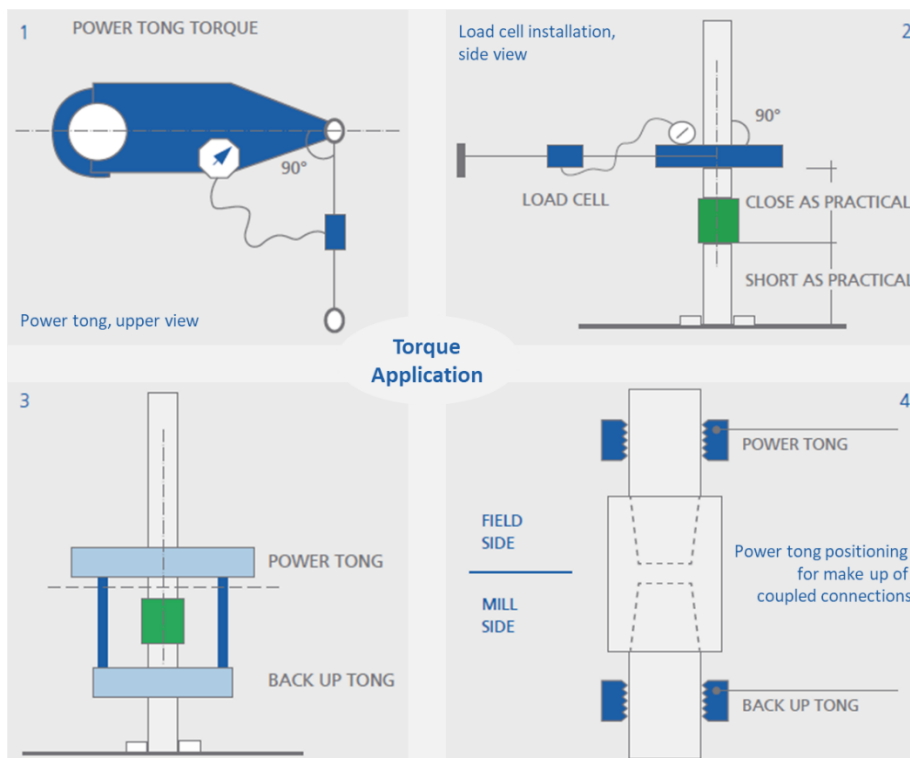

Figure B7. Torque application during make-up of coupled connections [8].

In general, the optimum torque falls within a range between maximum and minimum tabulated values, as is shown in Figure B8 for API 8 Round Connections and premium connections. Particularly, a typical torque profile of premium connections exhibits four basic component parts, namely (1) thread and seal interferences that can show an acceptable change in angle during seal engagement; (2) shoulder point; (3) delta torque and (4) delta turns. Given the criticality of the operation for both structural integrity and leak resistance, several criteria are closely monitored for not accepting a make up graph, such as low/high shoulder point, low/high final torque, short/incomplete graph, over torque with yield, erratic thread and seal build, not defined shoulder point, discontinuous delta torque [8] and many others. Similar care is taken during break-out operations, which are mainly carried out for inspection and replacement.
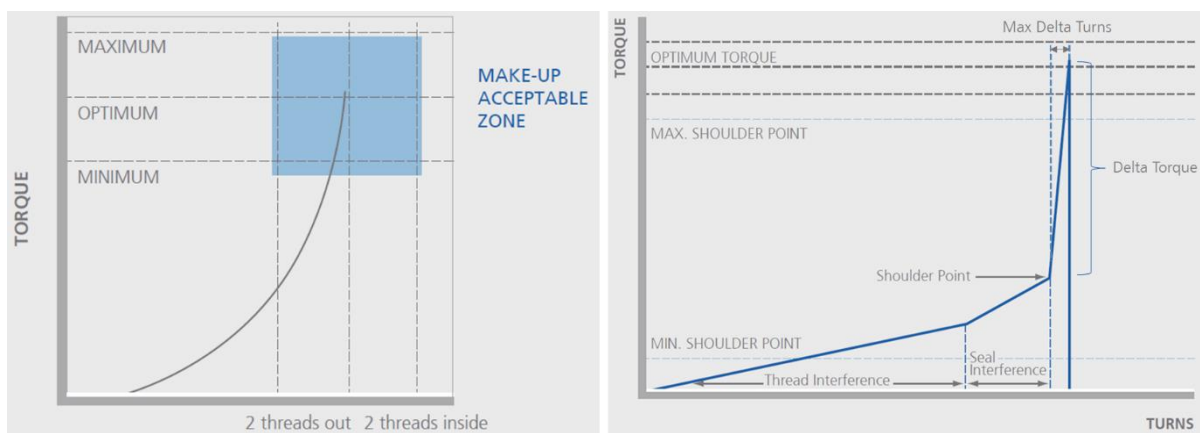

Figure B8. Typical Torque graph profile for API 8 Round Connections (left) and premium connections (right) [8].

B.5   Phosphate coating

The main failure mechanism associated with make-up/break-out operations is galling (Figure 4.2). The latter is a particular form of adhesive wear that involves the transfer of material between mating surfaces in contact. Galling causes functional failures such as oil and gas leakages and/or structural failures such as cracks and fatigue. From the previous statement, it follows that connection make-up affects sealing performance as nano- and micro-leaking channels may be created in between the mating surfaces. Hence, prior to connection make-up, the entire surface of the connections (threads, metal-to-metal seal, and shoulder surfaces) is usually treated by phosphating and subsequently coated with a thread compound to prevent galling [16]. The synergistic effect of phosphate coating and lubricant grease relies on the porosity given by the typical crystalline structure of phosphates acting as a good absorbent for the grease [125]. *Ernens and coworkers* [17] reported that the use of phosphate coating drastically improves surface damage prevention. For this purpose, surface finish, casing material grade and sliding conditions should also be taken into account in the realization of the tribological system that represents the premium connection. Besides, the porous structure helps in protection against corrosion during storage [126]. The deformation

capability of phosphate coatings allows them to absorb mechanical stresses during make-up and, presumably, maintaining an optimal sealing configuration [17] during the lifetime of the well.
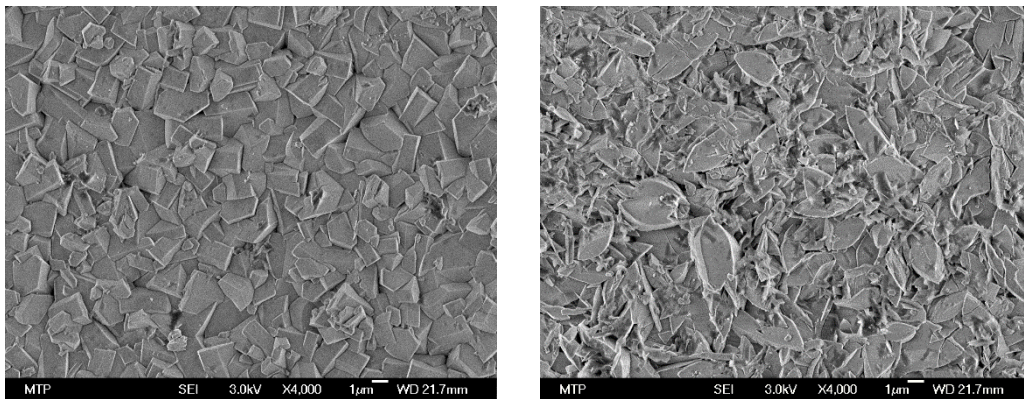

Figure B9. SEM images of steel surfaces treated with manganese (left) and zinc (right) phosphates. The scale bars represent 1 micrometer. The analyzed samples were provided by Shell.

Manganese and zinc phosphate are the most common types of coatings used. They exhibit characteristic plate and needle structures, respectively, as is shown in Figure B9. Although general trends suggest only coating one of the two sides of the connections is sufficient, Shell uses manganese phosphate on the box (coupling) and zinc phosphate on the pin. This choice probably depends upon the different mechanical properties of the two types of phosphates at the single asperity level, with zinc phosphate crystals showing higher nano-hardness compare to manganese phosphate. However, a so-called hard glaze layer is formed under continuous sliding for both materials [127].

C.   Fabrication methods of microchannels

The most common fabrication methods are listed below together with some useful tips:

▪ <u>Etching technology</u>. The substrate (glass, polymer or metal) is covered with an etchant-resistant protective layer (mask) that, in turn, is patterned so that the etched channels can have certain shapes (*e.g.* steps 3 in Figure C1 for silicon substrates). Different methods can be used to etch the substrates, namely a combination of wet/dry and anisotropic /isotropic etching processes [128]. In general, the geometry of the pattern (*e.g.* rectangles, squares and circles) affects the etching process and, therefore, the final shape of the channel. In wet etching, liquid chemicals (etchants) etch away from a wafer the material that is not protected by the mask. Lithography (see next method) is often used to pattern the masks on the wafers to reach precision in the order of micrometers. When the liquid chemicals remove materials at different rates depending upon the silicon crystalline plane that is exposed to the etchant, the process is called anisotropic wet etching. Instead, in case of isotropic wet etching, the material removal occurs at similar speed in both lateral and downward directions. Dry etching requires the use of plasmas or etchant gasses to etch away the substrate material. It can be (1) physical (dry) etching, which uses the high kinetic energy of

75

particle beams as etchant medium; (2) chemical (dry) etching, in which etchant gases chemically react to attack the substrate and (3) Reactive Ion Etching (RIE), *i.e.* a combination of both physical and chemical (dry) etching that is widely used in industry and research [129]. Dry etching is commonly used to etch glass and polymer substrates while wet etching is more suitable for metallic base materials [63]. Following channel etching, a glass or silicon wafer is bonded on top of the channel to close it. In such a way, it is possible to obtain various geometries.
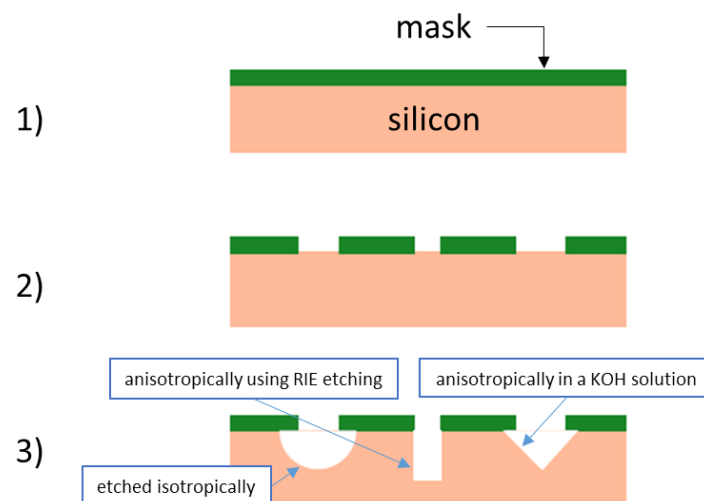

Figure C1. Steps for the etching of silicon substrates. 1) The silicon substrate is covered with a mask material. 2) The mask material is patterned and finally the 3) the silicon is etched to yield to microchannels [128].

- Lithography/photolithography. In a general sense, lithography refers to the method used to print "images" mainly on stones, metal plates, rubber and other plastics. Specifically for microfabrication, photolithography implies the use of light to transfer the geometric pattern onto a thin film of the substrate by means of a photomask, which allows light to pass through a defined pattern of holes [63]. In such a case, a light-sensitive chemical "photoresist" covering the wafer (for example applied by spin coating) is patterned by exposing it to light while it is protected by the photomask, as is shown in Figure C2. The resulting photoresist can be also used for future wet chemical etching or plasma etching. This expensive procedure is often applied to create microchannels in PDMS and PMMA.
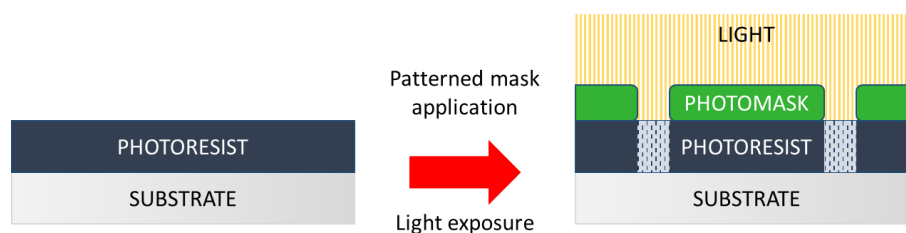

Figure C2. Patterning the photoresist during a photolithography process.

- Nanoimprinting. In a similar way as in nanoimprinting lithography (NIL), a mold with nanoscale protrusion patterns is used. The latter is placed over a very thin polymer layer on a substrate at elevated temperature and pressure in such a way that the displaced polymer will not completely fill the trenches on the mold. Nanochannels are then created as is shown in Figure C3. This single-step process can be applied to PMMA and many other polymer materials [130]. However, the mask fabrication represents a non-trivial obstacle.
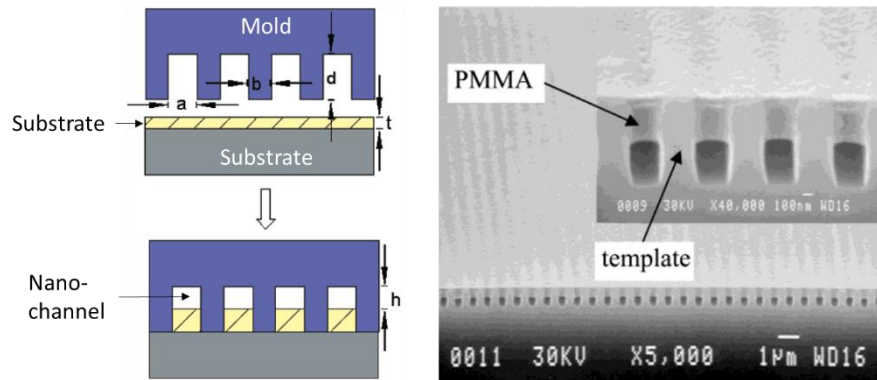

*Figure C3. Illustration of the key dimensional parameters for a multiple channel array template: **a**, trench width; **b**, ridge width; **d**, trench depth; **t**, initial thickness of the polymer layer; **h**, nanochannel height after NIL (left). SEM micrographs of imprinted nanofluidic channels having cross-sectional dimensions of 300 (width) x 500 nm (height) (right) [130].*

- Micromachining techniques. High-precision mechanical micro-cuttings allow to create ultra-precision components (*e.g.* microchannels) in a large number of materials, such as polymers and plastics, but also in steel, aluminum and brass. The most used mechanical cutting processes are micro milling and micro turning [63].
- Laser beam machining. In this process, a laser beam strikes the surface of the workpiece causing material ablation. The amount of energy of the photons is inversely proportional to the wavelength of the used laser. For this reason, shorter (UV) wavelength laser beams are more commonly used than longer infrared (IR) wavelength beams. Several kinds of laser sources are available in the market, from 145 nm wavelengths (UV) up to 10 μm, being 1064 nm the threshold between the two systems [63].
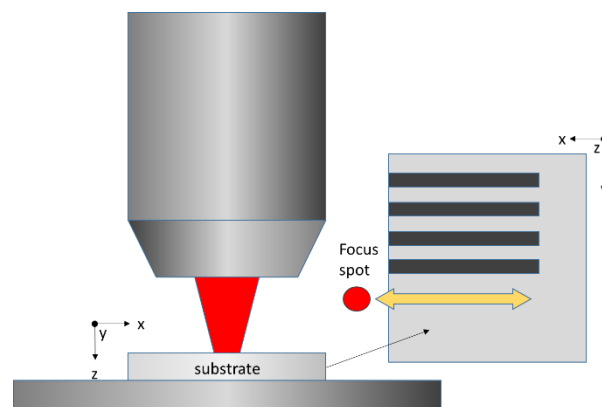

Figure C4. Example of laser set-up used for machining a workpiece.

- Thermal bonding of acrylic based microfluidics. This example represents a practical solution to bond two PMMA surfaces, one of which having open channels created with a method described above and the other serving as a lid. Referring to Figure C5, two aluminum plates can be used to apply pressure by screws from the top while heating the PMMA surfaces by a hot plate from the bottom, for a certain amount of time. The selection of a proper temperature for the material, the applied pressure, the bonding time and surface roughness determine the performance of the created bond [131].
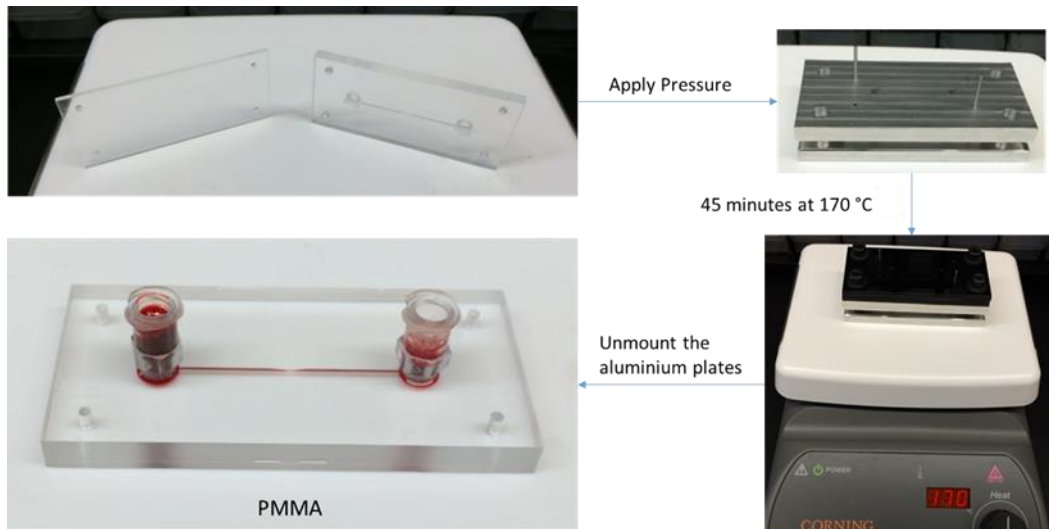

Figure C5. Using thermal bonding to prototype acrylic based microfluidics [131].

- "Cure and fix" method for PDMS-based microfluidic chips. In the case of PDMS microchannels, needles are often used as interconnection to the outside world by the "press-fit" method. Wang et al. [132] proposed a method to avoid damage of the PDMS chip due to unexpected bumps on the needles (Figure C6). As is shown in the right part of Figure C6, liquid PDMS is poured on top of the non-cured and fixed device before curing in such a way it will protect the interconnection and provide higher sealing.
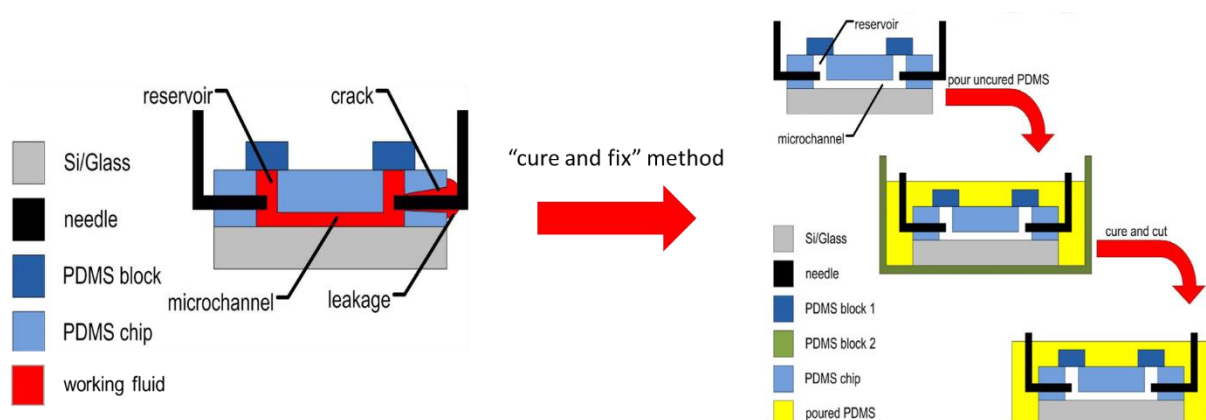

Figure C6. Mechanism of disturbance-caused leakage (left) and "cure and fix" method (right) [132].

- <u>Electrospinning</u>. Electrospinning can also be used to create microstructures [133]. This technique represents a versatile method to produce nanofibers. A polymer solution (*e.g.* PS) is placed into a syringe, which is fed by a syringe pump. A high-voltage power supply is connected to the needle of the syringe so that electrical forces stretch the jet of the polymer solution. Finally, fibers are collected onto a rotating collector [134]. A schematic representation of a typical electrospinning set-up is shown in Figure C7. The final fiber diameter depends upon relative humidity, temperature, flow rate (pump), applied voltage, viscosity and polymer type as well as its concentration [134] [135]. As is shown in Figure C8, in order to create microstructures from polymer fibers, the fibers are first aligned and then arranged in a solid matrix formed by a second polymer. The arranged fibers are subsequently dissolved by a selective solvent for the fibers, leaving a porous structure.
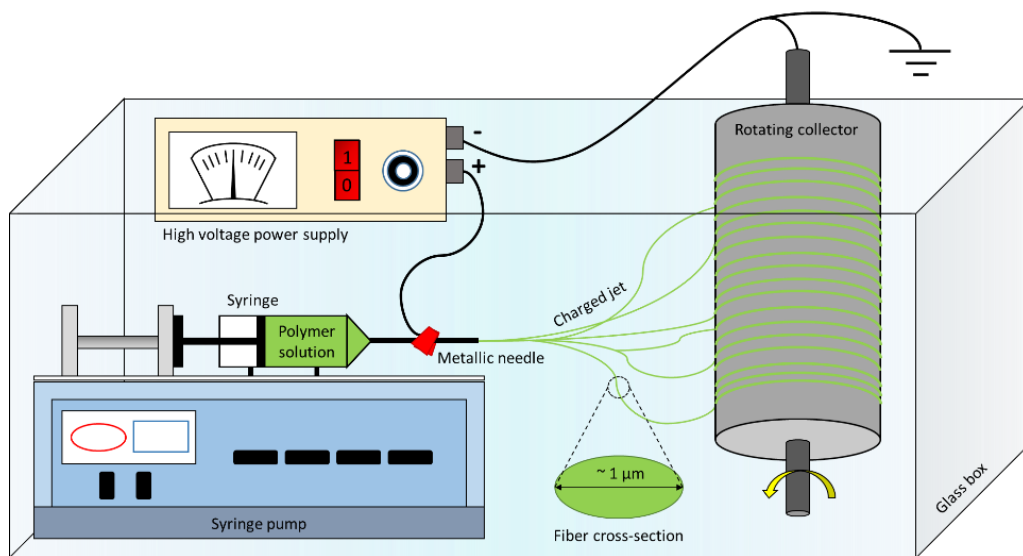

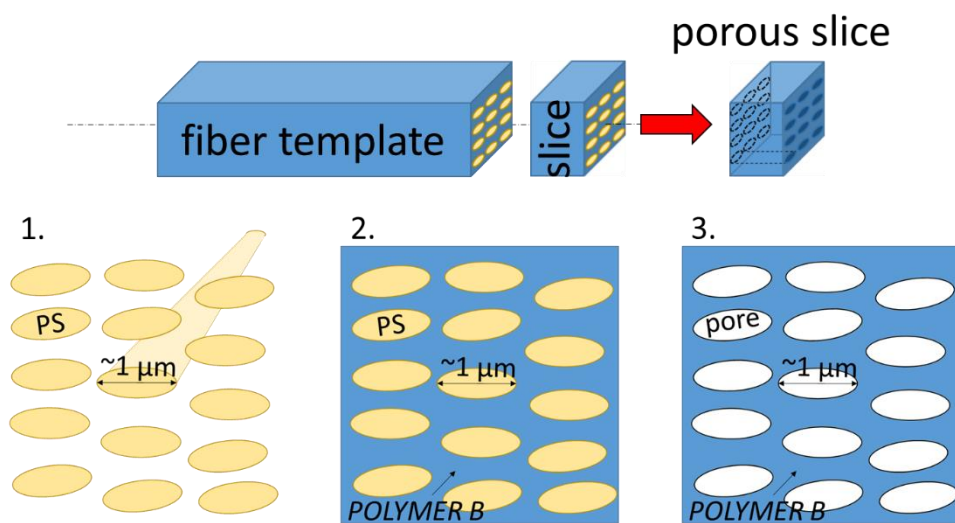*Figure C7. Schematic of a typical electrospinning set-up.*

Figure C8. Stages of the manufacturing process involving fibers in the realization of microstructures. 1. Fibers alignment; 2. Polymer-fiber template; 3. Porous polymer template.

D. Socio-technical system

Components of the environment
- Connection material
  L80, P110, Q125
- Coating
  Zinc and/or Manganese Phosphate
- Environ./Operational conditions
  Loading, contaminations

Physical mechanisms
Mechanical, Chemical, Thermal

Components of the artifact
- Base fluid
  Mineral oil
- Thickener
  Bentonite
- Group of additives
  Polymer particles
  Core-shell particles

Contexts
Oil and Gas
Wells
MTM seals
Tribology
Chemistry
Engineering
Viscoelasticity
Research

Effects
Environmental impact
Technical performance
Return of investment

Main project-involved Stakeholders
University (supplier)
Shell (customer)

Socio-technical system for the Design of an Environmentally Benign Thread Compound for Oil Well Joints

Artefact
Thread/Sealing Compound

External stakeholders

Operators
Health&safety
Make-up/break out/maintenance

Competitors
Thread Compound Manufacturers

Environmental Stakeholders
Organizations
Regulators

Technical Regulations
ISO, API, ASTM

Connection Thread Suppliers
Material grade/roughness/coating
Connection geometry

Feedbacks and resources
- human factors (supervisors, chemists, engineers, technicians)
- physical factors (materials, laboratories and test apparatus)
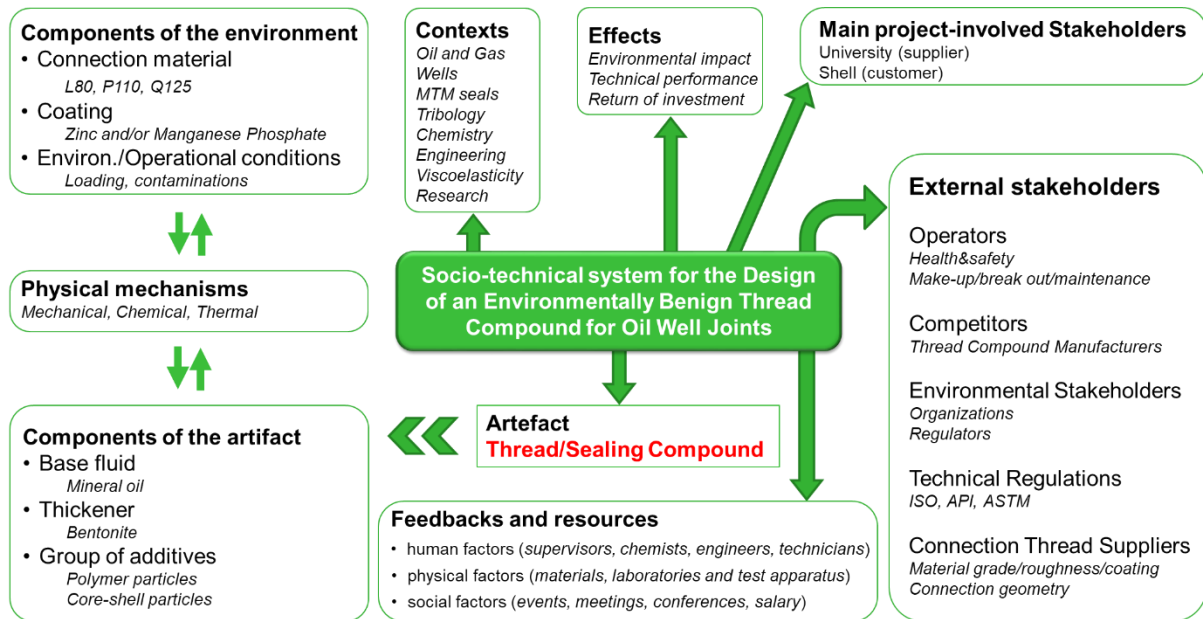- social factors (events, meetings, conferences, salary)

Figure D1. Socio-technical system for the design of an environmentally benign thread compound for oil well joints. Considering the context, the stakeholders are Shell, the university and other external stakeholders. The components of the artefact interact with each other and with the components of the artefact's environment (fixed by assumptions) by means of mechanical, chemical and thermal mechanisms. This interaction produces three main effects from three different perspectives. Human, physical and social factors are involved in the system.

E. Development phase: support figures and tables

Table E1. Comparison of weight loss percentages among base oil, base greases and API dope. Experimental conditions: oven, 250 °C, 55 hours, nitrogen environment.

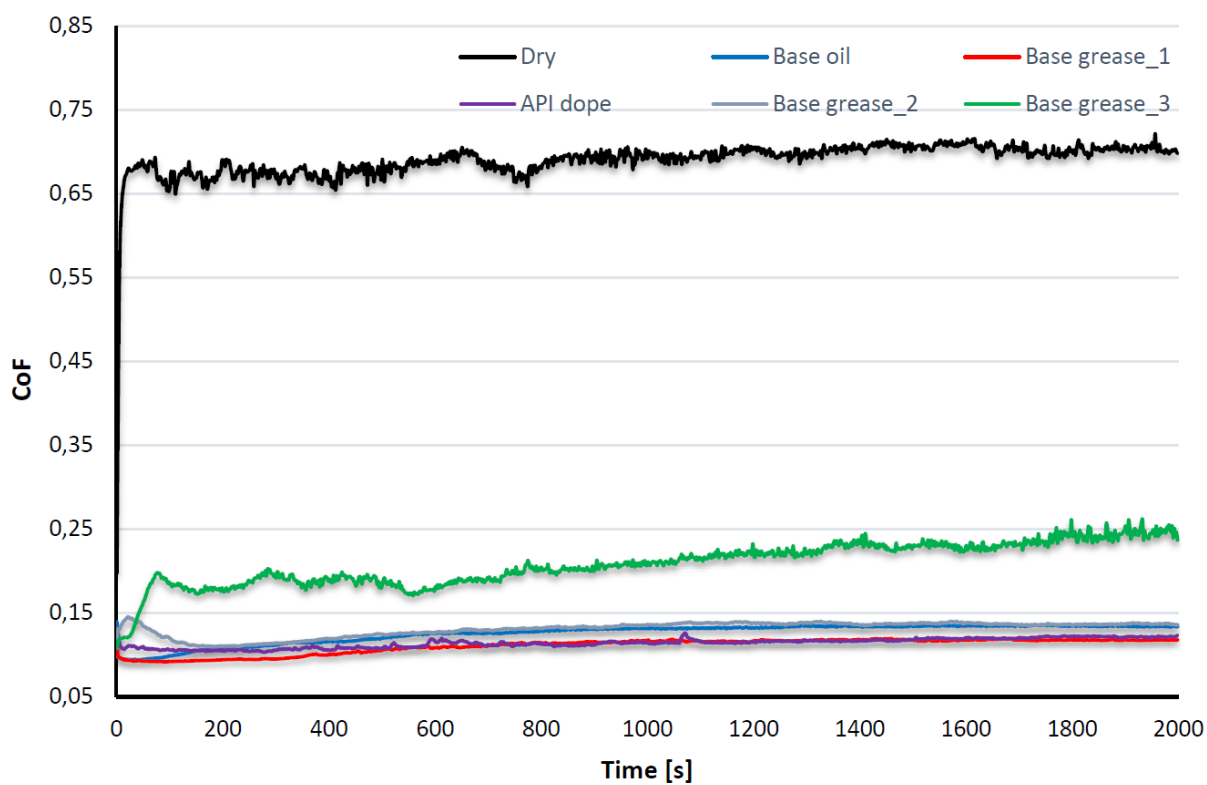| Sample name	Weight loss (%)
Base oil	49.4
Base grease_1	38.5
Base grease 2	67.1
Base grease_3	85.9
API dope	83.9

Figure E1. COF vs time (reciprocating pin-on-disc tests) for base oil, base greases and API dope in comparison with dry conditions.
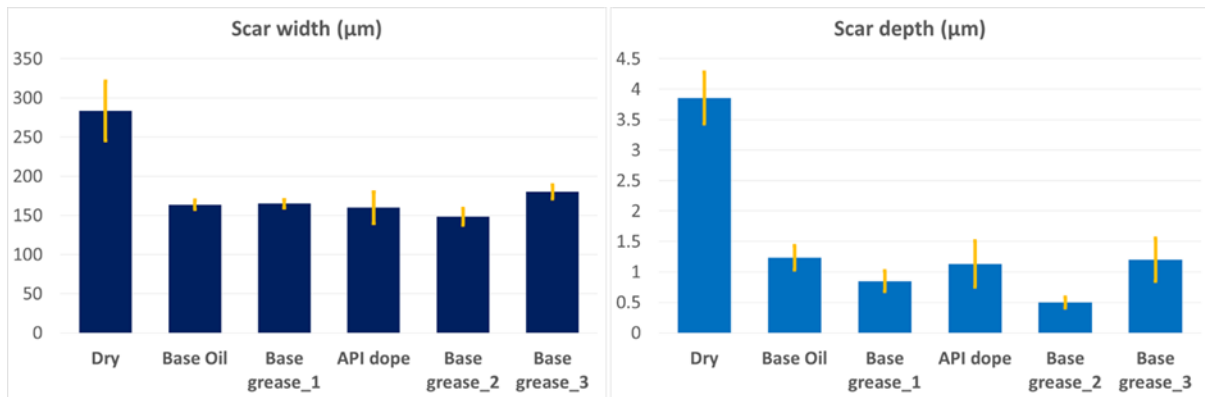
Figure E2. Scar width (left) and depth (right) as calculated from optical microscopy images for dry conditions, base oil, API dope and the three provided base greases. The error bars indicate the standard deviation (n=3).
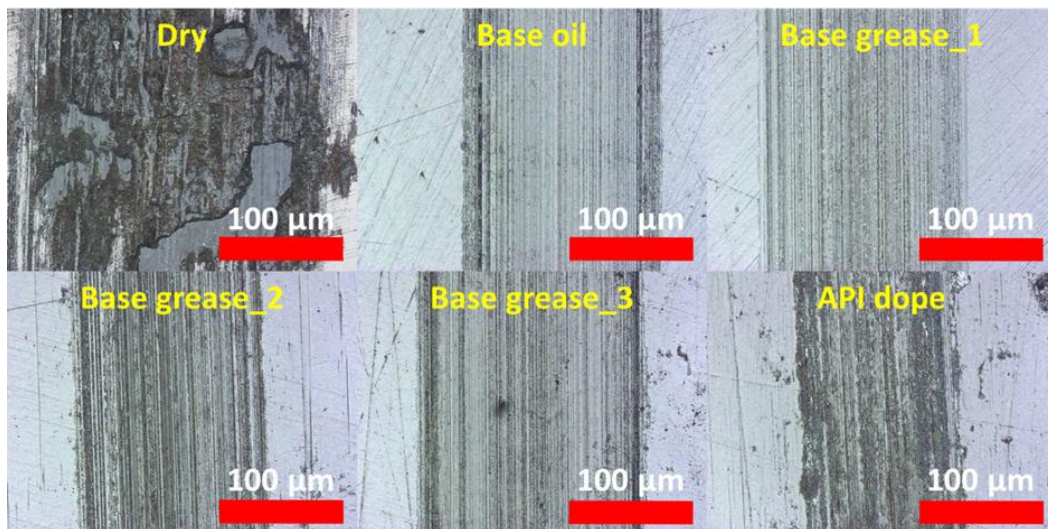

Figure E3. Confocal microscope images of wear scars after pin-on-disk tests for dry conditions, base oil, three base greases and API dope. The images were taken by confocal microscope and analyzed by VK Analyzer.
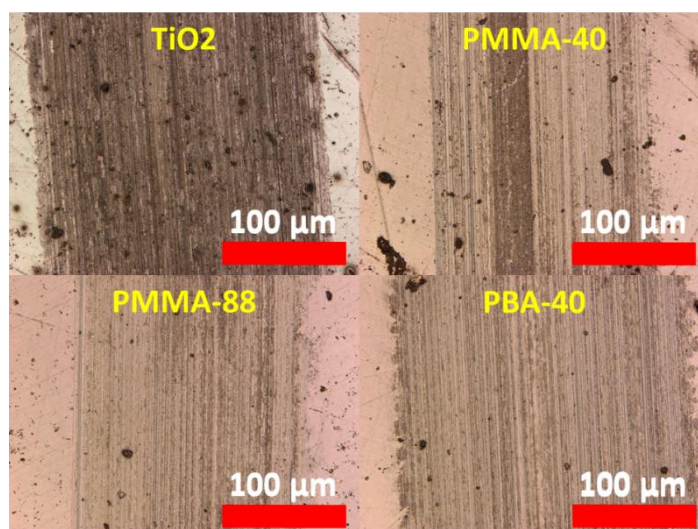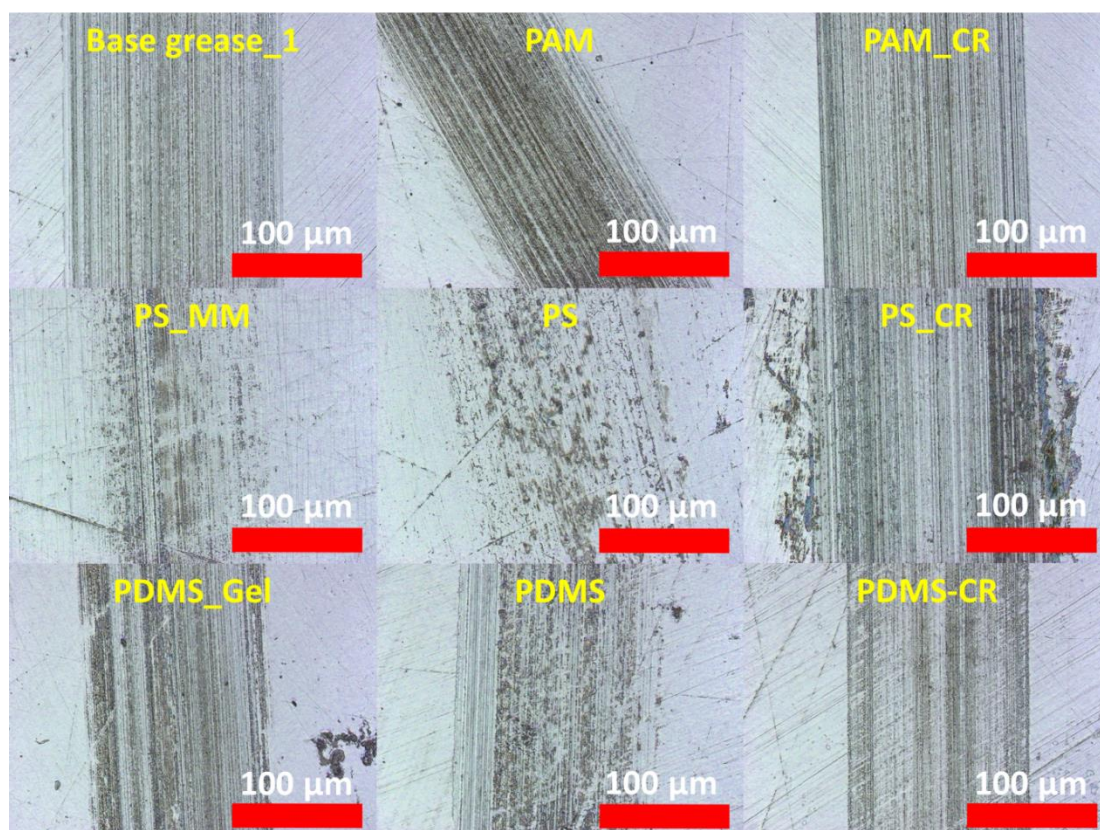
Figure E4. Confocal microscope images of wear scars after pin-on-disk tests of base grease_1 and thread compounds made with all the particles tested in this project. The images (in the previous page and above) were taken by confocal microscope and analyzed by VK Analyzer.
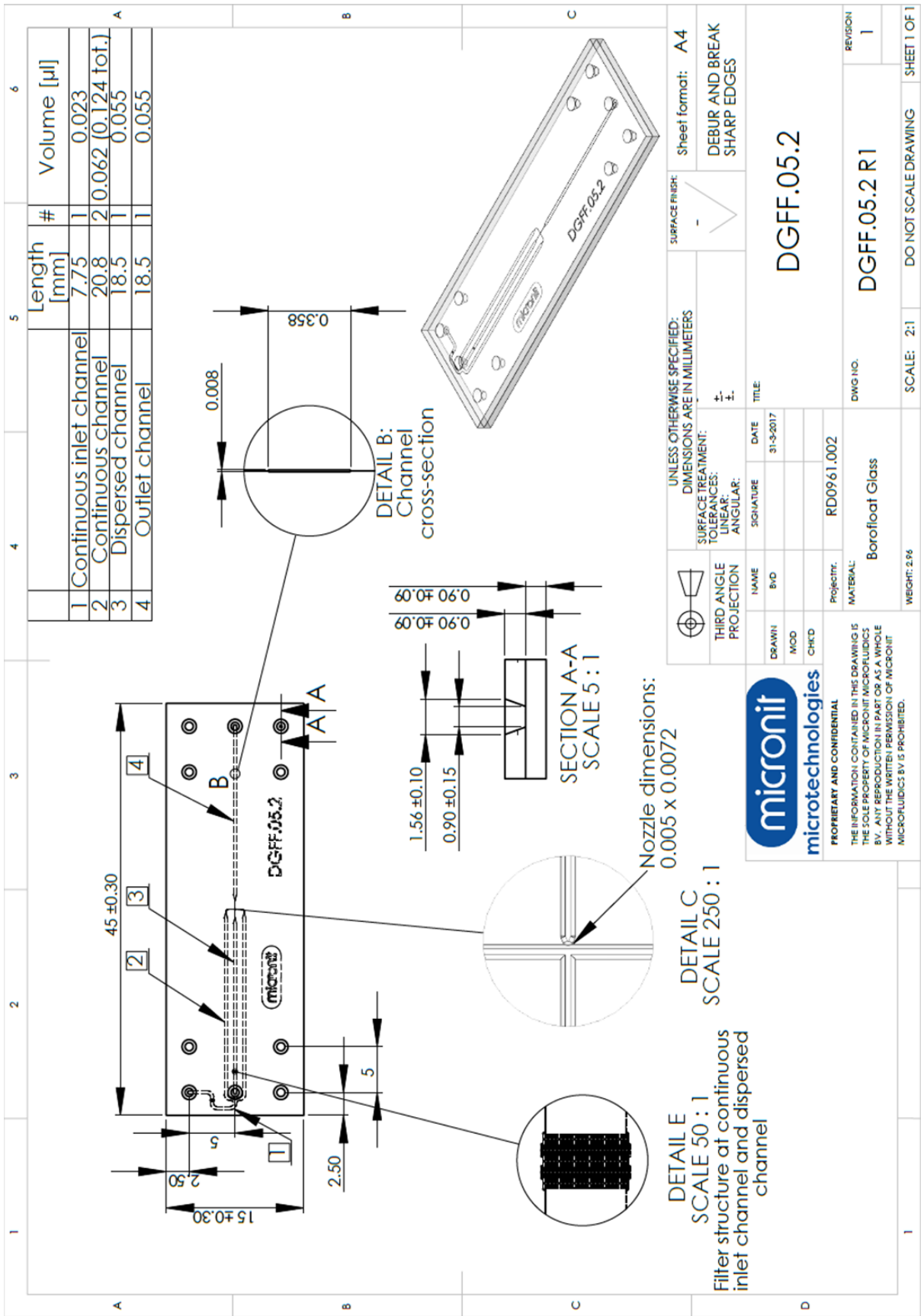
Figure E5. Technical drawing of Micronit microchip equipped with 5-µm nozzle.
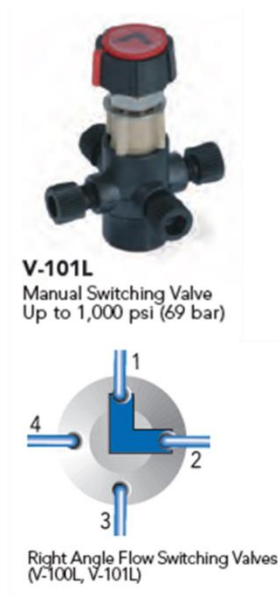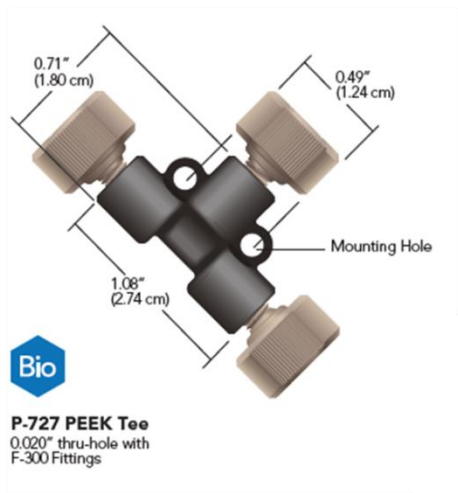
Part No.	Description	Threads	Includes	Thru-hole	Swept Volume	Pressure Rating	Qty.
PEEK TEES AND CROSSES							
P-727	PEEK Tee for 1/16" OD Tubing	10-32 Coned	(3) F-300	0.020" (0.50 mm)	0.57 µL	3,500 psi (241 bar)	ea.

Part No.	Description	Tubing/Fitting Size	Wetted Material	Configuration	Includes	Qty.
SWITCHING						
V-101L	4-Position, 4-Port, Bulkhead, 500 psi (34 bar)	1/4-28 Ports for 1/16" OD Tubing	PEEK, PTFE	Right-Angle "L"	**	ea.

Figure E6. Specifications and drawings of P-727 PEEK Tee and V-101L right angle flow switching valve.

The first specification table (0 psi to 250 psi):

Characteristic	0 psi to 250 psi Typ.	0 psi to 250 psi Max.	Unit	Note
Span	–	212 ±68	mV	1
Null offset	–	0 ±30	mV	2
Linearity (Best Fit Straight Line, P2>P1)	±0.2	±1.0	%span	3
Null shift (0 °C to 25 °C, 25 °C to 50 °C)	±1.0	–	mV	4
Span shift (0 °C to 25 °C, 25 °C to 50 °C)	±5.0	–	%span	5
Repeatability and hysteresis	±0.5	–	mV	6
Overpressure	–	250	psi	7

Symbol	Description
Vcc	supply
OUTPUT A	bridge positive output
GROUND	ground
OUTPUT B	bridge negative output

Characteristic	Min.	Typ.	Max.	Unit	Note
Supply voltage	2.5	10	12	Vdc	–
Input resistance	4	5	6	kOhm	–
Output resistance	4	5	6	kOhm	–
Time response	–	–	1	ms	2

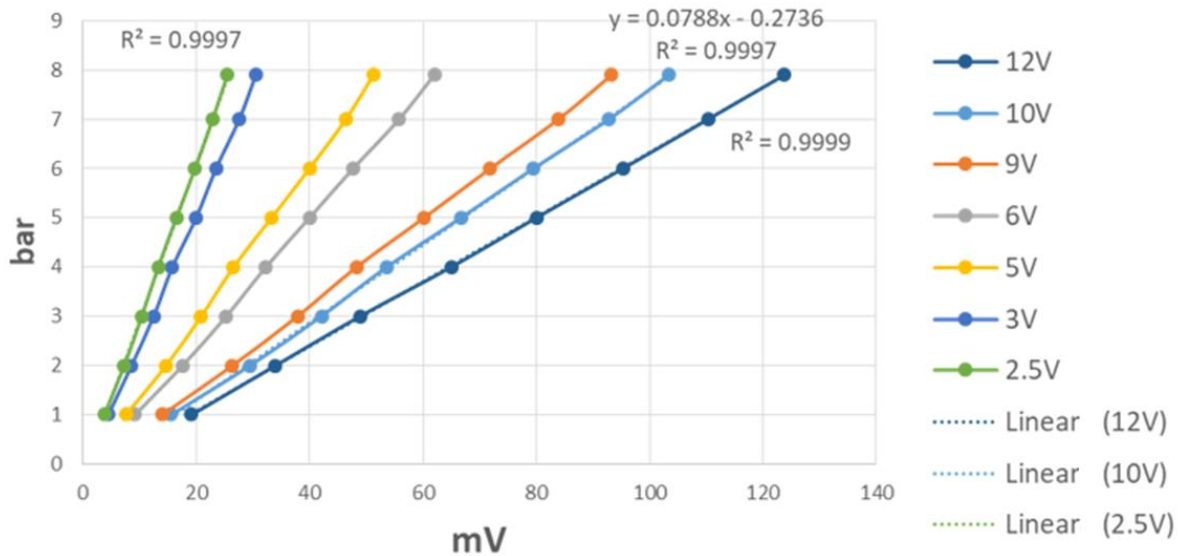*Figure E7. Specifications and drawings of Honeywell pressure transducer 24PCGFB6G.*

Figure E8. Calibration curve varying voltage from the power supplier.
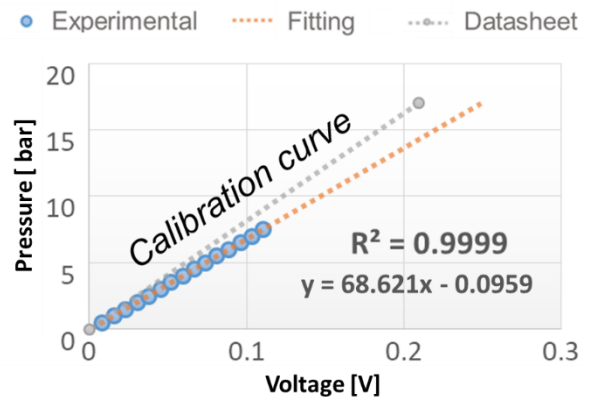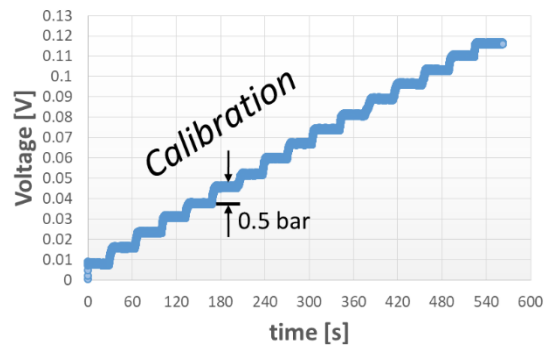
Figure E9. Manual calibration by multimeter (left) and corresponding calibration curve (right). Note that the coefficients of the curve are different from the previous graph because the calibration with 10 Volt (best) was performed again in a more accurate way.
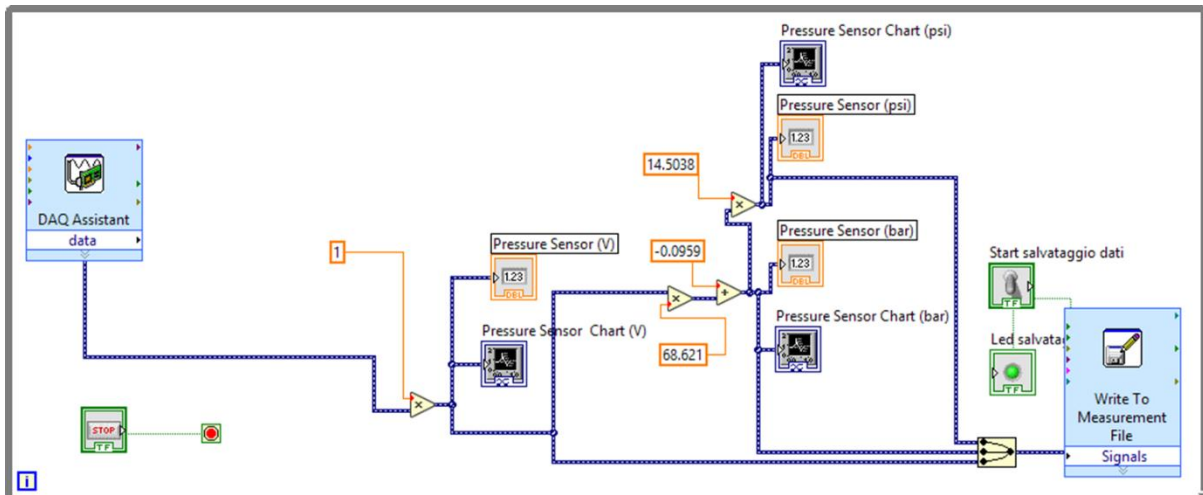

Figure E10. LabVIEW script used for the acquisition and the volt/psi/bar conversion based on the calibration curve.

DEVICE SPECIFICATIONS

NI USB-6008

USB, 8 AI (12-Bit, 10 kS/s), 2 AO (12-Bit), 12 DIO

The following specifications are typical at 25 °C, unless otherwise noted. For more information about the NI USB-6008, refer to the *NI USB-6008/6009 User Guide* available from *ni.com/manuals*.

Analog Input

Analog inputs	
Differential	4
Single-ended	8, software-selectable
Input resolution	
Differential	12 bits
Single-ended	11 bits
Maximum sample rate (aggregate)	10 kS/s, system dependent
Converter type	Successive approximation
AI FIFO	512 bytes
Timing resolution	41.67 ns (24 MHz timebase)
Timing accuracy	100 ppm of actual sample rate
Input range	
Differential	±20 V[1], ±10 V, ±5 V, ±4 V, ±2.5 V, ±2 V, ±1.25 V, ±1 V
Single-ended	±10 V
Working voltage	±10 V
Input impedance	144 kΩ

Figure E11. Specifications of the NI USB-6008 DAQ card. The red circle indicates the selected range to be used with LabVIEW.
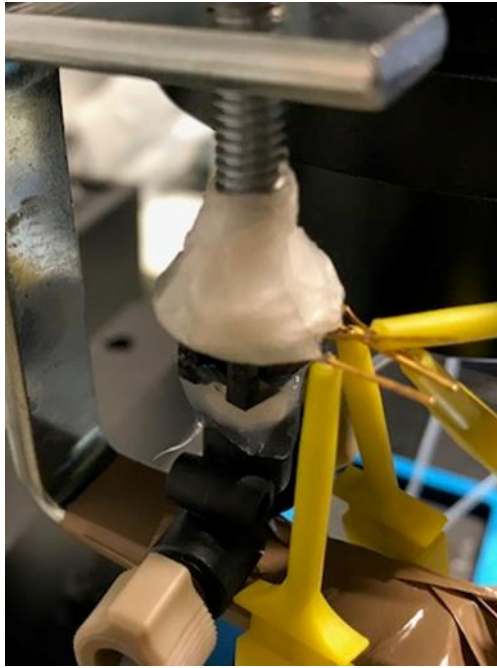
Figure E12. Connection of the pressure transducer to the tee junction and to the electric plugs. Note the pressure sensor was properly glued and kept in little compression (not affecting the measurements) for the overall duration of the testing period.
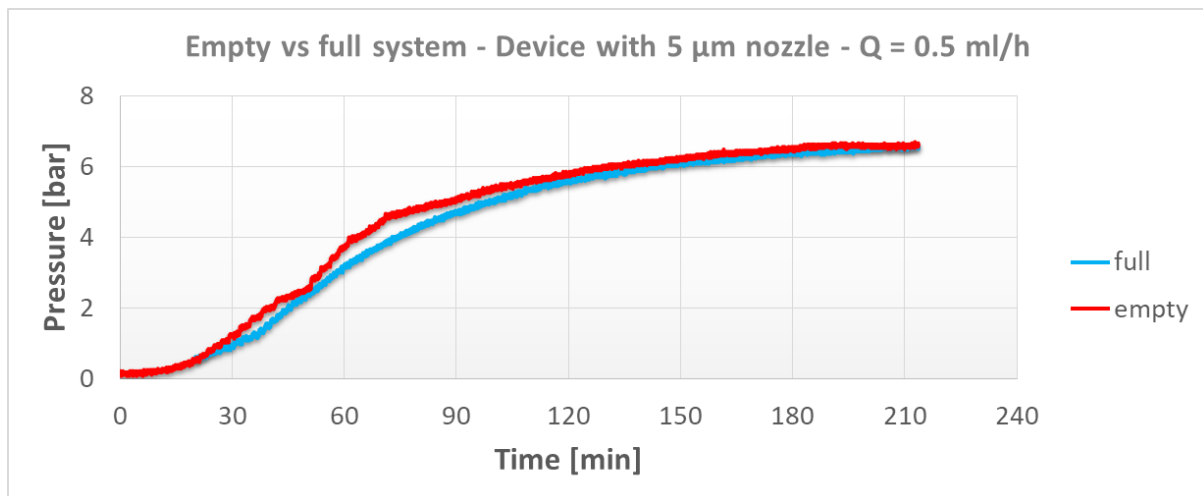
Figure E13. Effect of filling the microchannels (device with 5 µm nozzle) before test and effect of using a higher flow rate (Q = 0.5 ml/h) than 0.3 ml/h. In the test with empty channels, the hydraulic resistance is higher due to the friction with the walls and a certain time is needed for the flaw to stabilize (red curve). The blue line (flow inside an already filled microchannel), instead, is more gradual since the flow is facilitated by the presence of the previous amount of water, which reduces the force required to overcome the friction with the walls and allow the flow. At the set flow rate (0.5 ml/h), both curves show that the steady state is reached at p > 6 bar. Considering the limit of 10 bar given by the syringe (see calibration), the pressure range between pressure at the steady state and syringe limit is too small. For this reason Q = 0.3 ml/h was selected as a suitable flow rate for the sealing tests.
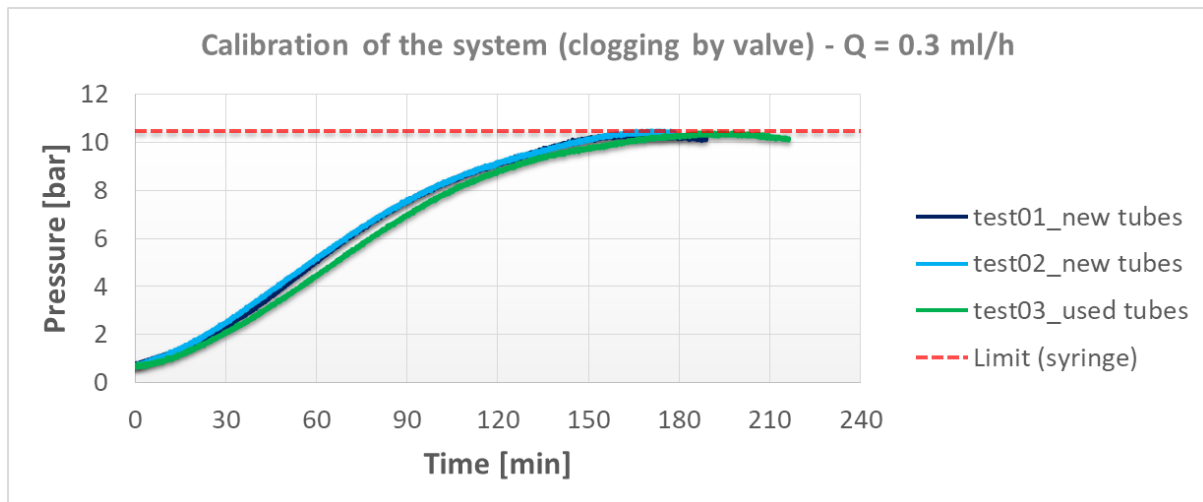
Figure E14. Calibration of the system closing the valve and measuring the pressure while sending a water flow at Q = 0.3 ml/h. Note that no device (neither microfluidic chip nor capillary tube) was used for the calibration. The red dashed line indicates the limit of the system given by the deformation of the plastic syringe. Note also the good reliability of the system given by the agreement between the three curves in the graph (the green curve refers to the repetition of test02 without changing tubes). The length of the tubes was kept constant for all the tests.

References

[1]   Exxon Neftegas Limited, "Sakhalin-1 Project - Project history," [Online]. Available: http://www.sakhalin-1.com/en-ru/company/about-us/about-sakhalin-1-project/history.

[2]   Society of Petroleum Engineers, *Petroleum Engineering Handbook - Drilling Engineering,* vol. 2, Austin, USA, Texas: Robert F. Mitchell, 2006.

[3]   H. O. Björnsson, *Casing Coupling for Extreme Temperature Setting,* Reykjavik University, 2015.

[4]   J. Xie, *Investigation of Casing Connection Failure Mechanisms in Thermal Wells,* Canada: WHOC, 2009.

[5]   API Spec. 5CT/ISO 11960, *Casing and Tubing,* American Petroleum Institute, 2005.

[6]   API RP 5A3/ISO 13678, *Thread Compounds for Casing, Tubing, and Line Pipe,* American Petroleum Institute, 2003.

[7]   F. P. Ràfols, *Modelling and Numerical Analysis of Leakage Through Metal-to-Metal Seals,* Luleå University of Technology. Department of Engineering Science and Mathematics, Division of Machine Elements, 2016.

[8]   Tenaris, "TenarisHydril Runnig Manual," 2016. [Online]. Available: https://www.google.nl/url?sa=t&rct=j&q=&esrc=s&source=web&cd=3&ved=0ahUK Ewilzu-e2PzWAhUIvBoKHepXALwQFghAMAI&url=http%3A%2F%2Fwww.tenaris.com%2F~ %2Fmedia%2FFiles%2FProductLiterature%2FLiteraturePremiumConnections%2FRun ningManual%2FTenarisHydril_RunningManu.

[9]   P. Gloeckner and F. Ebert, *Micro-Sliding in High-Speed Aircraft Engine Ball Bearings,* vol. 53, Tribology Transactions, 2010, pp. 369-375.

[10]   Y. Oku, M. Sugino, Y. Ando, T. Makino, R. Komoda, D. Takazaki and M. Kubota, *Fretting fatigue on thread root of premium threaded connections,* Japan: Elsevier. Tribology International, 2016.

[11]   Vallourec, "VAM Book," VAM, November 2017. [Online]. Available: http://www.vamservices.com/Library/files/VAM%C2%AE%20Book.pdf.

[12]   T. K. Frost, I. Nilssen, J. Neff, D. A. Battelle and K. E. Lunde, *Toxicity of Drilling Discharges,* 2006.

[13]   E. O. Aluyor and M. Ori-jesu, *Biodegradation of minaral oils - A review,* vol. 8, Benin City: African Journal of Biotechnology, 2009, pp. 915-920.

[14]   K. Matthews, "HDD Tech Talk: The Importance of Thread Compound," Trenchless Technology, 4 May 2018. [Online]. Available: https://trenchlesstechnology.com/importance-thread-compound-hdd/.

[15]   B. Chesnut, "Drill Pipe Under-Torque: The Devil in Disguise," Trenchless Technology, 19 April 2016. [Online]. Available: https://trenchlesstechnology.com/drill-pipe-torque-devil-disguise/prettyPhoto/0/.

[16]   K. Inose, M. Sugino and K. Goto, *Influence of Grease on High-Pressure Gas Tightness by Metal-to-Metal Seals of Premium Threaded Connections,* Japan: Tribology Online. Steel Research Laboratories, Nippon Steel and Sumitomo Metal Corporation, 2016.

[17]   D. Ernens, E. J. v. Riet, M. d. Rooij, H. R. Pasaribu, W. v. Haaften and D. J. Schipper, *The Role of Phosphate Conversion Coatings in Make-up and Seal Ability of Casing Connections,* SPE Drill Complet, 2018.

[18]   Engineering ToolBox, "Oil - Lubrication and Temperature Limits," 2009. [Online]. Available: https://www.engineeringtoolbox.com/oil-temperature-limits-lubrication-d_1492.html.

[19]   E. Booser, *CRC handbook of lubrication volume II: theory and design,* 1984.

[20]   A. v. Beek, *Advanced engineering design : lifetime performance and reliability,* TU Delft, 2012.

[21]   M. Paszkowski, *Some Aspects of Grease Flow in Lubrication Systems and Friction Nodes,* Tribology Fundamentals and Advancements, 2013.

[22]   R. Czarny, *Effect of changes in grease structure on sliding friction,* vol. 47, Industrial Lubrication and Tribology, 1995, pp. 3-7.

[23]   D. M. Pirro and M. W. E. Daschner, *Lubrication Fundemantals, Third Edition,* CRC Press, 2016.

[24]   J. Flink, Water-based chemicals and technology for drilling, completion and workover fluids, Elsevier, 2015.

[25]   Noria Corporation , "Solid Film Lubricants: A Practical Guide," 2006. [Online]. Available: https://www.machinerylubrication.com/Read/861/solid-film-lubricants.

[26]   R. B. PortWood, *Lubrication Requirements of Rotary Shouldered Tool Joint,* vol. 8, NLGI Spokesman, 1981.

[27]   M. Sateva, M. Koren-Markovic, L. Kondres, S. Zajcic and N. Janusic, "Thread compound developed from solid grease base and the relevant preparation procedure". Croatia Patent 5,885,941, 23 March 1999.

[28] H. C. Zweifel, "Lubricating and sealing composition of flake copper, powdered lead, graphite, and petroleum vehicle". USA Patent 2,543,741, 27 February 1951.

[29] N. L. Jacobs, "Graphite-containing lubricant composition". USA Patent 5,049,289, 17 September 1991.

[30] Wikibooks, "Introduction to Inorganic Chemistry/Metals and Alloys: Mechanical Properties," 2017. [Online]. Available: https://en.wikibooks.org/w/index.php?title=Introduction_to_Inorganic_Chemistry/Metals_and_Alloys:_Mechanical_Properties&oldid=3295097.

[31] K.Persson and M. Fathi-Najafi, *Desiderable particles: Greases containing solid particles,* Lubrisense White Paper, 2009.

[32] O. Rohr, *Bismuth – the new ecologically green metal for modern lubricating engineering,* vol. 54, Tribology, 2002, pp. 153-164.

[33] A. Mlynarczak, *The aftermarket additives used in lubricating oils,* vol. 20, Gdynia, Poland: Journal of KONES Powertrain and Transport, 2013.

[34] J. Burbank and M. Woydt, *Friction and wear reductions in slip-rolling steel contacts through pre-conditioned chemical tribofilms from bismuth compounds,* Vols. 360-361, Wear, 2016, pp. 29-37.

[35] S. Wan, A. K. Tieu, Y. Xia, H. Zhu, B. H. Tran and S. Cui, *An overview of inorganic polymer as potential lubricant additive for High temperature tribology,* vol. 102, TribologyInternational, 2016, pp. 620-635.

[36] G. Ngail, J. Cochran and D. Stark, *Formulation of polymer-based lubricant for metal forming,* vol. 221, Proc. IMechE. Part B: J. Engineering Manufacture, 2006.

[37] S. T. Krawiec, *The influence of polymer fillers in a grease lubricant on the tribological performance of friction nodes operating under mixed friction conditions,* vol. 7, Archives of Civil and Mechanical Engineering, 2007, pp. 121-128.

[38] R. M. Bielecki, E. M. Benetti, D. Kumar and N. D. Spencer, *Lubrication with Oil-Compatible Polymer Brushes,* vol. 45, Tribology Letters, 2012, pp. 477-87.

[39] E. F. Lucas, C. R. E. Mansur, L. Spinelli and Y. G. C. Queirós, *Polymer science applied to petroleum production,* vol. 81, Pure and Applied Chemistry, 2009, pp. 473-494.

[40] A. Z. Abidin, T. Puspasari and W. A. Nugroho, *Polymers for Enhanced Oil Recovery Technology,* vol. 4, Procedia Chemistry, 2012, pp. 11-16.

[41] J. E. Woodrow, J. N. Seiber and G. Miller, *Acrylamide Release Resulting from Sunlight Irradiation of Aqueous Polyacrylamide/Iron Mixtures,* vol. 56, Journal of Agricultural and Food Chemistry, 2008, pp. 2773-2779.

[42] K. Lee, Y. Hwang, S. Cheong, Y. Choi, L. Kwon, J. Lee and S. H. Kim, *Understanding the Role of Nanoparticles in Nano-oil Lubrication,* vol. 35, Tribology Letters, 2009, p. 127–131.

[43] D. X. Peng, Y. Kang, R. M. Hwang, S. S. Shyr and Y. P. Chang, *Tribological properties of diamond and SiO2 nanoparticles added in paraffin,* vol. 42, Tribology International, 2009, pp. 911-917.

[44] Z. J. Zhang, D. Simionesie and C. Schaschke, *Graphite and Hybrid Nanomaterials as Lubricant Additives,* vol. 2, Lubricants, 2014, pp. 44-65.

[45] N. Xu, M. Zhang, W. Li, G. Zhao, X. Wang and W. Liu, *Study on the selectivity of calcium carbonate nanoparticles under the boundary lubrication condition,* vol. 307, Wear, 2013, pp. 35-43.

[46] P. Rabaso, F. Ville, F. Dassenoy, M. Diaby, P. Afanasiev, J. Cavoret, B. Vacher and T. L. Mogne, *Boundary lubrication: Influence of the size and structure of inorganic fullerene-like MoS2 nanoparticles on friction and wear reduction,* vol. 320, Wear, 2014, pp. 161-178.

[47] J. Joly-Pottuz, F. Dassenoy, M. Belin, B. Vacher, J. M. Martin and N. Fleischer, *Ultralow-friction and wear properties of IF-WS2 under boundary lubrication,* vol. 18, Tribology Letters, 2005, pp. 477-485.

[48] M. Kao and C. Lin, *Evaluating the role of spherical titanium oxide nanoparticles in reducing friction between two pieces of cast iron,* vol. 483, Journal of Alloys and Compounds, 2009, pp. 456-459.

[49] Y. Y. Wu, W. C. Tsui and T. C. Liu, *Experimental analysis of tribological properties of lubricating oils with nanoparticles additives,* vol. 262, Wear, 2007, pp. 819-825.

[50] L. Zhang, L. Chen, H. Wan, J. Chen and H. Zhou, *Synthesis and Tribological Properties of Stearic Acid-Modified Anatase (TiO2) Nanoparticles,* vol. 41, Tribology Letters, 2011, pp. 409-416.

[51] L. Bogunovic, S. Zuenkeler, K. Toensing and D. Anselmetti, *An Oil-Based Lubrication System Based on Nanoparticular TiO2 with Superior Friction and Wear Properties,* vol. 59, Tribology Letters, 2015, p. 29.

[52] K. Matyjaszewski and X. Jianhui, *Atom Transfer Radical Polymerization,* vol. 101, Chemical Reviews, 2001, pp. 2921-2990.

[53] K. Matyjaszewski, *Atom Transfer Radical Polymerization (ATRP): Current Status and Future Perspectives,* vol. 45, Macromolecules, 2012, pp. 4015-4039.

[54] T. Galle, W. Waele, P. Baets and J. V. Wittenberghe1, *Influence of design features on the structural integrity of threaded pipe connections,* Ghent, Belgium: Sustainable Construction and Design, 2011.

[55] J. V. Wittenberghe, *Experimental Analysis and Modelling of the Fatigue Behaviour of Threaded Pipe Connections,* Gent: Ghent University. Department of Mechanical Construction and Production, 2011.

[56] C. Santus, *Fretting fatigue of aluminum alloy in contact with steel in oil drill pipe connections, modeling to interpret test results,* vol. 30, International Journal of Fatigue, 2008, pp. 677-688.

[57] L. Canhasi, *Numerical investigation on the effects of out-of-flatness on leakage in metal-to-metal seals,* Luleå University of Technology, 2017.

[58] API RP 5C5/ISO 13679, *Evaluation procedures for casing and tubing connections,* American Petroleum Institute, 2003.

[59] I. Nitta and Y. Matsuzaki, *Experimental Study of the Performance of Static Seals Based on Measurements of Real Contact Area Using Thin Films,* vol. 132, Journal of Tribology, 2010.

[60] S. Geoffry and M. Prat, *On the Leak Through a Spiral-Groove Metallic Static Ring Gasket,* vol. 126, Journal of Fluids Engineering, 2004, pp. 48-54.

[61] F. Robbe-Valloire and M. Prat, *A model for face-turned surface microgeometry. Application to the analysis of metallic static seals,* vol. 264, Wear, 2008, pp. 980-989.

[62] T. Nakamura and K. Funabashi, *Effects of directional properties of roughness and tangential force on pressure flow between contacting surfaces,* vol. 4, Lubrication Science, 1991, pp. 13-23.

[63] S. Prakash and S. Kumar, *Fabrication of microchannels: A review,* vol. 229, Proc. IMechE. Part B: J. Engineering Manufacture, 2014, pp. 1273-1288.

[64] P. Tabeling, *Introduction to Microfluidics,* Oxford University Press, 2005.

[65] H. Bruus, *Acoustofluidics 1: Governing equations in micrfluidics,* vol. 11, Lab on a Chip, 2011, p. 3742.

[66] Y. Ghasemi, *Aggregates in Concrete Mix Design,* Luleå, Sweden: Luleå University of Technology, 2017.

[67] F. Larrard, *Concrete Mixture Proportioning. A scientific approach,* vol. 9, London and New York: E & FN SPON. An Imprint of Routledge. Modern Concrete Technology, 2011.

[68] T. Hales, *A formal proof of the Kepler Conjecture,* 2 ed., vol. 6, Forum of Mathematics, Pi, 2017.

[69] G. D. Scott and D. M. Kilgour, *The density of random close packing of spheres,* Toronto, Canada: Department of Physics, University of Toronto, 1969.

[70] D. Cumberland and R. Crawford, *The packing of particles,* Amsterdam: Elsevier. Handbook of powder technology, 1987.

[71] S. Yamada, J. Kanno and M. Miyauchi, *Multi-Sized Sphere Packing,* Japan and U.S.A: Kyoto Sangyo University, Louisiana Tech University, NTT Communication Sciencce Labs, 2009.

[72] S. V. Kumar and M. Santhanam, *Particle packing theories and their application in concrete mixture proportioning: A review,* The Indian Concrete Journal, 2003.

[73] W. B. Fuller and S. E. Thompson, *The Laws of Proportioning Concrete,* vol. LIX, Transactions of the American Society of Civil Engineers, 1907, pp. 67-143.

[74] A. H. M. Andreasen, *Ueber die Beziehung zwischen Kornabstufung und Zwischenraum in Produkten aus losen Körnern (mit einigen Experimenten),* vol. 50, Kolloid-Zeitschrift, 1930, p. 217–228.

[75] J. E. Funk. and D. R. Dinger, *Derivation of the Dinger-Funk Particle Size Distribution Equation,* Boston: Predictive Process Control of Crowded Particulate Suspensions, 1994.

[76] P. Rosin and E. Rammler, *The Laws Governing the Fineness of Powdered Coal,* vol. 7, Journal of the Institute of Fuel, 1993, p. 29–36.

[77] S. A. A. M. Fennis and J. C. Walraven, *Using particle packing technology for sustainable concrete mixture design,* vol. 57, Delft, The Netherlands: HERON, 2012.

[78] Pegasus Vertex, Inc., *Seal the Formation Surface with Optimized Bridging Blend,* Houston: WHITE PAPER.

[79] F. Wenqiang and Y. Jienian, *Designing Drill-in Fluids by Using Ideal Packing Technique,* vol. 4, Beijing, China: Petroleum Science, 2007.

[80] C. C. Furnas, *The relations between specific volume, voids, and size composition in systems of broken solids of mixed sizes,* United States: Dept. of Commerce, Bureau of Mines, 1928.

[81] M. Gan, *The packing of cohesive particles,* Materials Science & Engineering. The University of New South Wales, 2003.

[82]   A. Kwan, K. Chan and V. Wong, *A 3-parameter particle packing model incorporating the wedging effect,* vol. 237, Powder Technology, 2013, pp. 172-179.

[83]   W. Toufar, M. Born and E. Klose, *Contribution of optimisation of components of different density in polydispersed particles systems,* Freiberger Booklet A, 1976, pp. 29-44.

[84]   P. Goltermann, V. Johansen and L. Palbøl, *Packing of Aggregates: An Alternative Tool to Determine the Optimal Aggregate Mix,* 435-443 ed., vol. 94, ACI Materials Journal, 1997.

[85]   T. Stovall, F. Larrard and M. Buil, *Linear packing density model of grain mixtures,* vol. 48, Powder Technology, 1986, pp. 1-12.

[86]   Danish Technological Institute, "4C-Packing - The software," [Online]. Available: https://www.dti.dk/4c-packing/the-software/2783.

[87]   F. Larrard and T. Sedra, *Optimization of ultra-high performance concrete by using a packing model,* vol. 24, Cement and Concrete Research, 1994, pp. 997-1009.

[88]   L. Burtseva, B. V. Salas, R. Romero and F. Wemer, *Multi-Sized Sphere Packings: Models and Recent Approaches Approaches,* Autonomous University of Baja California; Polytechnic University of Baja California; Otto-von-Guericke University, 2015.

[89]   J. B. A. B. A.B. Yu, *On the modelling of the packing of fine particles,* vol. 3, Powder Technology, 1997, pp. 185-194.

[90]   C. L. Feng, *The packing of particles and the effect of cohesive forces,* Australia: PhD thesis. University of New South Wales, 1998.

[91]   E. Ispirogullari, *Polymer particles as environmentally benign premium connection dope additives,* MSc report. MTP group. University of Twente, 2017.

[92]   J. Spanjers, *TiO2 Hybrid core-shell particles for lubrication and sealing of metal-to-metal-seals,* MSc report. MTP group. University of Twente, 2017.

[93]   J. He, Z. Zhang, M. Midttun, G. Fonnum, G. Modahl, H. Kristiansen and K. Redford, *Size effect on mechanical properties of micron-sized PS–DVB polymer particles,* vol. 49, Oslo: Polymer, 2008, p. 3993–3999.

[94]   I. Lilge and H. Schönherr, *Covalently cross-linked poly(acrylamide) brushes on gold with tunable mechanical properties via surface-initiated atom transfer radical polymerization,* vol. 49, European Polymer Journal, 2013, pp. 1943-1951.

[95]   A. Kuo, *Polymer Data Handbook - Poly(dimethylsiloxane),* Oxford University Press, 1999.

[96]   Houston Urethane and Composite, "What is the Advantage of Using Urethane Instead of Other Materials?," [Online]. Available: https://www.houstonurethane.com/technical/.

[97]   Y. Tokiwa, B. P. Calabria and C. U. Ugwu, *Biodegradability of plastics,* vol. 10, International Journal of Molecular Sciences, 2009, pp. 3722-3742.

[98]   Bangs Laboratories Inc, *Material Properties of Polystyrene and Poly(methyl methacrylate) (PMMA) Microspheres.*

[99]   AZO Materials, [Online]. Available: https://www.azom.com.

[100]   M. Kopeć, J. Spanjers, E. Scavo, D. Ernens, J. Duvigneau and G. J. Vancso, *Surface-initiated ATRP from polydopamine-modified TiO2 nanoparticles,* European Polymer Journal, 2018.

[101]   B. H. Chudnovsky, *Distribution, and renewable energy generation power equipment: aging and life extension techniques,* CRC Press, 2017.

[102]   J. He, Z. Zhang, H. Kristiansen, K. Redford, G. Fonnum and G. Modahl, *Crosslinking effect on the deformation and fracture of monodisperse polystyrene-co-divinylbenzene particles,* vol. 7, Express Polymer Letters, 2013, pp. 365-374.

[103]   T. Pakula, Y. Zhang, K. Matyjaszewski, H. Lee, H. Börner, S. Qin and G. Berry, *Molecular brushes as super-soft elastomers,* vol. 47, Polymer, 2006, pp. 7198-7206.

[104]   American Iron and Steel Institute, *Review of the wear and galling characteristics of stainless steels,* Washington: Committee of Stainless Steel Producers, 1978.

[105]   H. M. Wyss, D. L. Blair, J. F. Morris, H. A. Stone and D. A. W. Weit, *Mechanism for clogging of microchannels,* vol. 74, Physical review. E, 2007, p. 061402 .

[106]   C. Sun, F. Yin, A. Afacan, K. Nandakumar and K. Chuang, *Modelling and Simulation of Flow Maldistribution in Random Packed Columns with Gas-Liquid Countercurrent Flow,* vol. 78, Chemical Engineering Research and Design, 2000, pp. 378-388.

[107]   Z. B. Sendekie and P. Bacchin, *Colloidal Jamming Dynamics in Microchannel Bottlenecks,* vol. 32, Langmuir, 2016, pp. 1478-1488.

[108]   *Recommended guidelines for discharge and emission reporting,* Norwegian Oil and Gas Association, 2018, p. 33.

[109]   T. Tinga, *Principles of Loads and Failure Mechanisms,* Den Helder: Springer Series in Reliability Engineering, 2013.

[110]   T. Nguyen, *Introduction and API Standards of Casing,* Well Design, PE 413, Spring, 2011.

[111] Frank's International N.V., *PROSPECTUS. Common Stock,* 2013.

[112] API Spec. 5B, *Threading, gauging, and thread inspection of casing, tubing, and line pipe threads,* American Petroleum Institute, 1996.

[113] API RP 5A5, *Filed inspection of new casing, tubing and plain-end drill pipe,* American Petroleum Institute, 2005.

[114] API RP 5B1, *Threading, Gauging, and Thread Inspection of Casing, Tubing, and Line Pipe,* American Petroleum Institute, 1999.

[115] API RP 5C1, *Care and use of casing and tubing,* American Petroleum Institute, 1999.

[116] API Bull. 5A2, *Thread compounds,* American Petroleum Institute, 1988.

[117] API Bull. 5C2, *Performance properties of casing and tubing,* American Petroleum Institute, 1999.

[118] API Bull. 5C3, *Formulas and calculations for casing, tubing, drillpipe and line pipe properties,* American Petroleum Institute, 1994.

[119] API Bull. 5C4, *Round thread casing joint strength with combined internal pressure and bending,* American Petroleum Institute, 1987.

[120] Society of Petroleum Engineers, *Petroleum Engineering Handbook - Drilling Engineering,* vol. 4, Austin, USA, Texas: Robert F. Mitchell, 2006.

[121] J. X. a. G. Tao, *Analysis of Casing Connection Subjected to Thermal Cycle Loading,* Edmonton, Alberta, Canada: SIMULIA Customer Conference, 2010.

[122] C. Sches, E. Desdoit and J. Massaglia, *Fatigue resistant threaded and coupled connector for deepwater riser systems: design and performance evaluation by analysis and full scale tests,* ASME 27th International Conference on Offshore Mechanics and Arctic Engineering, 2008.

[123] R. C. Griffin, S. Kamruzzaman and R. D. Strickler, *Casing drilling drill collars eliminate downhole failures,* Offshore Technology Conference, 2004.

[124] K. Yamamoto, K. Kobayashi and e. al, *Stress Analysis of Premium Threaded Connection "FOX" by Finite Element Method,* vol. 20, Kawasaki Steel Giho, 1989, pp. 202-207.

[125] Russel Products. Industrial Coating Apllications, "Phosphate - Steel Protection," [Online]. Available: http://www.russprodco.com/phosphate/.

[126] D. Weng, P. Jokiel, A. Uebleis and H. Boehni, *Corrosion and protection characteristics of zinc and manganese phosphate coatings,* vol. 88, Surface and Coatings Technology, 1997, pp. 147-156.

[127] D. Ernens, M. d. Rooij, H. Pasaribu, E. J. v. Riet, W. v. Haaften and D. J. Schipper, *Mechanical characterization and single asperity scratch behaviour of dry zinc and manganese phosphate coatings,* vol. 118, Tribol Int, 2018, p. 474–83.

[128] R. W. Tjerkstra, M. D. Boer, E. Berenschot, J. G. E. Gardeniers, A. V. D. Berg and M. Elwenspoek, *Etching technology fro microchannels,* IEEE Computer Society, 1997, pp. 147-152.

[129] A. P.Nayak, V. J. Logeeswaran and M. S. Islam, *Wet and Dry E,* Davis, California: University of California,.

[130] L. J. Guo, X. Cheng and C.-F. Chou, *Fabrication of Size-Controllable Nanofluidic Channels by Nanoimprinting and Its Application for DNA Stretching,* vol. 4, Nano Letters, 2003, pp. 69-73.

[131] S. Khetarpal, "Prototyping Acrylic Based Microfluidics Using Thermal Bonding," 2015. [Online]. Available: http://www.khetarpal.org/thermal-bonding/.

[132] S. Wang, H. Yu, W. Wang and Z. Li, "Easy and robust interconnection methods for PDMS-based microfluidics," 2012. [Online]. Available: http://blogs.rsc.org/chipsandtips/2012/01/20/easy-and-robust-interconnection-methods-for-pdms-based-microfluidics/?doing_wp_cron=1533469452.6422669887542724609375.

[133] J. F. Sakamot, M. Tuszynski and T. Gros, "High aspect ratio template and method for producing same for central and peripheral nerve repair". Patent US 2009/0202605 A1, 2009.

[134] W. Liu, C. Huang and X. Jin, *Electrospinning of Grooved Polystyrene Fibers: Effect of Solvent Systems,* vol. 10, Nanoscale Research Letters, 2015, p. 237.

[135] T. Uyar and F. Besenbacher, *Electrospinning of uniform polystyrene fibers: The effect of solvent conductivity,* vol. 49, Polymer, 2008, pp. 5336-5343.